INVESTIGATION OF ANTIPHASE DOMAIN BOUNDARY ENERGETICS
IN GAAS-ON-SI(001)

By

CALEB SHUAN CHIA BARRETT

A DISSERTATION PRESENTED TO THE GRADUATE SCHOOL
OF THE UNIVERSITY OF FLORIDA IN PARTIAL FULFILLMENT
OF THE REQUIREMENTS FOR THE DEGREE OF
DOCTOR OF PHILOSOPHY

UNIVERSITY OF FLORIDA

2017

To all those who came before

TABLE OF CONTENTS

LIST OF TABLES

LIST OF FIGURES

9

LIST OF ABBREVIATIONS

ABF	Annular bright field
AFM	Atomic force microscopy
ALD	Atomic layer deposition
APB	Antiphase domain boundary
BF	Bright field
CMOS	Complimentary metal oxide semiconductor
DEZn	Diethylzinc
DF	Dark field
DFT	Density functional theory
EDS	Energy dispersive spectroscopy
EELS	Electron energy loss spectroscopy
FIB	Focused ion beam
FWHM	Full width at half maximum
HAADF	High angle annular dark field
HRTEM	High resolution transmission electron microscopy
MBE	Molecular beam epitaxy
MOCVD	Metal-organic chemical vapor deposition
MOSFET	Metal oxide semiconductor field effect transistor
nMOS	n-type metal oxide semiconductor
pMOS	p-type metal oxide semiconductor
RTA	Rapid thermal anneal
SEM	Scanning electron microscopy
SIMS	Secondary ion mass spectrometry
STEM	Scanning transmission electron microscopy

TBAs	Tertiarybutylarsine
TEM	Transmission electron microscopy
TMGa	Trimethylgallium
XRD	X-ray diffraction
XTEM	Cross-sectional transmission electron microscopy

Abstract of Dissertation Presented to the Graduate School
of the University of Florida in Partial Fulfillment of the
Requirements for the Degree of Doctor of Philosophy

INVESTIGATION OF ANTIPHASE DOMAIN BOUNDARY ENERGETICS
IN GAAS-ON-SI(001)

By

Caleb Shuan Chia Barrett

August 2017

Chair: Kevin Jones
Major: Materials Science and Engineering

GaAs was once called the material of the future for the semiconductor industry. Significant effort was directed towards the integration of high-performance GaAs on large Si wafers, but GaAs-on-Si devices never became economically feasible compared to Si devices. With the recent push for researching alternative transistor channel materials to replace Si, interest has been renewed in GaAs and the other III-V compound semiconductors. However, many of the same challenges to integrate GaAs on Si still remain. In particular, during the epitaxial growth of GaAs on Si, antiphase domain boundaries (APBs) can nucleate at the GaAs/Si interface and propagate throughout the entire GaAs layer. Much effort has been placed towards achieving APB-free GaAs through various avenues, e.g. substrate preparation and changing growth conditions. Still little is known about how different factors affect the energetic stability of APBs in GaAs. This work investigates these factors at different stages of processing of GaAs films grown on Si(001) by metal-organic chemical vapor deposition (MOCVD). First, it is shown that APB density is quantitatively correlated to the presence of contamination at the GaAs/Si interface. Second, it is demonstrated that the MOCVD growth temperature directly affects the tendency of APBs to change habit planes and

self-annihilate. Third, post-growth annealing is shown to drive the dissolution of grown-in APBs. Finally, Fermi level-induced modulations in antisite defect formation energies are investigated as a method of affecting the APB stability.

CHAPTER 1
INTRODUCTION

1.1 Motivation

Technological progress in the microelectronics industry has traditionally been

dictated by Moore's Law. The observation first made by Gordon Moore in 1965

predicted that the number of transistors on a single silicon chip would double every one

to two years [1]. Adherence to Moore's Law has since been accomplished by simply

shrinking the individual transistor size. This decrease in size brings a proportional

increase in electrical performance, as explained by the Dennard scaling law [2]. A key

component of the Dennard scaling law is that as transistors are scaled down the power

density should also remain constant. However, this rule has broken down in recent

years as leakage currents in devices have become a greater concern [3–5]. Classical

Dennard scaling of Si-based transistors at the rate given by Moore's Law is therefore no

longer sustainable. In an attempt to extend the life of Moore's Law, industry has turned

towards non-planar device architectures as well as alternative transistor channel

materials to replace Si.

The most likely group of materials to replace Si in future transistors are the III-V

compound semiconductors, so called because they are composed of elements from

groups III and V of the periodic table. III-V materials such as GaAs, InAs, and their

ternary alloy InGaAs have much better electron transport properties than Si, including

higher electron mobilities [6]. Transistors made from these materials can theoretically

obtain much higher drive currents at similar supply voltages relative to Si-based

devices. However, it is impractical to use III-V wafers as the basis for future devices

because they are generally more expensive to produce [7], cannot be made as large as

Si wafers [8], and are fragile compared to Si wafers [9]. Therefore, research has been devoted to integrating III-V materials on Si to combine their respective beneficial properties.

Epitaxial growth is a common method of fabricating III-V layers on Si wafers. The growth of GaAs on Si specifically has been well studied since the 1980s. Much of the early work was focused on obtaining good quality GaAs-on-Si to replace more expensive bulk GaAs in photonics applications, with the goal of eventually combining these devices with transistors in integrated circuits [10]. However, as with other III-Vs, the epitaxial layers continued to be plagued by a variety of growth-related defects and the cost and performance of GaAs-on-Si devices never rivaled that of bulk GaAs. Therefore, work in the area of GaAs growth on Si was largely shelved until the recent push for new transistor materials in microelectronics applications. This renewed interest has sparked a need for research to fill the gaps left previously in the understanding of how these different defects can be suppressed or eliminated.

One type of defect that is unique to the epitaxy of a polar material such as GaAs on a nonpolar material such as Si is antiphase domain boundaries (APBs). APBs are high energy planar defects composed of antisite bonds and can be treated as a special type of grain boundary separating regions of crystal with reversed polarity. They can propagate through the entire thickness of an epitaxial layer and lead to degradation of electrical properties [11]. Therefore, from an engineering standpoint, it is critical to develop processes that either prevent the nucleation of APBs or achieve complete suppression of antiphase domains within the epitaxial film but that are also practical for implementation in complex industrial process flows. These breakthroughs require

18

knowledge of the fundamental characteristics of APBs and how their energetics are affected by different conditions. Even though several decades of research have been spent on GaAs growth on Si, still little is known about the energetics and thermal stability of APBs. Successful integration of GaAs and other III-Vs on Si will never occur without a thorough understanding of these factors.

1.2 The Role of GaAs in Future Transistors

In its most common usage in modern electronic devices, the transistor functions as a switch between two different states for logic gates, either "1" when it is on or "0" when it is off. Therefore, the two most important properties that define a transistor are the on-state drive current, I_{on}, and the off-state leakage current, I_{off}. A good transistor must have a high ratio of I_{on} to I_{off} in order for the two states to be distinguishable. The breakdown in scaling of Si-based devices has arisen largely because I_{off} has gotten very large due to decreases in the gate dielectric thickness and the transistor threshold voltage [4]. As well, increasing the supply voltage to increase I_{on} is not feasible due to heat dissipation concerns [6].

On paper, the III-V compound semiconductors have much more attractive properties for use in metal-oxide-semiconductor field-effect transistors (MOSFETs) over Si. For n-type MOS (nMOS) devices, the electron mobility at room temperature of InGaAs and InAs is more than 10 times that observed for Si [6]. III-V compounds may also be used for p-type MOS (pMOS), as the hole mobility of materials such as GaSb is greater than that of Si [6, 12]. Thus, marked improvements in I_{on} can theoretically be made for III-V devices over Si devices even at lower operating voltages. In practice, integrating III-Vs on Si for future devices comes with a number of challenges, not least of which is the issue of growth-related defects. The lattice constant mismatch in

particular can be quite large. For example, InAs and Si have a lattice mismatch of ~11%. The lattice mismatch can lead to a high density of threading dislocations that will, in combination with the antiphase disorder, degrade the quality of the layer and adversely affect device performance [13].

Buffer layers are commonly implemented in the epitaxial growth of III-V compounds on Si to alleviate growth-related defects [12, 14]. The buffer layer material must be chosen such that it has an intermediate lattice constant between that of the substrate and the subsequent layer. It must also form good interfaces with the substrate material and the next growth layer. GaAs is a good candidate for a buffer layer material. While future transistor devices could be based on GaAs, larger gains in performance would be made by using other III-V compounds, such as InAs, instead. In the role of a buffer layer material, GaAs has several beneficial properties. In particular, it has a lattice constant larger than Si but smaller than InAs, it can make ternary alloys with InAs with variable lattice constant, and there is already a wealth of history of research on the growth of GaAs on Si. Another advantage of using GaAs as a buffer material is its relatively large bandgap (1.42 eV at room temperature) which makes it semi-insulating when it is undoped [15]. This property provides electrical isolation for the active channel layer in a transistor. Thus, the first step towards realizing III-V devices on Si substrates is the growth of GaAs layers on Si with good crystal quality and suppression of defects.

1.3 History of GaAs Epitaxy on Si

Since the early reports on the semiconducting nature of III-V compounds in the 1950s [16], GaAs has displayed significant promise for device applications. It has many attractive properties relative to Si, particularly for high-frequency, high-temperature, and high-radiation environment applications [17]. However, the technology for Si in general

integrated circuits applications matured much more rapidly and it became the standard of the semiconductor industry. The cost of Si devices was also much lower compared to GaAs in part due to the larger wafer size of Si which allowed for higher throughput. It was realized that in order to make GaAs devices economically feasible for large-scale manufacturing, GaAs would need to be integrated onto Si wafers [13]. Thus, significant effort towards researching GaAs epitaxy on Si began in the 1980s.

There are two primary growth methods for GaAs epitaxy on Si. One is molecular beam epitaxy (MBE) and the other is metal-organic chemical vapor deposition (MOCVD). Briefly, MBE takes place in ultrahigh vacuum (~10^{-9} Torr) and evaporates the elemental sources onto a substrate, while MOCVD takes place at higher pressure (~1 Torr to 760 Torr) and uses gas-based metal-organic precursors that are flowed across the substrate [18, 19]. MBE is considered to be a technique that is further from equilibrium and can be used to form high purity films with good stoichiometric control. However, the ultrahigh vacuum environment of MBE makes it inefficient for large-scale production compared to MOCVD [19]. Therefore, MOCVD has been the dominant method used in industry.

1.3.1 Two-Step Growth Process

Successful growth of GaAs films on Si with good morphology was demonstrated for both MBE [20] and MOCVD [21] systems in 1984. The critical breakthrough in both of these studies was the use of a two-step growth process for GaAs to reduce defect densities and achieve good crystal quality. The first step is a thin nucleation layer grown at a relatively low temperature, typically 400-600 °C [21]. The growth temperature is then raised to the range of conventional GaAs homoepitaxy, 600-700 °C, in the second

step for the remainder of the film growth. Attempts to nucleate GaAs on Si at typical

GaAs homoepitaxy temperatures resulted in rough films with high defect densities [22].

The advantage of a low temperature nucleation layer is manifested in the number

and size of nuclei that form during the initial stages of growth. There are three generally

accepted modes of growth for epitaxial films [23]: two-dimensional (2-D) layer-by-layer

growth (Frank-van der Merwe mode), three dimensional (3-D) island growth (Volmer-

Weber mode), and a combination of the two (Strankski-Krastanov mode). For highly-

strained films, such as GaAs on Si, it is difficult to maintain stability of 2-D layer growth.

This can be seen in a wetting surface energy inequality relationship. Layer-by-layer

growth is only favorable if the following is true:

$$\gamma_{substrate} > \gamma_{film} + \gamma_{interface} \tag{1-1}$$

where $\gamma_{substrate}$, γ_{film}, and $\gamma_{interface}$ are the surface energies of the substrate, film, and

substrate-film interface, respectively [23, 24]. A strained film creates a large γ_{film} which

can then reverse this inequality and thus favor the growth of 3-D islands. The number of

nuclei that will form at the initial stages of growth can be related to the degree of

undercooling, set by the growth temperature, T [25]:

$$r^* \propto \frac{1}{T_m - T} \tag{1-2}$$

where r^* is the critical nucleus radius and T_m is the equilibrium solidification temperature

of the film. A low temperature presents a large undercooling and thus promotes the

formation of many, small nuclei allowing for earlier coalescence of the film [26–28]. As

well, the islands at a low growth temperature are more likely to still be fully strained, i.e.

pseudomorphic, before the film coalesces [22, 28]. For a high growth temperature,

fewer islands form and can grow quite large and form a high density of dislocations

before they meet and coalesce [22]. Misoriented nuclei can also form and lead to a polycrystalline film. Thus, the nucleation temperature should be kept as low as possible. Nucleation of GaAs on Si at temperatures as low as 225 °C has been shown for MBE [26]. The nucleation temperature for GaAs on Si by MOCVD is limited to ~400 °C since the temperature at the substrate surface must still be high enough to crack, or pyrolyze, the precursor molecules [29, 30]. It should also be noted that once the film is nucleated, it no longer is advantageous to grow at a low temperature as this hinders the growth rate and the annihilation of any existing defects [31].

1.3.2 Substrate Surface Preparation

The preparation of the Si substrate is also critical in achieving successful growth of GaAs on Si. Contaminants present on the Si surface prior to growth can degrade the quality of the epitaxial GaAs layer and lead to higher defect densities [13]. Interfacial amorphous contaminant particles have been directly linked to the formation of growth defects [32, 33] and it is speculated that they may also be able to nucleate APBs [13]. The primary sources of contamination on the Si surface are oxygen from the native oxide of Si and carbon from the environment. Carbon contamination is typically more difficult to remove than oxygen [34]. Most early methods of Si substrate preparation involved some combination of degreasing in organic solvents then dipping in HF to remove the native oxide [13, 21]. Other studies found it was advantageous to intentionally oxidize and etch the Si surface in repeated steps to gradually reduce the amount of carbon [35–38]. After a number of oxidation and etch cycles, the substrates would be transferred to the growth chamber and annealed at 800-1000 °C to thermally desorb the remaining oxide prior to film growth. Eventually, it became widely accepted that a wet chemical treatment involving HF followed by a high temperature anneal near

1000 °C in the growth chamber was sufficient in reducing the surface contamination [38, 39].

1.3.3 Substrate Orientation

Early work by Kroemer et al. [40–43] proposed the use of (112)-oriented Si wafers to reduce the antiphase disorder in GaAs and other III-V compound films. The supporting theory was that the pattern of dangling bonds on the (112) Si surface would cause a preference for either Ga or As adatoms to stick to specific sites. Therefore, GaAs islands nucleating on different areas of the (112) surface would have the same orientation and not form APBs when they coalesced. However, since Si technology in industry was and still is based on (001)-oriented wafers, the (112) solution was not adopted. The focus of this work will also remain on (001)-oriented Si for its technological relevancy.

1.3.4 Growth-Related Defects

As mentioned above, the various strategies for GaAs growth on Si are all aimed at reducing the density of defects in the GaAs layer. The primary growth-related defects that typically occur, in order of defect formation energy, are [44, 45]: threading dislocations, stacking faults, twin boundaries, and APBs. Stacking faults and twin boundaries are planar defects that result from errors in the stacking sequence of atomic planes during growth. These errors can usually be avoided by optimizing growth conditions. The nucleation of threading dislocations (from interfacial misfit dislocations) and APBs is mostly unavoidable for conventional GaAs on Si epitaxy. There are already numerous studies on the reduction of threading dislocation densities in III-V layers grown on Si. The main strategies are the use of strained-layer superlattices [46–51] to deflect the propagation of threading dislocations away from the film surface and, more

recently, aspect ratio trapping [52–59] to encourage the termination of dislocations and other defects at oxide sidewalls. The elimination of APBs in III-V films is more complex and not as well understood. They are also particularly interesting defects because of their large formation energy and uniqueness in semiconductor processing. Literature relating to APB formation and energetics will be discussed herein.

1.4 Antiphase Boundaries in GaAs-on-Si

1.4.1 GaAs Crystal Structure

To understand the formation of APBs in GaAs grown on Si, one must begin by analyzing the crystal structure of GaAs as compared to Si. GaAs has the zinc blende crystal structure and Si has the diamond cubic crystal structure. While differing in name, these crystal structures are very similar. Each atom in the lattice shares four bonds with neighboring atoms. The basic unit cell for GaAs is a face-centered cubic (FCC) sublattice of one atom type (Ga or As) with additional atoms that are of the opposing type at the four tetrahedral sites. The four tetrahedral atoms are a part of an equivalent FCC sublattice with the origin at a_0(¼, ¼, ¼), where a_0 is the lattice constant. Figure 1-1A shows a GaAs unit cell based on the Ga sublattice with As atoms at the tetrahedral sites. The diamond cubic structure is identical in terms of atom positioning, but the two FCC sublattices are composed of the same type of atom.

Since the sublattices in GaAs are of opposing atom types, not all configurations are structurally alike. This difference is most notable in the <110> projections of the GaAs crystal structure. Figure 1-1B shows a GaAs unit cell along the [110] viewing direction. The classic "dumbbell" structure is apparent and shows the polar nature of GaAs with As-polarity in the +z direction. If the lattice is rotated by 90° (or, equivalently, inverted) and viewed along the [-110] direction (Figure 1-1C), the direction of bond

25

polarity is reversed. Therefore, if GaAs in nucleated in regions with orientations offset by 90°, the crystal structures will have opposing polarity and the Ga- and As-sublattice positions are switched. For Si homoepitaxy this is a nonissue as the sublattices are identical. Likewise, for GaAs homoepitaxy, Ga and As adatoms will energetically prefer to be incorporated in the correct sublattice and follow the ordering of the substrate. However, during the heteroepitaxy of GaAs on Si, this ordering preference no longer applies and structural defects can result.

It is also important to note that in comparing Figure 1-1B and Figure 1-1C, if the two unit cells are offset by a single atomic layer, equivalent (002) planes will be offset by one quarter of the lattice constant, or one half of the (002) plane spacing, in the +z direction. Thus, the (002) plane is sensitive to any dispersions in the GaAs crystal ordering arising from such monolayer offsets. This factor will become relevant for the detection of APBs in GaAs.

1.4.2 Formation of Antiphase Boundaries

The possible formation of APBs in GaAs was first predicted by Holt in 1969 [60]. This prediction was based on the characteristic dual sublattices of the GaAs zinc blende structure which allows for regions of crystal with opposite polarity, i.e. are antiphase with respect to the other. Thus, if these two types of domains formed in a bulk crystal, a planar boundary would form at their intersection. This boundary was termed an antiphase domain boundary, or antiphase boundary for short. The atomic bonds across the boundary would be forced to be antisite bonds, i.e. Ga-Ga or As-As bonds, due to the differing allocation of Ga and As atoms in the sublattices in the two orientations. Antiphase domains were first experimentally observed in GaAs epitaxial layers by Morizane in 1977 [61] for GaAs grown on Ge. The degree of antiphase disorder in

epitaxial GaAs layers can be extensive. Figure 1-2 shows a plan view scanning electron microscope (SEM) image of a GaAs layer grown on Si(001) with a large areal density of APBs. APBs in GaAs must form closed loops, i.e. domains, and cannot intersect in triple points since there are only two sublattices [44].

The surface of the substrate is the key to the formation of APBs in epitaxial GaAs layers. The (001) surface of Si is known to exhibit a 2x1 dimerized reconstruction [13]. The dimers form between atoms with dangling bonds at the surface in order to lower the surface energy [62, 63]. The orientation of the dimer bond on the Si surface will depend on the sublattice that terminates the surface. Thus, two distinct domains can exist on the surface. This difference is evident with the presence of a step on the Si(001) surface that is a single atom in height. These types of steps will be referred to as single-steps. Figure 1-3 shows how the orientation of dimerization is rotated by 90° across single-steps.

Surface steps will always be present on a real Si(001) surface [10, 43], mainly because of entropy and the fact that slices of Si wafers from the boule are never perfectly flat. It follows that if GaAs growth is nucleated on either side of a single-step on the Si surface, the crystal will be rotated by 90° to follow the orientation of the substrate and the respective crystal polarities will be reversed. Therefore, when the two nucleated islands coalesce, an APB will form above the surface step. Figure 1-4 shows a <110> projection of an epitaxial GaAs layer on a Si(001) substrate with the presence of surface steps. An APB is nucleated at a single-step in Figure 1-4A and propagates vertically along a {110} type plane. The reversal of bond polarity across the APB from As-polar to Ga-polar can be observed, along with the alternating antisite bonds of Ga-Ga and As-As

27

along the APB plane. If an APB propagates along a habit plane that is inclined relative to the substrate normal, e.g. {111}, then it may self-annihilate with another APB, as seen in Figure 1-4B. The antisite bonds along the {111} habit plane are all the same type; in this case, As-As. This type of habit plane is considered to be non-stoichiometric and may not be energetically favorable. In the case of a surface step that is two atomic layers in height, i.e. a double-step, the sublattice ordering of the epitaxial GaAs layer is reset and no APB forms, as seen in Figure 1-4C. In addition to physical surface steps, it is suspected that the presence of contaminant particles on the Si substrate may act analogously to steps and contribute to the nucleation of APBs [13].

1.4.3 Suppression of Antiphase Boundaries

As depicted in Figure 1-4C, the presence of all double-steps on the Si(001) surface would theoretically prevent the nucleation of APBs. Therefore, most of the initial efforts to suppress antiphase disorder in epitaxial GaAs films grown on Si were based on achieving a perfect step-doubling of the Si substrate. For as-prepared Si(001) wafers the most common step-height is a single atomic layer [64, 65]. One approach focused on deliberately misorienting the Si(001) wafers by off-cutting the wafer some angle from the (001) plane which would increase the step density. It was found that these vicinal Si(001) wafers exhibited higher percentages of double-steps with increasing annealing temperature (up to 1000 °C) in ultra-high vacuum environments [66–68]. The preference for double-steps with substrate misorientation was theorized to stem from a reduction in the elastic interaction energy between steps since the terrace distance is reduced with greater misorientation and higher step density [69, 70]. The reconstruction of adjacent single-steps into a double-steps increases the average terrace width and creates a single domain surface.

Other studies found that step-doubling could be achieved even for nominally on-axis Si(001) wafers, i.e. no off-cut, with high temperature annealing. Sakamoto and Hashiguchi [71] first showed a two-domain Si(001) surface with single-steps reconstructed to a single-domain surface via conversion of the single-steps to double-steps after annealing at 1000 °C for 20 min in a MBE system. Later work speculated that this result, and the step-doubling result from off-cut substrates, was due to an energetic preference for a specific step edge [64, 72]. Figure 1-5 shows the two types of terraces that will exist on a Si(001) surface with steps. Type A terraces have dangling bonds running perpendicular to the step edge and Type B terraces have dangling bonds running parallel to the step edge. Type B terraces and the corresponding step edges were thought to be more energetically favorable [64] and in particular Type B double-steps were theorized to be favored over either type single-steps [65, 72]. More recent work has corroborated this energetic preference for double-height steps with dangling bonds parallel to the step edge [73, 74]. Therefore, there is a driving force for a surface made of single-steps of either type, i.e. a normal Si(001) surface, to reconstruct to form only Type B double-step edges with annealing. Misorienting the substrate simply reduces the distance that atoms at unfavorable step edges need to diffuse to reach a favorable step edge.

The accepted method of Si substrate preparation for optimal GaAs growth and reduced antiphase disorder involves some degree of off-cutting followed by a high temperature pre-growth anneal near 1000 °C [38]. The pre-growth anneal has the additional benefit of reducing the amount of surface contamination, including native oxide, that may contribute to higher densities of APBs and other defects. Several

studies in the late 1980s were able to demonstrate the growth of APB-free GaAs films by MBE and MOCVD using this procedure [75–77] and it continues to be employed for the growth of GaAs and other III-V compounds in more recent years [78–80]. However, the use of misoriented substrates and high temperature anneals is not necessarily practical for integration into large-scale industrial processes. In particular, established process flows for integrated circuit manufacturing are based on nominally on-axis Si(001) wafers. Moving to misoriented substrates would require a complete revamping of these process flows and so is cost prohibitive. High temperature anneals should also ideally be avoided since there may be other existing layers or devices on the Si wafer before the deposition of GaAs that would be affected [10]. Thus, it is unlikely that the nucleation of APBs can be completely prevented for GaAs films grown on Si(001) substrates with no intentional off-cut.

Film thickness is a variable that may help to suppress any nucleated APBs in GaAs-on-Si. Georgakilas et al. [11] showed through depth profiling of a GaAs layer grown on a misoriented Si(001) substrate that the APB density decreased with increasing GaAs thickness. Therefore, APBs must be self-annihilating during growth. This evidence corresponds with experimental observations in transmission electron microscopy (TEM) that APBs in GaAs have a tendency to change habit planes during growth [81–85] which is conducive for self-annihilation. Figure 1-6 is a composite cross-sectional TEM (XTEM) image showing the meandering path of an APB propagating through a GaAs layer grown on Si(001). It is likely that the early studies of GaAs growth on Si that grew good quality films took advantage of this effect, whether intentionally or

not. GaAs-on-Si film thicknesses for device fabrication were commonly on the order of a few microns [13, 75].

In theory, based on the evidence for APB self-annihilation, APBs can be completely suppressed in a film regardless of the nucleated density if growth is continued indefinitely. However, there is an upper limit on GaAs film thickness due to the difference in the coefficient of thermal expansion with Si. The cool down from the high growth temperature can induce large stresses in the film and lead to cracking, depending on the film thickness [38]. For typical GaAs-on-Si heteroepitaxial growth ranges, the critical thickness is approximately 4 µm [86–88]. In addition to the potential for film cracking, growing thick GaAs films on the order of microns should be avoided to reduce cost and dwell time in industrial processes.

Growing another group IV layer on top of the GaAs layer also will not necessarily reset the atomic ordering and suppress antiphase disorder. Jia and Fitzgerald [89] showed that APBs will propagate through a GaAs film with Ge interlayers. Thus, the misordering induced by single-steps is being preserved even through the Ge layers. Self-annihilation of APBs must then be achieved completely in the GaAs film with minimal thickness. To this end, it becomes important to understand the energetics of APBs and how their propagation can be affected.

1.5 Antiphase Boundary Energetics

1.5.1 Calculations of Formation Energies

The first attempt at calculations of APB energetics in GaAs were made by Petroff in 1986 [90]. These calculations were based on a simple analysis of the wrong bond energy and wrong bond densities for given APB planes. Petroff found that {110} and {112} APBs should have a lower formation energy than {111} or {100} APBs. However,

subsequent work by Vanderbilt and Lee in 1992 [91] showed that this approach was insufficient because it neglected the electrostatic contribution of wrong bonds to APB formation energy. The Ga-Ga bond has a net charge of $-q/2$ and the As-As bond has a net charge of $+q/2$, where q is the elementary electron charge. APBs on {110} type planes are self-compensated in that they are stoichiometric and will have equal numbers of Ga-Ga and As-As bonds. On the other hand, {111} APBs are non-stoichiometric and will be fully formed of the same type of wrong bonds, either As-As or Ga-Ga. Thus, APBs that are stoichiometric should generally be energetically favored over non-stoichiometric APBs. The first principles calculations by Vanderbilt and Lee found that {110} APBs had lower formation energies than non-stoichiometric {111} or {100} APBs.

The most recent analysis of APB formation energies for GaAs was made by Rubel and Baranovskii in 2009 [92] using density functional theory (DFT) calculations. They expanded upon the work of Vanderbilt and Lee by calculating formation energies for {112} APBs which are fully stoichiometric and {113} APBs which are partially stoichiometric. As with {111} APBs, these higher-index planes would also be conducive for self-annihilation. The APB formation energies calculated by Rubel and Baranovskii are listed in Table 1-1. It was once again determined that {110} APBs have the lowest formation energy (28 meV/$Å^2$). APBs along {112} and {113} have an identical formation energy (39 meV/$Å^2$) that is lower than that found for {111} APBs (43 meV/$Å^2$). The low formation energy of {110} APBs agrees with TEM observations that show {110} planes as the most common for APB propagation [83, 93]. However, the evidence for APB self-annihilation [11] indicates that APBs must be kinking to higher index planes, even if they

are higher formation energy. Thus, {112} and {113} planes may be good candidates as APB habit planes to facilitate annihilation.

It should be noted that while {110} APBs are commonly observed in TEM and have relatively low formation energies, APBs can theoretically exist on any set of crystal orientations. When observed in plan view, such as in Figure 1-2 or in the work of Cohen and Carter [94], APBs are not always faceted along {110} planes forming rectangular domains. Rather, the APBs are faceted along various planes including {110} and sometimes are apparently curved. Vertical APBs connecting {110} segments could exist in any configuration between {110} and {100}, e.g. {120} or {130}. The formation energies of APBs along these planes have not been calculated, nor have they been calculated for curved APBs, likely in part since these orientations do not facilitate self-annihilation. The work of Beyer et al. [95] also showed that nucleated APBs can be templated by the underlying Si surface structure. It is possible that APBs nucleate along various facets including {110} to follow the Si step structure and then otherwise follow the shortest distance to form a closed loop. This configuration would minimize the total line length of APBs that form and lead to the sometimes curved and wandering nature of APBs seen in Figure 1-2. There is an energy balance between the formation energy of APBs along these orientations and the overall energy added to the system by the total line length of APBs. The lowest energy configuration of APBs may be revealed by annealing experiments.

In general, the existence of any APB in GaAs should be unfavorable due to the large associated energy. As a comparison, the formation energy of a stacking fault in GaAs is ~3 meV/Å^2 [45, 96], about an order of magnitude lower than the formation

energy for APBs. Only zero-dimensional defects, i.e. point defects, should be present at thermal equilibrium [44]. In GaAs-on-Si APBs are forced to form because of single-steps on the Si surface. It follows from the thermodynamic instability of APBs that there should be an energetic driving force for the self-annihilation of APBs. This driving force is likely what leads to the kinking of APBs from {110} planes to higher-index planes, even if these planes are theoretically a larger energy cost.

1.5.2 Fermi Level Effects

Since APBs are composed entirely of antisite bonds, their energetic stability may be affected by the relative stability of antisite defects in the GaAs layer. The Ga-Ga wrong bond will have an associated Ga_{As} defect and the As-As wrong bond will have an associated As_{Ga} defect. Recall that these bonds have a net charge; Ga-Ga bonds will act as acceptors and As-As bonds will act as donors. Walukiewicz presented a model in which the Fermi energy in heavily-doped GaAs is stabilized by amphoteric native defects that compensate the dopant species [97]. In other words, the formation energy is lowered for a given native defect, depending on the type of dopant used. As the Fermi level approaches the conduction band edge, i.e. for more n-type GaAs, the formation of Ga_{As} antisite defects and Ga vacancies (V_{Ga}) that act as compensating acceptors is favored. Towards the valence band edge, i.e. for more p-type GaAs, formation of As_{Ga} antisite defects and As vacancies (V_{As}) that act as compensating donors is favored. These native defects in compound semiconductors work to stabilize the Fermi energy and shift it away from the band edges closer to an equilibrium charge-neutral level [98].

The Fermi level effect on point defect energies was later corroborated with DFT calculations by Chroneos et al. [99]. This work focused only on the formation energies of Ga_{As} and As_{Ga} antisite defects as a function of Fermi level, but showed a similar trend

to the work by Walukiewicz. The formation energy of As_{Ga} is lower near either the valence or conduction band edge. The formation energy of Ga_{As} tends to decrease moving from the valence band edge to the conduction band edge, where it is lower overall in energy compared to the As_{Ga} defect.

Experimental work has supported this model of dopant compensation by native point defects for Si-doped InGaAs [100]. However, no study has reported on the effect of doping on APB energetic stability in GaAs or other III-V arsenides.

1.5.3 Kinetics of Transformation

While APBs are a unique defect for polar-on-nonpolar systems in semiconductor epitaxy, they are hardly unique to compound semiconductor material systems as a whole. APBs can exist in any crystal in which there are multiple equivalent sublattices such that the polarity can be reversed from one grain to a neighboring grain. They are well documented in other compounds, including metals and metal oxides. Some of the earliest reports on the possible existence of APBs were made for copper-gold alloys in the 1930s [101–103]. Cu_3Au, for example, has a FCC lattice with four equivalent simple cubic sublattices [103]. Various studies found that these alloys exhibited antiphase domains in their ordered states [104–106]. Notably, these studies also found that the antiphase domain size changed with annealing treatments [106, 107]. The domain growth for these systems typically obeys the following equation [107, 108]:

$$D^2 - D_0^2 = kt \tag{1-3}$$

where t is the annealing time, D is the domain size at time t, D_0 is the initial domain size, and k is a rate constant. Equation 1-3 is identical to the equation used to describe the kinetics of grain growth [109]. The temperature dependence of domain growth can be then described by an Arrhenius relationship:

$$k = k_0 e^{-E_a/k_B T} \tag{1-4}$$

where k is the rate constant from Equation 1-3 at a given temperature T, k_B is

Boltzmann's constant, and E_a is the activation energy.

As is the case in grain growth, Allen and Cahn [110] theorized that the evolution

of APBs is driven by a reduction in curvature. Over time, as domains grow, both the

mean curvature and total surface area of APBs should decrease. This transformation

lowers the overall free energy of the system. Allen and Cahn derived a equation for this

transformation similar to Equation 1-3:

$$[S_v(t)]^{-2} - [S_v(0)]^{-2} = 2\varphi M t \tag{1-5}$$

where S_v is the APB surface area per unit volume as a function of time, t, φ is a

dimensionless constant, and M is a rate constant similar to k from Equation 1-3 with

units of m^2/s. S_v can be related to APB density which is simply the line length of APBs

per unit area in plan view. Therefore, the change in APB density should also have a $t^{-1/2}$

dependence. This time dependent APB density evolution has been observed during

growth of epitaxial Fe_3O_4 films [111] and with annealing [112], but has not been studied

for APBs in GaAs.

1.6 Thermal Effects on III-V Antiphase Boundaries

Although there has been extensive work on the effects of thermal treatments on

APBs in other material systems, thermal effects on APB evolution in GaAs and other III-

V compounds is not well understood. There are two primary avenues for affecting APB

energetics in epitaxial GaAs films grown on Si via application of thermal energy. The

first is to increase the growth temperature which may affect the tendency of APBs to

change habit planes. The second is to anneal the samples after growth which may allow

neighboring APBs to diffuse towards each other and self-annihilate, similar to grain growth. Studies on the effects of growth temperature and annealing on APBs in GaAs and other III-V compounds will now be discussed.

1.6.1 Growth Temperature Effects

If APBs in GaAs-on-Si(001) layers propagated entirely parallel to the substrate normal on the lowest energy {110} planes, they would never self-annihilate. However, the work of Georgakilas et al. [11] strongly indicated that APBs have a tendency to change their plane of propagation during growth. It follows that the tendency of APBs kink to higher index planes that are conducive for self-annihilation may be a function of the growth temperature.

While MOCVD is not an equilibrium process [30], increasing the temperature in the system should bring it closer to equilibrium conditions. Based on the high formation energy of APBs, the equilibrium state for a GaAs-on-Si layer should be APB-free or, at the very least, with minimized APB interfacial area. Figure 1-7 shows an arbitrary free energy diagram for a GaAs-on-Si system in two different states: B, a GaAs layer with APBs propagating vertically along {110} planes, and A, a GaAs layer with self-annihilated APBs. The transition between the two states may be kinetically limited by different factors during growth. Thus, there is an activation energy, E_a, that must be satisfied by increasing the growth temperature.

The effect of growth temperature on APBs has been examined for GaP films grown on Si(001) by MOCVD [113, 114]. For bulk growth temperatures near 450 °C, APB propagation along {110} planes was favored and these APBs extended to the surface of the film. When the bulk growth temperature was raised to 625 °C, the majority of APBs were oriented along {111} and {112} type planes leading to complete

suppression of antiphase domains in the film. The transition between majority {110} APBs to majority {112} APBs with the increase in growth temperature indicates there is a kinetic barrier for APB propagation along these higher index planes.

1.6.2 Annealing Effects

Using the same rationale for the effect of growth temperature, post-growth annealing should also drive the GaAs-on-Si system to its equilibrium state. Thus, it may be possible for annealing to dissolve APBs as long as the temperature is high enough to satisfy the energy required to diffuse APBs. Qualitatively, the energetic barrier for an antiphase domain wall to move would likely be substantial, as it would require the diffusion of an entire plane of antisite defects.

The effect of annealing on APBs in GaAs grown on Si(001) by MOCVD was briefly examined by Chu et al. in 1988 [115]. The films were between 1.9 µm and 5.5 µm thick and had a high degree of antiphase disorder. The study found that APB density in the films decreased, i.e. antiphase domains grew, with 2 hr anneals for a temperature range from 700 to 800 °C. No remarks were made about the activation energy for APB diffusion. However, the results do demonstrate that the diffusion of an APB in GaAs is possible which is consistent with what has been reported for annealing of APBs in other material systems. Further, the anneals indicate that the lowest energy state for the GaAs-on-Si films is in fact APB-free and that annealing helps to reduce the total APB interfacial area.

The evolution of APBs with annealing was recently investigated for GaP films grown on Si by MBE [116]. The study examined the ratio of antiphase crystal to main phase crystal using data obtained by X-ray diffraction reciprocal space mapping for an

as-grown sample and a sample annealed at 600 °C for 10 min. It was found that the ratio of antiphase to main phase crystal increased after annealing, in addition to increased surface roughness as determined by atomic force microscopy (AFM). The authors theorized that this result occurred in part because the APBs were grown in along {111} type orientations. Annealing the sample caused APBs to reconfigure along {110} planes that are more energetically stable [92]. The enhanced migration of atoms in an APB near the surface of the film during this volumetric redistribution would cause pits to form and make the surface very rough. This theory contradicts the hypothesis that the equilibrium state for a film with APBs should be APB-free. If APBs reconfigured along {110} planes during annealing then they would never annihilate. More work is needed to understand the effect of annealing on APBs in GaAs and other III-V compounds.

1.7 Summary and Statement of Research Goals

While the epitaxy of GaAs on Si has been studied for several decades, there are still significant gaps in literature regarding the characteristics of APB defects. Many early studies took advantage of methods to suppress antiphase disorder that are not practical for industrial integration. The use of GaAs and other III-V compounds in future electronic devices will require a more complete understanding of factors influencing the nucleation and energetic stability of APBs in GaAs-on-Si. This work will examine these characteristics of APBs at different stages of processing for GaAs-on-Si films. First, the quantitative relationship between substrate surface contamination and nucleated APB density will be developed. Second, the influence of MOCVD growth temperature on the annihilation rate of APBs and the associated activation energy will be investigated. Third, the effect of post-growth annealing on grown-in APBs and the associated

39

activation energy for APB diffusion will be studied. Finally, the effect of in situ doping on

grown-in APB density will be examined.

Table 1-1. GaAs APB formation energy on different habit planes as determined by DFT calculations. Values from Rubel and Baranovskii [92].

GaAs APB Plane	Formation Energy (meV/Å^2)
{110}	28
{111}	43
{112}	39
{113}	39
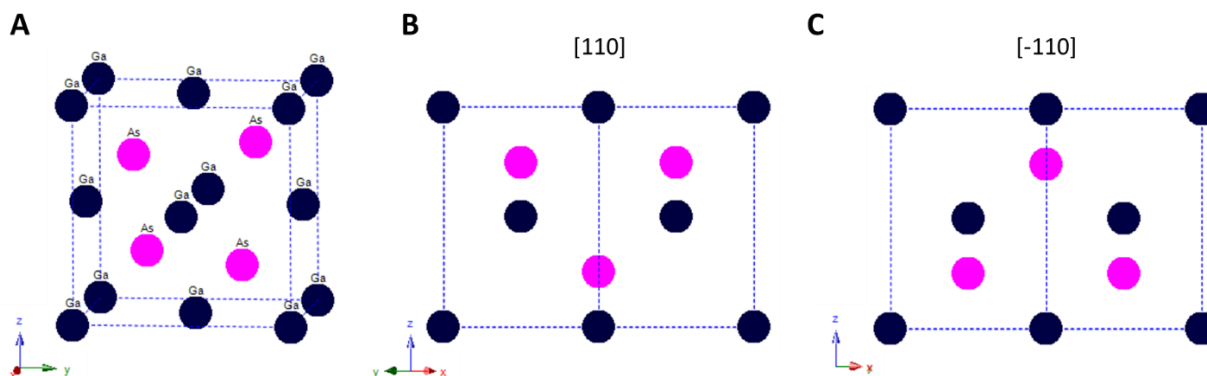
Figure 1-1. GaAs unit cell along various viewing directions. A) Offset view showing atom positions. B) Viewed along the [110] projection showing the Ga-As dumbbell structure. C) Viewed along the [-110] projection showing the reversal of Ga-As dumbbell polarity when the lattice is rotated by 90°. Images made with CrystalMaker® software. CrystalMaker Software Ltd, Oxford, England (www.crystalmaker.com).
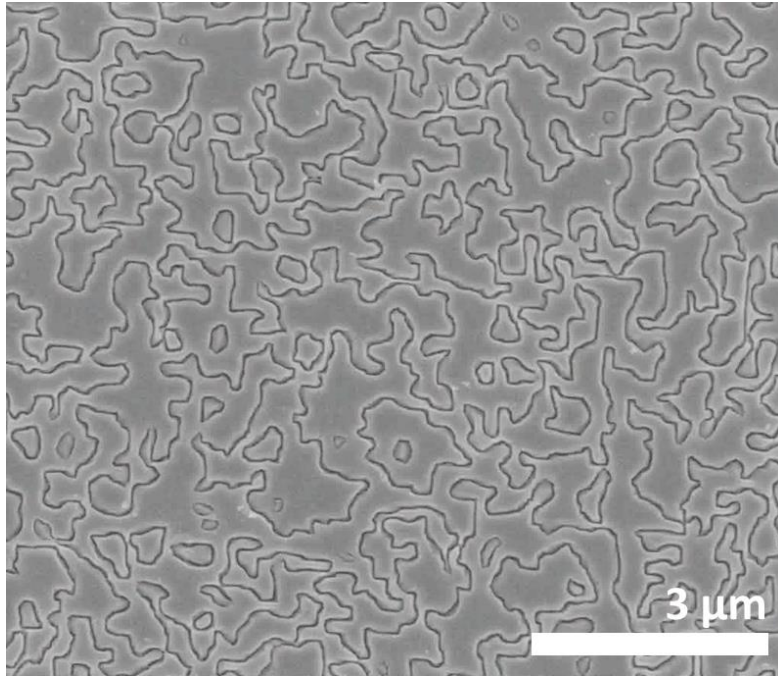
Figure 1-2. Plan view SEM image of GaAs layer grown on Si(001) with high APB density. APBs are visible as linear features of dark contrast.
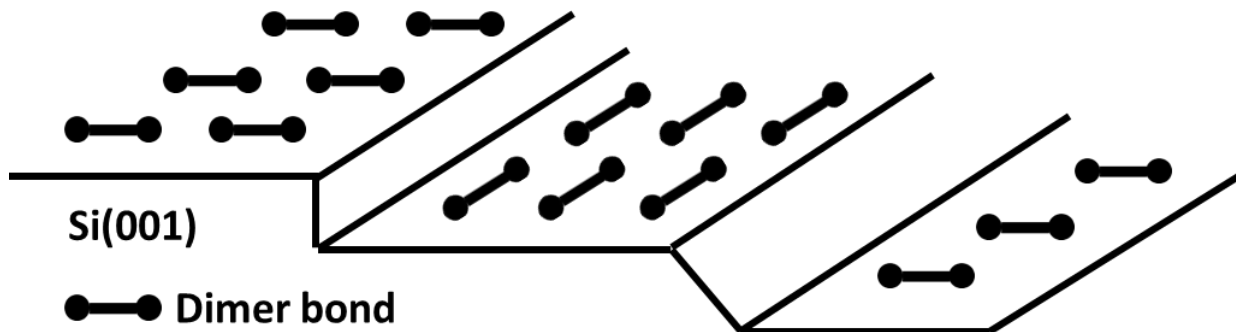
Figure 1-3. Schematic drawing of dimer bonds on the Si(001) surface showing the rotation of dimers by 90° across single-steps.
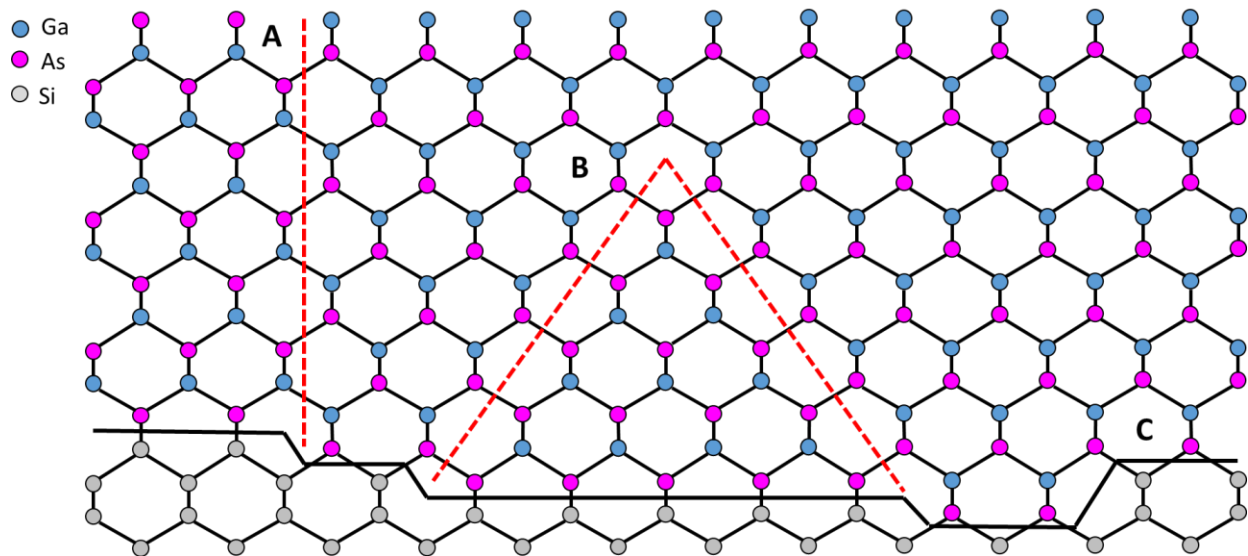
Figure 1-4. <110> projection of an epitaxial GaAs layer on a Si(001) substrate with APBs. A) An APB is nucleated at a single-step and propagates along a {110} plane. B) APBs may also nucleate along inclined planes, e.g. {111}, and self-annihilate. C) Double-steps suppress the formation of APBs by resetting the atomic ordering of the epitaxial layer.
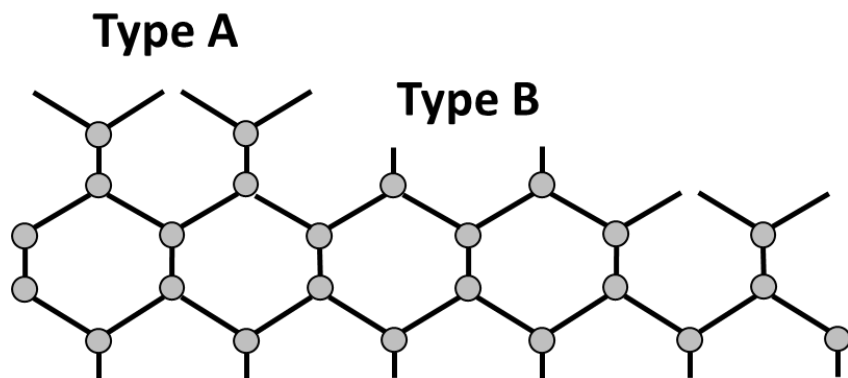
Figure 1-5. <110> projection of a Si(001) surface showing the two types of terraces that will exist. Type A terraces have dangling bonds perpendicular to the step edge and Type B terraces have dangling bonds parallel to the step edge.
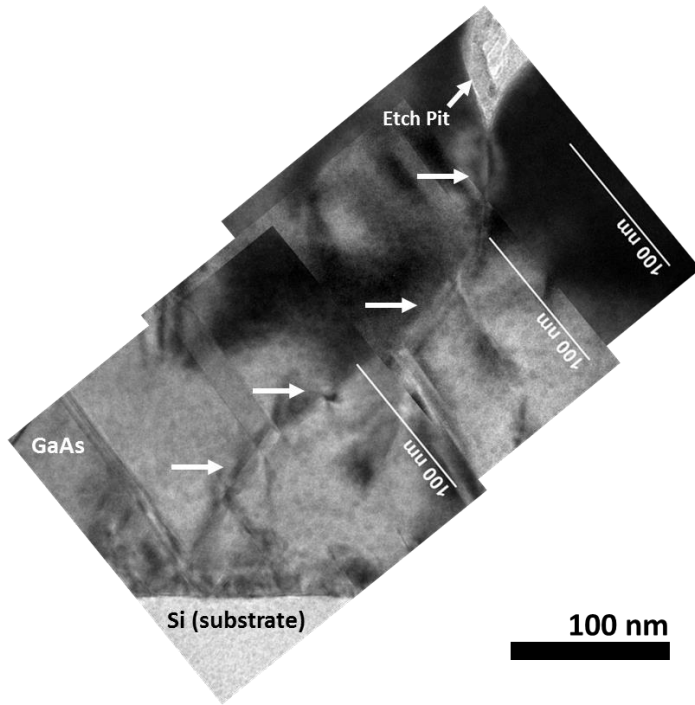
Figure 1-6. Composite XTEM image showing the meandering path of an APB (marked by arrows) through a GaAs-on-Si(001) layer.
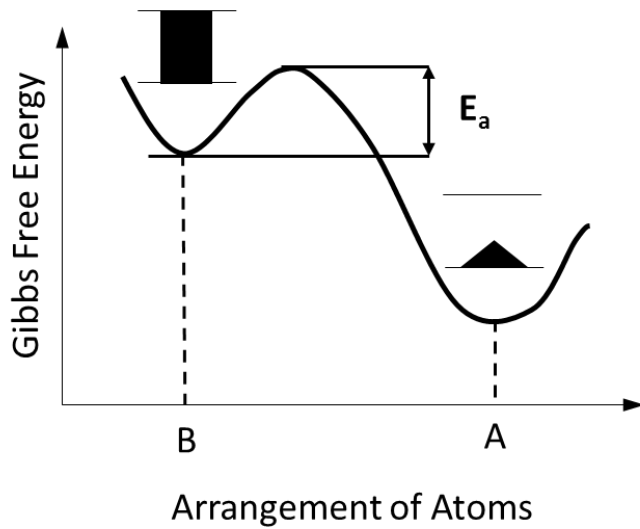
Figure 1-7. Arbitrary Gibbs free energy diagram for a GaAs-on-Si system with two different states: B, a GaAs layer with APBs propagating vertically through the film, and A, a GaAs layer with self-annihilated APBs suppressed in the film. Arrangement A should be thermodynamically favored but the transition between the two states may be kinetically limited by an energy barrier, E_a.

CHAPTER 2
EXPERIMENTAL METHODS

In any study on APBs in III-V films grown on Si, it is critical to know the complete background of sample processing conditions as these can have a large impact on the severity of antiphase disorder. An overview of the methods used to prepare, grow, and process all samples for the experiments in this work will be discussed in the following sections. Details that are pertinent for specific experiments will be given in the respective chapters. The latter portion of this chapter is dedicated to sample characterization methods with an emphasis on how certain techniques can be used to detect and quantify antiphase disorder.

2.1 Materials Processing

2.1.1 Substrate Preparation

All substrates used in this work were commercially available double side polished 300 mm Si(001) wafers with no intentional off-cut. There is typically some degree of unintentional wafer misorientation due to uncertainties in processing from the boule of up to 0.5° [117].

Prior to film growth, the native oxide and other contaminants on the Si substrates were removed in a novel process developed by Applied Materials known as a Siconi^{TM} clean. The details of this cleaning procedure have been discussed elsewhere [118]. Briefly, the substrates are placed under vacuum and transferred to a dedicated cleaning chamber where they are exposed to a dry NF_3/NH_3 based plasma. The plasma species have high selectivity for the Si native oxide and forms reaction products that are easily sublimated at temperatures near 100 °C. This Siconi^{TM} cleaning process has several advantages over conventional substrate cleaning methods. First, it is a low temperature

process. Second, the substrates are transferred from the cleaning chamber to the growth chamber under vacuum. The vacuum transfer prevents any oxide reformation from exposure to the ambient. This exposure is unavoidable if dipping in HF is used to remove the native oxide.

After transferring the substrates to the growth chamber, a high temperature bake is performed under hydrogen gas flow near 900 °C. This pre-growth bake helps to promote the formation of double-steps on the Si surface. The combination of the substrate clean and pre-growth bake is critical for reducing defect densities in the epitaxial GaAs films. The effect of residual surface contamination after Siconi™ cleaning on APB density will be discussed in Chapter 3.

2.1.2 GaAs Film Growth

GaAs film growth in this work was performed in an Applied Materials III-V MOCVD system. A simplified schematic of a typical MOCVD growth system is shown in Figure 2-1. In the MOCVD growth process, the substrate is loaded into the chamber on a rotating chuck or susceptor. The temperature of the susceptor, and thereby the temperature of the substrate, is controlled using heating elements such as lamp arrays or filaments. The metal-organic precursors are contained outside of the growth chamber. Hydrogen gas is flowed through the containers to carry vaporized precursor molecules into the growth chamber. The flow rate of the individual precursors can be easily modulated. The precursor molecules contained in the hydrogen gas flow towards the heated substrate where they react and decompose forming solid phase material with the metallic element and gaseous organic by-products. The by-products are then pumped out of the chamber.

The key parameters for the growth of GaAs on Si via MOCVD are the growth temperature, i.e. the substrate temperature, and the ratio of the partial pressures of the group V and group III precursor gases, i.e. the V/III ratio. The growth temperature must be sufficient to decompose the precursor molecules and also can affect the growth rate. The V/III ratio must be greater than unity in order to form purely solid phase GaAs due to the relatively high volatility of group V elements [30].

The baseline recipe for GaAs film growth in this work has been developed and optimized by Applied Materials. The precursors used for Ga and As are trimethylgallium (TMGa) and tertbutylarsine (TBAs), respectively. The V/III ratio is approximately an order of magnitude greater than unity. The chamber pressure is maintained in the typical reduced pressure MOCVD processing range of 10-100 Torr [30]. A standard two-step growth process is used, unless otherwise stated, with growth temperatures in the range of 500 to 700 °C.

2.1.3 Thermal Processing

The thermal processing of GaAs can be very challenging and it is one of the reasons as to why GaAs never overtook Si as the primary material of the semiconductor industry in the 1980s. Thermal treatments are essential in semiconductor processing for the diffusion and activation of dopant impurities. The temperatures required can easily reach 850 °C to over 1000 °C for anneal times up to 60 min [119]. These temperatures pose no issue for Si which is only limited by its melting point of ~1400 °C. However, for a binary semiconductor such as GaAs, the surfaces are prone to dissociation before the actual melting point of the solid. GaAs is known to suffer significant surface degradation at temperatures above 650 °C [120]. At this point, known as the congruent evaporation point [121], As leaves the surface preferentially over Ga leaving behind a non-

stoichiometric surface. Ga droplets can then form which etch away underlying material and roughen the surface [120]. Several strategies have been developed to protect the GaAs surface during thermal treatments and to suppress the loss of As.

2.1.3.1 Prevention of surface degradation

One of the methods to prevent GaAs surface degradation during annealing is to provide an overpressure of As in the annealing environment. The overpressure is typically accomplished by flowing an As-based gas or by heating liquid or solid source As in a separate chamber and flowing the vapor into the compartment containing the GaAs sample [120]. The higher partial pressure of As at the GaAs surface reduces the tendency of As to evaporate, thus increasing the upper temperature limit of the anneals. This technique is not popular due to the inherent safety concerns involved with handling toxic As-based gases and other sources.

An alternative means of providing a local As overpressure at the GaAs surface is to physically place another piece of material in contact with the GaAs sample. This technique is called proximity capping. The cap material is typically another piece of GaAs, but Si may also be used. The presence of the proximity cap suppresses the outdiffusion of As to atmosphere from between the two surfaces, i.e. any evaporated As is essentially trapped near the GaAs surface. Therefore, further degradation of the surface is prevented. The proximity cap method can be effective for temperatures up to about 900 °C [120].

Instead of using a proximity cap, it is also possible to protect the GaAs surface by depositing a thin dielectric film encapsulant. Early encapsulating films used were Si_3N_4, SiO_2, and AlN [120] since these materials can be easily deposited at relatively low temperatures, form good interfaces, and are stable at elevated anneal temperatures. As

evaporation is suppressed for processing temperatures of up to 900 °C for 10 s [122]. More recently, Al_2O_3 films grown by atomic layer deposition (ALD) have been used as a successful encapsulant material for InGaAs [100, 123]. The interest in ALD Al_2O_3 films was spurred by the need for an effective gate dielectric material for future MOSFET devices based on III-V arsenides, e.g. GaAs and InGaAs. It has been demonstrated that the process of depositing Al_2O_3 on GaAs via ALD has the secondary effect of cleaning the native oxide present on the GaAs surface [124, 125].

For the anneals performed in this work, the majority of GaAs-on-Si samples were capped with Al_2O_3 films deposited by a Cambridge Nano Fiji 200 ALD system in the Research Service Centers (formerly Nanoscale Research Facility) cleanroom at the University of Florida. Films thicknesses varied between 15 and 30 nm. The precursors for Al and O were trimethylaluminum (TMAl) and water, respectively. The O source was changed to an oxygen plasma for select recipes which will be discussed in Chapter 5. The deposition temperature was between 200 °C and 250 °C. Additional annealed GaAs-on-Si samples were proximity capped with either a polished semi-insulating GaAs wafer or another piece of GaAs-on-Si with the two GaAs films in contact.

2.1.3.2 Furnace anneals

Long term anneals (≥ 4 min) in this study were performed in a standard 2.5" quartz tube furnace. Due to the long ramp rate that is characteristic of tube furnaces with heating coils, shorter anneals are not reliable. Samples were loaded surface of interest down on a Si carrier wafer in a quartz boat. The temperature of the furnace was controlled using an external digital controller and checked with a thermocouple prior to inserting the boat with the samples. Care was taken to ensure that the thermocouple

measured the temperature of the furnace at the same location along the tube as where the samples would sit. During the anneals, inert Ar gas was flowed through the tube at about 3 L/min.

2.1.3.3 Rapid thermal anneals

Short term anneals (≤ 4 min) in this study were performed in an AG Associates HeatPulse 4100 rapid thermal anneal (RTA) system. A RTA system uses high intensity lamps to heat samples inside of a quartz chamber. The quartz is transparent to the radiation emitted by the lamps which allows for much faster and direct heating of the samples [126]. Samples were placed surface of interest down on a Si carrier wafer on top of a quartz tray inside the anneal chamber. The chamber was filled with inert Ar gas during the anneals. The temperature was monitored by a thermocouple placed between the Si carrier wafer with the samples and an additional Si wafer underneath. The temperature ramp rate used for the RTA recipes in this work was approximately 25 °C/s.

2.2 Sample Characterization

2.2.1 Transmission Electron Microscopy

TEM is a useful method for microstructural characterization of semiconductor materials down to the atomic scale. The ability analyze features at this scale has become increasingly more important with the ever decreasing physical length scales of transistors, now approaching the sub-10 nm regime. TEM operation is relatively complex so a brief background on the subject is necessary before beginning the discussion of APB characterization.

In TEM, an electron beam is generated and accelerated towards a specimen. The operating voltage is typically between 100 and 300 kV. Along the way, the beam focused by a series of magnetic lenses and also passes through a number of different

apertures. The specimen sits near the middle of the TEM column with lenses and apertures above and below it. The electrons in the beam are scattered by the specimen as they pass through it before they finally reach a detector. This interaction can be used to develop images of the specimen since the interaction depends on the specimen structure. The exact information that can be gained from TEM imaging depends on numerous factors including the mode of TEM operation (i.e. the setup of the beam), the orientation of the specimen, and the crystalline nature of the specimen. For the purposes of this work, only background on TEM imaging of single crystal materials is relevant.

The interaction of the electron beam with a single crystal specimen generates a characteristic diffraction pattern with spots from specific families of crystal planes. The scattering of the electron beam by these planes is determined by Bragg's Law:

$$\lambda = 2dsin\theta \tag{2-1}$$

where λ is the electron wavelength, d is the crystal plane spacing for a set of planes, and θ is the angle of incidence of the electron beam on the sample. The diffraction pattern depends on the orientation and crystal structure of the specimen. For most of the TEM in this work, specimens are imaged in cross-section along <110> type crystallographic directions. Figure 2-2 shows the diffraction pattern that is expected from a GaAs-on-Si sample along a [110] zone axis. Note that GaAs and Si will have similar diffraction patterns due to equivalent positioning of atoms in their crystal structures, but the spacing of the diffraction spots, or Bragg spots, will differ due to the dissimilar values of d for their respective sets of crystal planes. The 002 type Bragg spots are forbidden reflections for Si because every atom in its crystal structure is identical which

51

cancels out the intensity. These spots will appear, although weakly, for GaAs as superlattice reflections because it has two distinct Ga and As based FCC sublattices that will scatter the electron beam differently [127]. The 002 Bragg spots in turn can be used to detect antiphase disorder because these planes are sensitive to the non-equivalent ordering of Ga and As atoms on the sublattices across an APB, as was discussed in Chapter 1.

The primary modes of TEM operation are bright field (BF), dark field (DF), and high resolution (HR). In BF imaging, the objective aperture of the TEM is centered on the direct spot (Figure 2-2) so that it is the only contributing beam. The factors affecting contrast in BF imaging are mass-thickness of the specimen and diffraction of the beam. Regions of the sample that strongly diffract the electron beam will appear dark and regions in which the beam passes through relatively unperturbed will appear bright. Thicker samples or samples with atoms of higher Z will also appear darker due to greater scattering of the electron beam. DF is performed by using one of the Bragg spots for imaging instead of the direct spot. The sample is usually tilted such that the scattering intensity for the desired Bragg spot is enhanced, thereby leading to better contrast. The contrast is opposite that of BF, with strongly diffracting areas of the sample now appearing bright. This aspect of DF imaging makes it useful for the analysis of crystal defects. HRTEM imaging utilizes phase contrast, i.e. the difference in phase of the electrons in the beam after they interact with the sample, in addition to diffraction and mass-thickness contrast. The objective aperture must be placed around the direct spot and multiple Bragg spots so that they all simultaneously contribute to imaging. Lattice fringes corresponding to atomic planes in the sample become visible in HRTEM

images because the difference in phase between electrons depends on whether they travel directly down columns of atoms or in between them [128]. The variation in intensity is periodic with a spacing that corresponds to the atomic plane spacing. High angle annular DF scanning TEM (HAADF-STEM) is a special mode of TEM operation that can provide atomic resolution images with excellent Z contrast. Therefore, for III-V compounds with differing atoms, it is possible to directly observe and discern the group III and group V atoms and their specific sublattice allocation.

2.2.1.1 Identification of antiphase boundaries

DF imaging using the 002 superlattice reflection has previously been used to confirm the presence of APBs in GaAs and other III-V compounds [11, 79, 82, 89, 113]. Due to the reversal of the Ga-As dumbbells across an APB, the g_{002} reflection for the crystal on one side of the APB is equivalent to the $g_{00\text{-}2}$ reflection for the crystal on the other side [129]. Therefore, when performing DF imaging using only one of these spots, the contrast from diffraction intensity should also be reversed. That is, the region inside of an antiphase domain should appear bright relative to the main phase crystal, or vice versa. This contrast reversal can be seen in Figure 2-3 for a <110> DF XTEM image of a GaAs film grown on Si made using the g_{002} reflection. The contrast can be enhanced by tilting the sample to also excite g_{115} and g_{117} type spots along with the g_{002} type spot [113]. For a [1-10] cross-section, the g_{115} and $g_{11\text{-}7}$ spots should be excited. This tilting increases the diffraction intensity of the g_{002} type spots used for imaging.

APBs can also be identified in high resolution TEM images (either HRTEM or HAADF-STEM) by Fourier filtering the images using the 002 spots [130, 131]. The filtered images show a series of lines corresponding to the (002) planes in the crystal. The (002) planes are misaligned by ½ plane spacing across an APB. Thus, at the

location of an APB in the filtered image, the lines are disrupted and misaligned by the same proportion. Fourier filtering of TEM images in this work was accomplished using ImageJ software [132]. Figure 2-4 shows the procedure for Fourier filtering a HAADF-STEM image of an APB in a GaAs-on-Si sample (A). First, a fast Fourier transform (FFT) is taken of the original TEM image (B). Second, a mask is created encircling only the 002 spots and the direct spot (C). Finally, the inverse FFT of this masked FFT is taken, which gives the Fourier filtered image (D). The misalignment of the (002) planes at the location of the APB is clearly visible. The procedure for processing HRTEM images and identifying APBs is identical as long as the HRTEM image is of sufficient magnification and resolution for lattice imaging.

2.2.1.2 Preparation of samples

Samples for XTEM imaging in this study were prepared using a Focused Ion Beam (FIB) system. The primary tools used were FEI Strata DB235 and FEI Helios NanoLab 600 dual beam FIB/SEMs located at the University of Florida Research Service Centers. The recipe for sample preparation is similar to that published by Schaffer et al. [133]. Briefly, Ga^+ ions are used to mill out a thin lamella (~10 μm long x 5 μm tall x 1 μm thick). The lamella is attached to an Omniprobe micromanipulator and separated from the rest of the sample. The lamella is then attached to a specialized Cu Omniprobe TEM grid where it is thinned to a final thickness of ~100 nm. It is important to protect the sample surface during milling from the ion beam to prevent amorphization. Initially, a carbon rod evaporator system was used to coat samples with a thin C film. However, based on work by Park et al. [134], it was determined that coating the samples with Sharpie permanent marker ink was sufficient and this method was

subsequently used. Further surface protection is afforded by depositing a 1 μm thick Pt

bar on top of the C layer over the area of interest in the FIB system.

2.2.2 Chemical Etching and Scanning Electron Microscopy

Chemical etching by wet or dry methods is a widely used tool in semiconductor

processing. The diversity of materials present in the fabrication of any integrated circuit

device require an equally diverse array of chemistries that will selectively etch away

material with high spatial and temporal precision. These same etching chemistries can

also be effective in the identification and quantification of defects. The defects present in

a given material, such as APBs in a GaAs-on-Si film, are not visible to the naked eye

and may not even be visible in the as-grown material under a high-powered microscope

amongst the typical surface morphology. Selectively etching these defects would allow

for a quick and accurate count of the defect densities.

Wet chemical etching, in combination with a SEM for imaging, is used for the

quantification of APB density in this work. Wet chemistries for etching are binary, having

one component for oxidizing some material in a sample and a second component for

reducing and removing the newly oxidized material. The sequence repeats itself until

the etch process is stopped, typically by immersing the sample in water to neutralize

and dilute the etchant. SEM is a good tool for imaging defects with the scale and

distribution of APBs since it can quickly take several images over a large area (> 100

μm^2) with excellent spatial resolution (< 1 nm). Selectively etching APBs would cause

etch pits to form along their entire length. Thus, the APBs will show up in secondary

electron mode SEM images with dark contrast relative to the surrounding material.

Fewer secondary electrons are able to escape from the material inside the etch pits and

reach the detector, thereby giving lower intensity of signal in those areas. The SEM used for imaging in this work was a FEI Nova NanoSEM 430 at the University of Florida Research Service Centers operating at 5 kV.

An etchant that is selective for APBs in GaAs has been reported on previously [11, 115, 135]. The chemistry involves HNO_3 as the oxidizing agent, HF as the reducing agent, and water as the diluting agent for control of etch rate. In this study, a ratio of 20:1:7 of of HF(49%):HNO_3(69%):H_2O by volume was used. This etchant will henceforth be referred to as the HF/HNO_3 etching solution. A typical etch time of 10 s at room temperature was found to be effective in developing strong contrast of APBs in SEM (see Figure 1-3 for a representative image). The HF/HNO_3 solution is commonly used in semiconductor processing for the etching of Si. It is likely selective for APBs in GaAs due to the high associated energy of APBs. However, a more accurate description would be to say that the etchant is more selective for APBs over other defects and the GaAs film over the time scale of the etch. Some thickness of the overall GaAs film is still removed but the APBs are etched at a faster rate. Figure 2-5 shows BF XTEM images of a GaAs film grown on Si as-grown (A) and then after etching for 10 s in the HF/HNO_3 solution (B). The etch pits that form at the location of APBs which give rise to the strong contrast of APBs in SEM are clearly visible in Figure 2-5B. The as-grown GaAs film thickness is about 450 nm. After etching, about 50 nm of GaAs is removed and the etch pits extend a further 100-150 nm into the film. Thus, the etch rate of the APBs (~15-20 nm/s) is three to four times that of the overall GaAs film (~5 nm/s).

The selectivity of the HF/HNO_3 solution for APBs over other crystallographic defects was also confirmed with XTEM. Figure 2-6 shows a HRTEM image of a

developed etch pit in a GaAs film on Si. At the bottom point of the etch pit, an APB can be observed extending down into the film. A stacking fault can be seen intersecting the sidewall of the etch pit. The lack of an additional smaller pit or depression at the site of the stacking fault intersection with the etch pit demonstrates that it is not attacked preferentially by the HF/HNO3 solution over the APB. Therefore, the etched features visible in SEM can unambiguously be identified as APBs.

The APB density in samples etched with the HF/HNO$_3$ solution is quantified by tracing the line length of APBs in a given plan view SEM image using ImageJ software [132]. Figure 2-7 shows an example of the tracing procedure for APBs in a plan view SEM image. APB features are traced by hand using the freehand line tool in ImageJ. The total line length counted is then divided by the area of the image. Therefore the units for APB density are defined as μm^{-1}. In order to obtain a representative count of the APB density for a sample, multiple images are taken in different areas of the sample surface. A total area of at least 500-1000 μm^2 is counted, depending on the relative APB density in the sample. The APB density reported for a sample is the average of the APB densities in each SEM image and the error is the standard deviation.

While having an APB-selective etchant is a helpful tool for identifying APBs, an isotropic non-selective etch is useful if depth profiling of APB density is desired. There are several reported etchants for GaAs [136]. A mixture of H_3PO_4 and H_2O_2 was previously used for the depth profiling of APB density in GaAs films [11] and was selected for the same purpose in this study. The composition used for this work was $CH_3OH:H_3PO_4(85\%):H_2O_2(30\%)$ in a ratio of 10:1:1 by volume. This etchant will henceforth be referred to as the H_3PO_4/H_2O_2 solution. The etch rate of the H_3PO_4/H_2O_2

solution at room temperature for GaAs was determined to be ~120-130 nm/min. The

non-selectively of the etchant was also confirmed. Figure 2-8 shows a BF XTEM image

of a GaAs-on-Si sample after the removal of ~380 nm of GaAs. The surface of the film

is still relatively smooth and the defects in the film are not preferentially attacked. The

HF/HNO$_3$ solution can then be applied to determine the APB density at a given depth in

the film.

2.2.3 X-Ray Diffraction

X-ray diffraction (XRD) is a method that can help to determine the crystal quality

of a sample. The X-rays will interact with the sample and constructively interfere when

the Bragg condition is met for a set of atomic planes (Equation 2-1). This constructive

interference will give a peak of intense signal for a given Bragg angle, or reflection. In

theory, for an ideal crystal, the signal for these satisfied reflections should be linear.

However, scattering from perturbations in the crystal lattice, such as defects that induce

local strain, lead to broadening of the peak.

Specific lattice plane reflections can be analyzed that are sensitive to the

presence of crystalline defects. For epitaxial GaAs grown on Si, the fundamental (004)

reflection can be used to determine the threading dislocation density in the films that

arises from the lattice mismatch [80, 137, 138]. The threading dislocation density is

related to the full width at half maximum (FWHM) of the (004) peak by [137]:

$$D = \frac{\beta^2}{9b^2}$$

(2-2)

where D is the threading dislocation density, β is the FWHM in radians, and b is length

of the Burgers vector for the dislocation. For classic 60° dislocations, the value of b is

√2/a, where a is the GaAs lattice constant.

XRD can also be used to detect the presence of antiphase disorder in a crystal [13, 116, 139]. For GaAs and other III-V films grown on Si, the superlattice (002) reflection is sensitive to the antiphase disorder in XRD for the same reasons as in TEM. The presence of antiphase domains in the film with inequivalent atomic ordering on (002) planes leads to broadening of the (002) peak. The peak broadening more specifically is related to the average separation between APBs, i.e. the average domain size. For samples with less separation between APBs, i.e. higher APB density, the peak broadening is more severe. The average domain size was determined for GaP-on-Si samples with additional processing of the XRD data [116, 139]. The downside to XRD is that it does not provide direct imaging of APBs. It should also be noted that there is an upper limit on antiphase domain size that can be resolved by XRD which is around 300 to 500 nm [13, 116], depending on the XRD system used. Therefore, for comparing antiphase disorder between different sets of samples, selective etching and SEM is a more reliable method of quantifying APB density.

2.2.4 Ellipsometry

Spectroscopic ellipsometry can be an effective method for determining the thickness of a thin film. A multiple-wavelength polarized light source is set at an angle to the sample such that the light reflecting off the film reaches a detector. The detector measures changes in the amplitude and phase of the light as a function of the wavelength. Light reflecting off of the sample surface and light traveling through the film can have a phase difference and interfere, thereby affecting these changes [140]. Any light absorption by the layer will also affect this interference for a given wavelength of incident light. A model is fit to the data, assuming a layer composition with specified optical properties, to extract the film thickness. Ellipsometry can be used to measure

59

film thicknesses from the sub-nm level up to approximately a micron. XTEM can also be used to measure layer thicknesses, but ellipsometry is advantageous in that it is a non-destructive process and measurement of several samples can be completed in a relatively short period of time. Ellipsometry is used in this study as the primary method to measure thicknesses of GaAs films after the non-selective H_3PO_4/H_2O_2 solution etch. The ellipsometer used for measurements was a J.A. Woollam M88 at the University of Florida Research Service Centers. The accuracy of models for fitting GaAs film thicknesses was confirmed with selected XTEM samples.

2.2.5 Secondary Ion Mass Spectrometry

Secondary ion mass spectrometry (SIMS) is used to determine the chemical composition of a sample with depth-sensitivity. The sample is sputtered from the surface using an ion beam, typically Cs^+. The ejected secondary ions are accelerated towards and analyzed by a mass spectrometer. The spectrometer separates the ions by their mass-to-charge ratio to determine a number of counts for an element. Comparison to known standards allows for conversion to a more quantitative concentration value. By knowing the sputtering time and measuring the depth of the sputtered crater, the concentration of a given element can be tracked as a function of its depth in the sample. SIMS can detect atomic concentrations on the order of 10^{15} cm^{-3} or lower which makes it ideal for analyzing dopant concentrations in semiconductor thin films. SIMS will be used in this study when necessary to determine the concentrations of impurity atoms, dopants or otherwise, at the GaAs/Si interface and in the GaAs film.

2.2.6 Hall Effect

Hall effect measurements are a widely use method in semiconductor research to determine the electrical properties of samples, including carrier type and concentration

and carrier mobility. Measurements are commonly made with contacts at the four corners of a square sample, known as the Van der Pauw configuration. A known current is applied across a pair of contacts in opposite corners in the presence of a magnetic field with a known strength. The Lorentz force from the magnetic field deflects the charge carriers by some amount and induces an equivalent electric field to oppose this force. The voltage associated with this induced electric field is measured at the remaining two contacts. This voltage is called the Hall voltage, V_H, and can be used to determine the sheet carrier density, N_s, by the relation:

$$N_s = \frac{IB}{q|V_H|} \tag{2-3}$$

where I is the applied current, B is the applied magnetic field strength, and q is the elementary electron charge. The sign of the Hall voltage will change depending on the carrier type, i.e. negative for electrons and positive for holes. Sheet carrier density, or sheet number, is an areal density and can be used to determine the concentration of carriers by dividing by the thickness of the film or doped layer. The carrier mobility can be calculated from the sheet number by:

$$\mu = \frac{1}{q N_s R_s} \tag{2-4}$$

where R_s is the measured sheet resistance. The measurements are repeated for all sets of contacts, and then again with the magnetic field reversed for a more accurate determination of the Hall voltage.

Hall effect measurements using the van der Pauw method are used in this study to determine carrier concentrations and mobilities in GaAs-on-Si films. Samples are 1 cm by 1 cm square with contacts made in the corners using pressed-on In metal. For

undoped GaAs, it can be difficult to make the ohmic contacts required for an accurate

Hall effect measurement [17]. Annealing is typically needed after depositing the contact

material to form a more conductive alloy at the surface [141]. For this work, a 2 min

furnace anneal in Ar ambient at 425 °C was found to be sufficient in making ohmic

contacts to nominally undoped GaAs. Highly doped GaAs samples (> 10^{18} cm^{-3} carriers)

did not require any annealing step after pressing on the In contacts.
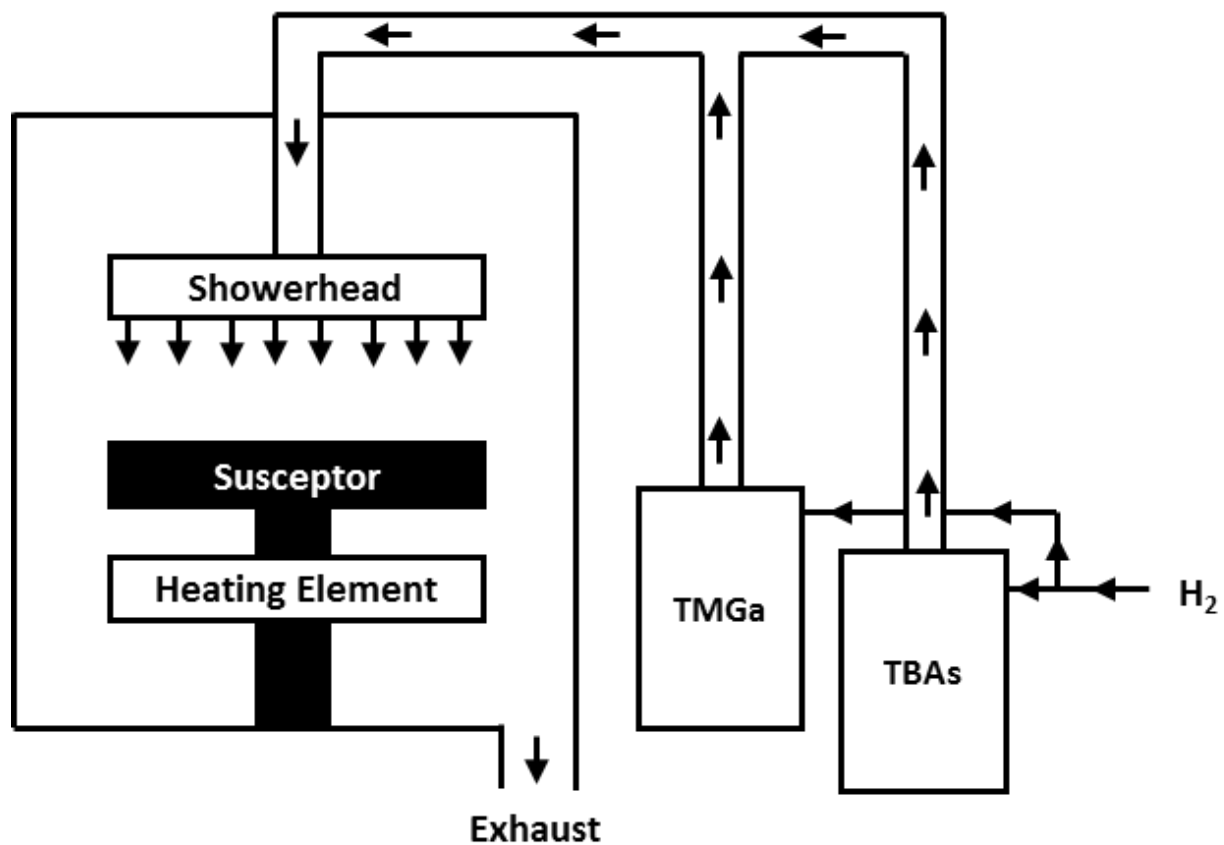
Figure 2-1. Simplified schematic drawing of MOCVD chamber. Precursors (TMGa, TBAs) are carried with hydrogen gas into the growth chamber through a showerhead to evenly distribute the precursor molecules across the wafer. The wafer sits on a heated and rotating susceptor.
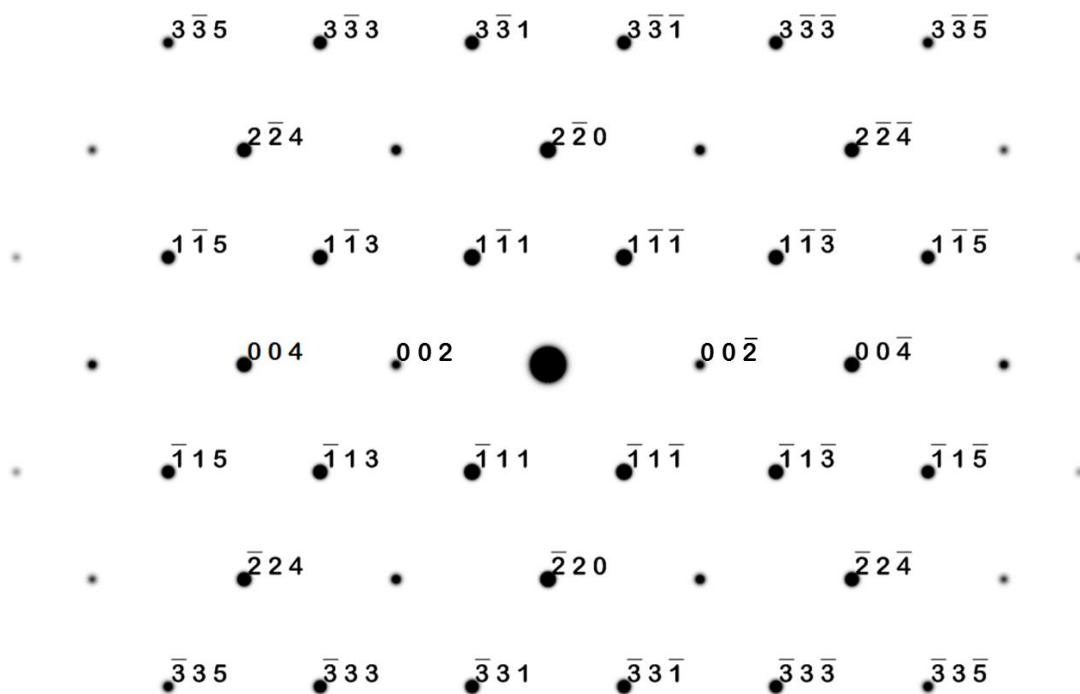
Figure 2-2. Simulated diffraction pattern for GaAs along the [110] zone axis. The g_{002} and $g_{00\text{-}2}$ spots are superlattice reflections and are sensitive to antiphase disorder in the GaAs crystal. Generated with SingleCrystal® software, CrystalMaker Software Ltd, Oxford, England (www.crystalmaker.com).
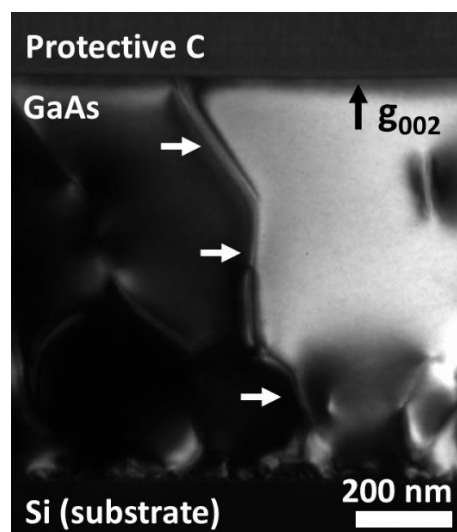
Figure 2-3. DF XTEM image of a GaAs layer on Si(001) made using the g_{002} Bragg reflection. The contrast reversal in the GaAs layer across an APB (marked by arrows) can be observed under these conditions.
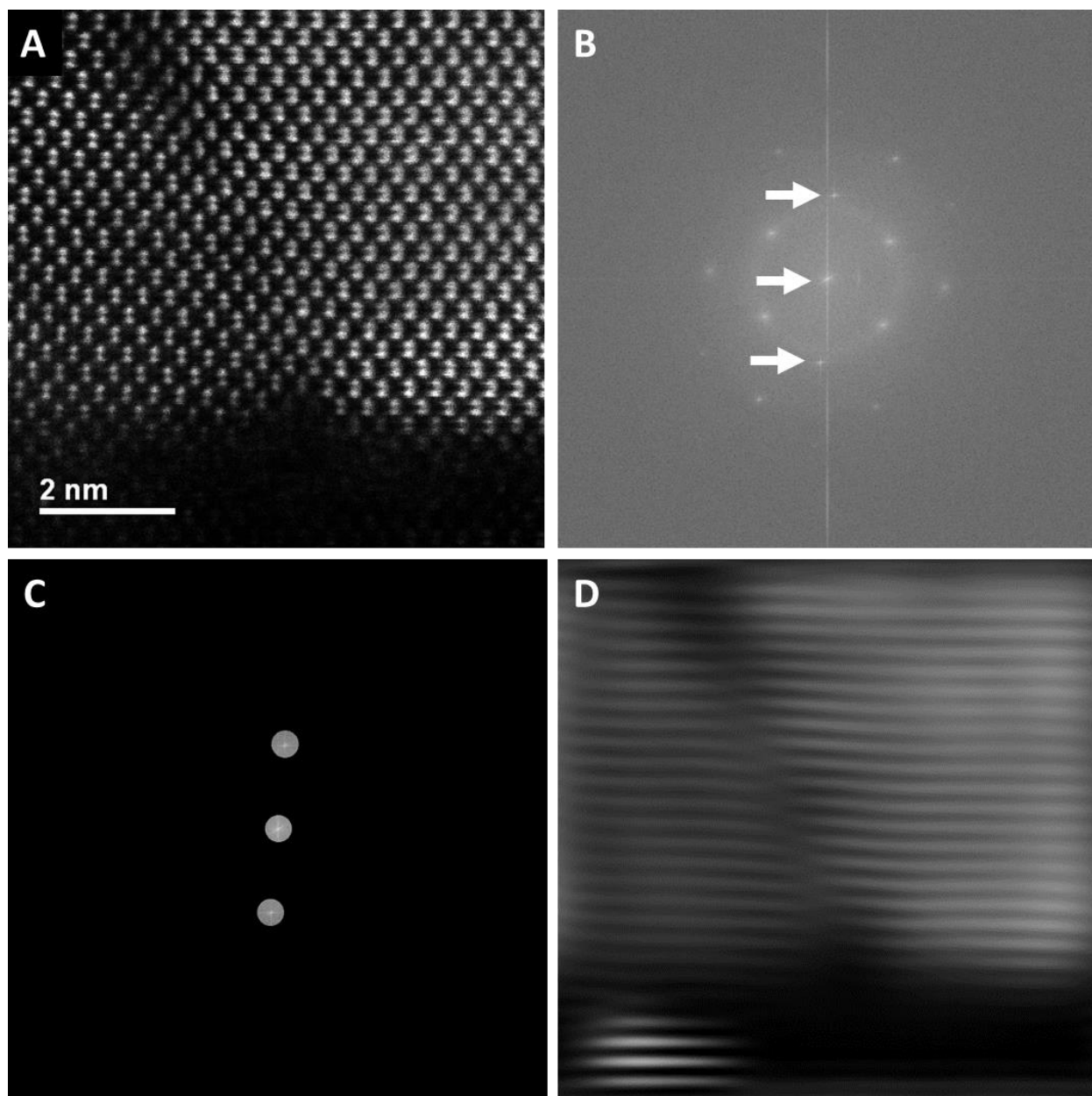
Figure 2-4. Procedure for Fourier filtering a HAADF-STEM image of a GaAs-on-Si film. A) Original HAADF-STEM image. B) FFT of the original image with 002 and direct spots marked by arrows. C) A mask is created using the 002 spots and the direct spot. D) Finally, the inverse FFT is generated giving the Fourier filtered image. The misalignment of (002) planes at the location of an APB in clearly visible.
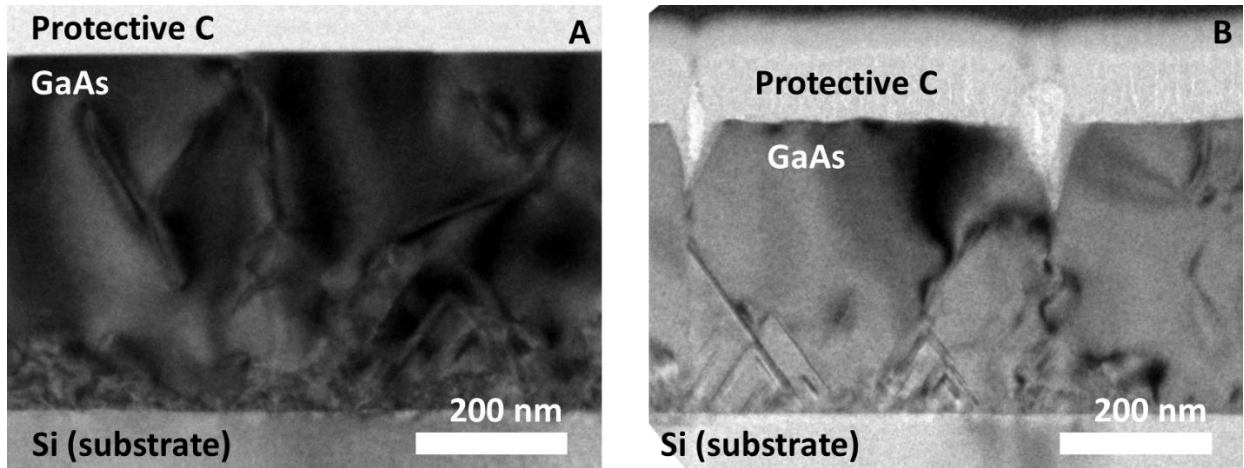
Figure 2-5. BF XTEM images of a GaAs-on-Si(001) film before and after etching with HF/HNO$_3$ solution. A) As-grown film. B) After etching for 10 s in the APB-selective HF/HNO$_3$ solution. The etch rate is enhanced at the location of APBs leading to the formation of pits. About 50 nm of GaAs is removed and the etch pits extend a further 100-150 nm into the film.
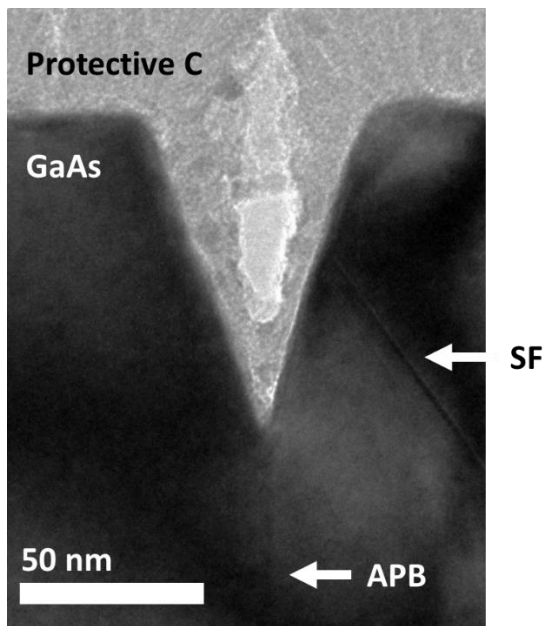
Figure 2-6. HRTEM image of a developed etch pit at the site of an APB in a GaAs-on-Si layer demonstrating the selectivity of the HF/HNO$_3$ etchant for APBs. A stacking fault (SF) can be seen intersecting the sidewall of the etch pit and is not preferentially attacked by the etchant relative to the APB.
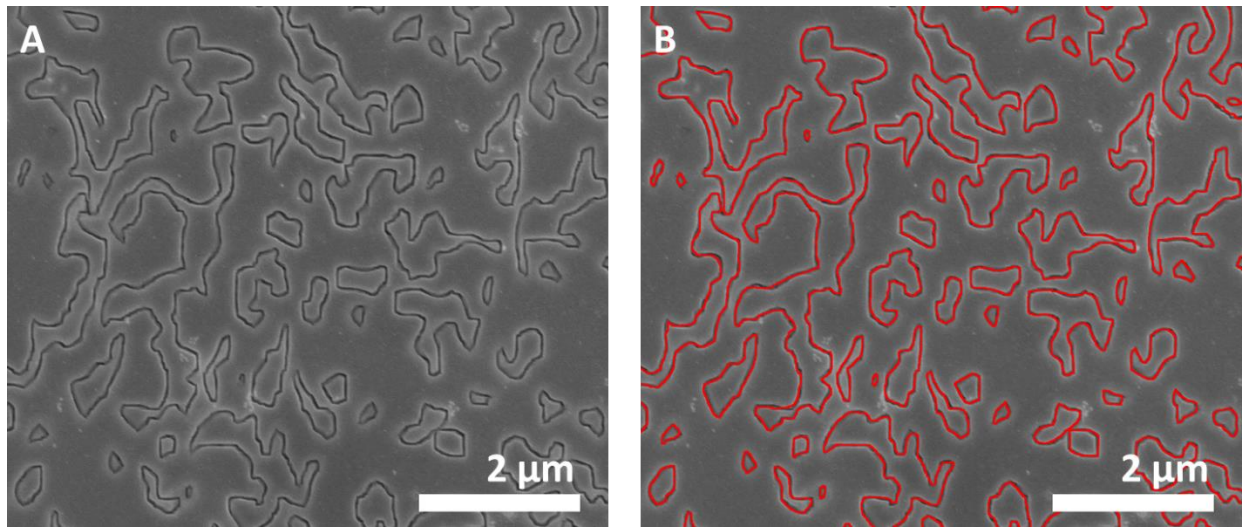
Figure 2-7. Example of tracing procedure of APBs in plan view SEM images. A) Original SEM image of GaAs-on-Si film with APBs. B) After tracing APBs using the freehand line tool in ImageJ software. The APB density is defined as the total line length of traced APBs divided by the area of the image giving units of μm^{-1}.
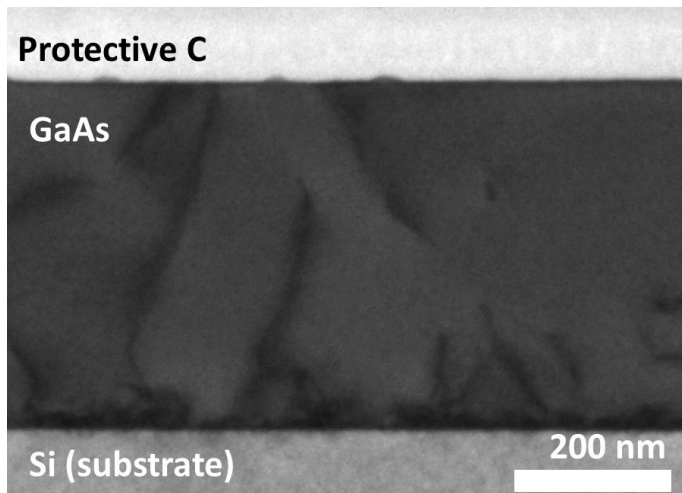
Figure 2-8. BF XTEM image of a GaAs-on-Si sample after the removal of ~380 nm of GaAs using the non-selective H_3PO_4/H_2O_2 solution. The surface of the layer is still relatively smooth and defects are not preferentially attacked.

CHAPTER 3
THE EFFECT OF INTERFACIAL CONTAMINATION

3.1 Background

The prospect of integrating III-V materials such as GaAs on Si for future

transistors and other electronic devices is hindered by a number of growth-related

defects in the epitaxy of these compounds on Si. In particular, APBs can nucleate at the

GaAs/Si interface and propagate through the film, degrading electrical and optical

properties [13]. Single-steps on the Si surface are well established to be a source of

APB nucleation. However, the role of residual contamination on the Si surface on APB

formation is not as well studied. Contamination present on substrate surfaces is known

to contribute to higher densities of stacking faults and dislocations in epitaxial layers

from disruption of the growth kinetics [13, 32, 142]. APBs have been found to be

associated with the presence of amorphous interfacial impurities through XTEM

analysis [33] leading to speculation that these impurities may also nucleate APBs in

addition to those nucleated by single-steps. The exact relationship is still unclear and

the effect of surface contamination on APB density has not been quantified.

The ideal Si surface for epitaxy should be pristine and free of native oxide or

other contaminants. In practice, it is exceedingly difficult to completely remove these

contaminants, most commonly oxygen and carbon, from the surface. The most widely

used method is to perform a dip of the Si wafer in HF to etch away the native oxide

followed by a high temperature anneal at 1000 °C in the growth chamber to desorb any

residual oxide [38, 39]. This procedure has the disadvantage of needing to expose the

wafer to ambient after dipping in HF and before transferring the wafer to the growth

chamber. The Siconi^{TM} etch process [118] is a low temperature method of removing

native oxide via a fluorinated plasma and can be performed under vacuum in a chamber attached to the growth chamber. The combination of the Siconi^{TM} clean with a pre-growth anneal near 900 °C leads to a dramatic reduction in APB density for GaAs-on-Si films compared to conventional preparation. Figure 3-1 shows plan view SEM images of the APB densities for GaAs films grown on nominally on-axis Si(001) by MOCVD with the Siconi^{TM} clean only (A) and the Siconi^{TM} clean plus a 900 °C pre-growth anneal (B). The GaAs film thickness for both samples is ~450 nm. The samples were etched with a HF/HNO$_3$ solution to selectively delineate APBs. The APB density in Figure 3-1A is comparable to the densities expected in films with conventional preparation of Si substrates with no deliberate off-cut to suppress APB nucleation [77]. The low APB density in Figure 3-1B is much more advantageous for achieving complete suppression of antiphase disorder via APB self-annihilation. It is especially notable that the low density was achieved on a Si(001) substrate with no intentional misorientation.

Despite the promising results from preparing Si substrates with the Siconi^{TM} clean and pre-growth bake, there is still a need to understand the role of substrate surface contamination on APB formation. The Siconi^{TM} process provides a useful method for controlling the relative amount of residual contamination on the Si surface. The goal of this experiment is to examine the effect of interfacial contamination on APB density in GaAs grown on Si(001) by MOCVD and to develop a quantitative relationship. The work in this chapter has been published in Barrett et al. [143].

3.2 Experimental

A 300 mm (001) oriented Si wafer with no intentional off-cut was utilized as the substrate in this study. The substrate was cleaned prior to growth using the Siconi^{TM} etch process [118]. The clean was varied across the wafer in order to affect the relative

amount of residual contamination from the wafer center to the wafer edge (Figure 3-2). Modulating the residual contamination on a single wafer ensures that specimens taken from different areas of the wafer experienced similar growth conditions. A pre-growth bake at ~900 ℃ was then performed in the growth chamber under hydrogen ambient to help promote the formation of double-steps.

An Applied Materials III-V MOCVD system was used for the growth of the GaAs film. The precursors for Ga and As were trimethylgallium (TMGa) and tertiarybutylarsine (TBAs), respectively. GaAs growth was carried out using the conventional two-step growth method for III-V epitaxy to improve crystal quality [26, 75]. The GaAs film was first grown at a low temperature of 530 °C for ~200 nm followed by a high temperature layer grown at ~610 °C for an additional ~200 nm. The total film thickness was ~450 nm. Figure 3-3 shows a schematic diagram of the GaAs film structure. The chamber was maintained at reduced pressure and the V/III ratio was in the typical process range for MOCVD.

Oxygen and carbon concentration depth profiles in the GaAs film were obtained using SIMS to confirm a variation in interfacial contamination across the wafer. Samples were selected from the wafer center to the wafer edge. The samples for SIMS were sputtered using Cs^+ ions. The depth resolution was ~1 nm. The amount of interfacial oxygen and carbon contamination for the samples was calculated by integrating the corresponding peaks at the GaAs/Si interface to obtain a dose.

The APB density in the GaAs film was also measured across the wafer. Samples were taken in sequential order from the wafer center to wafer edge. The selective $HF(49\%):HNO_3(69\%):H_2O$ (10:1:7 by volume) etchant was used to delineate APBs prior

to imaging in SEM. The samples were dipped in the HF/HNO$_3$ solution at room temperature for 10 s. Plan view SEM images were collected in various areas of the samples to obtain accurate counts of APB density. The APBs in SEM images were traced using ImageJ software [132]. The APB density is defined as the line length of APBs per unit area, giving units of μm^{-1}.

Analysis of the GaAs/Si interface and associated defects was accomplished using XTEM. Samples for XTEM were prepared using a FEI Strata DB235 dual beam FIB/SEM. HRTEM imaging of the GaAs layer and GaAs/Si interface was performed using a JEOL 2010F operating at 200 kV. Additional microscopy with annular bright field scanning transmission electron microscopy (ABF-STEM) and high-angle annular dark field scanning transmission electron microscopy (HAADF-STEM) imaging was carried out using a probe aberration-corrected JEM-ARM200cF operating at 200 kV. The resolution of STEM imaging on this instrument is ~0.78 Å. HAADF-STEM images were acquired with a probe convergence semi-angle of 11 mrad and collection angles of 76-174.6 mrad.

3.3 Results and Discussion

3.3.1 SIMS Measurements

SIMS measurements of oxygen and carbon concentrations in the GaAs film were made for samples at the center, +6 cm from the center, +8 cm from the center, +10 cm from the center, and edge of the wafer. The depth profiles were first normalized to the actual GaAs layer thickness as determined by XTEM. Figure 3-4 shows BF TEM images of the GaAs layer at the center of the wafer (A) and the edge of the wafer (B). The film thickness varies from ~455 nm at the center to ~445 nm at the edge. Film thicknesses for intermediately located samples on the wafer were then linearly

interpolated from this difference. There is also a notable difference in defect densities for the GaAs layer at the center versus the edge.

Figure 3-5A and 3-5B show the interfacial peaks for the selected SIMS samples of oxygen and carbon, respectively. There is some widening of the peaks, i.e. distortion of the true spatial distribution of oxygen and carbon near the interface, due to limitations of the SIMS depth resolution particularly from ion beam mixing. The peak oxygen concentration in Figure 3-5A at the center of the wafer is notably higher than the concentration near the middle of the wafer at +6 and +8 cm from the center. However, there is an overall trend of increasing oxygen concentration from center to edge and the peak concentration is greatest at the edge of the wafer. The interfacial carbon profiles determined by SIMS are shown in Figure 3-5B. Carbon also has a trend of increasing peak concentration from center to edge. There is a noticeable shoulder to the carbon depth profile which likely stems from incorporation of the MOCVD precursor reaction products in the GaAs layer [144]. However, there is still a distinguishable interfacial peak, as highlighted by the inset in Figure 3-5B, that likely arises from residual carbon contaminants on the Si surface prior to growth. This area will be used to determine the interfacial carbon dose. The SIMS measurements indicate that the variation in the pre-clean procedure was effective in changing the amount of residual oxygen and carbon contamination on the Si wafer surface from center to edge.

Figure 3-6 shows the interfacial carbon and oxygen doses as a function of position on the wafer. The interfacial doses are calculated by integrating the area under the respective interfacial peaks from Figure 3-5. This process helps to correct for distortion in oxygen and carbon distribution near the interface from the SIMS resolution.

Oxygen and carbon contaminants are expected to be concentrated at the GaAs/Si interface with negligible dispersion into the GaAs layer. Error bars for the interfacial doses were obtained by shifting the position of the interface ±15 nm from the depth determined by XTEM. The results of the calculated integrated doses corroborate the trend observed in Figure 3-5 of increasing amounts of oxygen and carbon interfacial contamination from center to edge of the wafer. The interfacial carbon dose is over two orders of magnitude greater than that of the interfacial oxygen dose across the wafer. The oxygen dose increases from 7.3×10^{11} atoms/cm^2 at the center to 4.0×10^{12} atoms/cm^2 at the edge, while the carbon dose increases from 1.9×10^{14} atoms/cm^2 at the center to 1.7×10^{15} atoms/cm^2 at the edge. The carbon dose at the edge corresponds to ~3 monolayers (6×10^{14} atoms/cm^2).

3.3.2 APB Density Measurements

After determining that there was a variation in residual oxygen and carbon contamination across the wafer, the APB density was also measured at corresponding locations using the selective HF/HNO$_3$ etch. Figure 3-7 shows representative plan view SEM images of the APB density in the GaAs film at the center of the wafer (A), +8 cm from the center (B), and at the edge of the wafer (C). The APB density increases from 0.14 µm^{-1} to 3.2 µm^{-1} over this distance and there is a marked increase of the average antiphase domain size from center to edge. The domains at the center of the wafer are on the order of a few hundred nanometers in diameter and the APBs demonstrate faceting along crystallographic planes. The APBs at the edge of the wafer tend to curve and extend for relatively long distances such that it becomes difficult to distinguish individual domains.

Figure 3-8 shows all of the APB density counts for samples measured in 2 cm increments from the center of the wafer to the edge. The increase in APB density corresponds well to the increase in interfacial contamination across the wafer. There is a large jump in the APB density from +6 cm from the center to +10 cm from the center of the wafer. The APB density begins to plateau at the edge, suggesting that there is a maximum value that can be reached. This maximum value likely stems from the self-annihilation of APBs once they are close enough to interact.

3.3.3 XTEM Characterization of Interface

The GaAs/Si interface and associated structural quality of the GaAs layer was examined with XTEM. Samples were prepared from the center of the wafer, +8 cm from the center, and the edge of the wafer. Distinct amorphous particles were observed at the GaAs/Si interface only for the edge sample which had the highest oxygen and carbon interfacial doses. Figure 3-9 is a HRTEM image showing the spatial distribution of these particles along the interface in an edge sample. The particles were associated with the formation of several defects including stacking faults. Examining the particles at higher magnifications demonstrated their physical relationship with defects. Figure 3-10 shows a series of HRTEM images of amorphous interfacial particles. The particles are a source of nucleation for stacking faults and twins. It is notable that in Figure 3-10D, the stacking fault nucleated by the particle is terminated ~15 nm away from the interface. This image is strikingly similar to the observation made by Liliental-Weber et al. [33] in which a stacking fault was terminated by an APB above an amorphous layer. The authors speculated that both the stacking fault and APB were nucleated by the amorphous layer. The termination of stacking faults and other defects at the location of APBs has been observed in additional studies [11, 130]. This termination likely due to

the high energy and degree of lattice disorder associated with an APB. Therefore, it is plausible to conclude that the stacking fault in Figure 3-10D is terminated by an APB. The close proximity of the APB with the interfacial particle, in turn, gives evidence for the nucleation of APBs by contaminant particles.

Further analysis of the GaAs/Si interface for a sample from the edge of the wafer was performed with STEM imaging. Figure 3-11 shows a region of the interface in ABF-STEM (A) and HAADF-STEM (B). An amorphous particle is clearly observed at the GaAs/Si interface in Figure 3-11A (indicated by the arrow). It is difficult to tell whether the Ga-As dumbbells are reversed in any region of Figure 3-11B. Even though HAADF-STEM has excellent Z contrast, Ga and As only have an atomic number difference of 3. After processing the HAADF-STEM image in Figure 3-11B via Fourier filtering with the 002 spots, the presence of an APB becomes evident (Figure 3-11C). The (002) atomic planes are disrupted by ~½ plane spacing at the location of the APB. The APB extends back towards the interface to the exact location of the amorphous particle. This observation corroborates the findings from HRTEM imaging (Figure 3-10D) indicating the direct nucleation of APBs by interfacial contaminant particles. These APBs would form in addition to those nucleated by single-steps on the Si surface and contribute to an overall greater APB density in the GaAs layer compared to samples with lower amounts of interfacial contamination, e.g. the center of the wafer in this study.

3.3.4 Discussion of Source of Particles

The chemical identity of the particles observed in XTEM, i.e. whether they are oxygen or carbon based, is still unclear. Energy dispersive spectroscopy (EDS) and electron energy loss spectroscopy (EELS) scans were inconclusive. It is possible to gain further insight by performing a basic calculation of the expected spatial distribution

of particles along the GaAs/Si interface if they were oxygen or carbon based particles (see Appendix A.1 for full calculation). First the typical particle size is measured from the XTEM observations in Figure 3-10 and found to be ~20 nm long with a height of ~2 nm. The particles are assumed to be circular and so their total volume can be calculated. A further assumption is made that if the particles are oxygen based they are SiO_2 and if they are carbon based then they are SiC. Using the known values of atomic density for SiO_2 and SiC, the number of oxygen and carbon atoms per particle can be determined. The oxygen and carbon interfacial doses for the edge sample were 4.0×10^{12} atoms/cm^2 and 1.7×10^{15} atoms/cm^2, respectively, as determined by the SIMS analysis. Thus, the areal density of particles along the interface can be found by dividing the interfacial doses of oxygen and carbon by the corresponding number of atoms per particle. Finally, the expected spacing of particles along the interface can be obtained by multiplying the particle areal density by the thickness of the lamella produced by FIB for XTEM imaging of ~50 nm. If the particles are carbon based SiC, the expected distribution is ~40 nm which is consistent with the observations from Figure 3-9. If the particles are oxygen based SiO_2, the expected spacing is ~17 μm meaning that it would be fortuitous to observe even a single interfacial particle in a given XTEM sample (observable area is typically ~10 μm or less). It appears that carbon is the only source of contamination that is present in significant enough quantity to account for the presence of the amorphous particles at the GaAs/Si interface in the edge sample.

3.3.5 Correlation or Causation?

It is now concluded that the interfacial particles associated with the formation of APBs and other defects such as stacking faults in this study are likely composed of

carbon. Figure 3-12 shows the APB density in samples from the center to edge of the wafer versus the corresponding interfacial carbon doses. There is a logarithmic correlation between APB density and interfacial carbon dose. The plateau in APB density after ~4x10^{14} atoms/cm^2 of carbon may stem from an upper limit on the total APB density in the layer from the inherent self-annihilation of neighboring APBs. Otherwise, it is plausible to assume that APB density would increase on an approximate linear trend with increasing interfacial carbon dose, i.e. the trend of APB density prior to ~4x10^{14} atoms/cm^2 of carbon. This quantitative correlation between APB density in GaAs-on-Si films and interfacial carbon underscore the importance of reducing the amounts of residual contamination on substrates prior to epitaxy. Extrapolating back to zero APB density in Figure 3-12, interfacial carbon should ideally kept below a density of ~2x10^{14} atoms/cm^2. Some amount of carbon contamination from incorporation of precursor reaction products or desorption from the chamber walls during the pre-growth bake, in addition to any residual carbon contamination after the Siconi^{TM} clean, is unavoidable. Some APBs will undoubtedly form because of single-steps on the Si surface, but lowering the amount of residual contamination allows for suppression of antiphase disorder via APB self-annihilation with minimal GaAs layer thickness.

While there is a clear quantitative correlation between APB density and interfacial contamination, in addition to qualitative association in XTEM, it cannot be definitively stated that the contaminant particles are in fact nucleating APBs. It is possible that the amorphous particles disrupt the atomic ordering of the epitaxial GaAs film in a manner similar to single-steps. However, an alternative explanation for the correlation is that the interfacial contaminant particles are associated with steps on the Si surface. Carbon is

known to preferentially agglomerate at the site of steps on a Si(001) surface [145]. It follows that if these steps with agglomerated carbon particles are single-steps, they are essentially passivated, i.e. the dangling Si bonds are satisfied. Therefore these steps would be less likely to reconstruct into double-steps during the pre-growth bake. If GaAs growth then occurs in islands on either side of this passivated single-step, an APB would form when the islands coalesce due to the rotation of the GaAs lattice. This APB would then be approximately located directly above the carbon particle leading to a structural association as observed in XTEM (Figure 3-10D and Figure 3-11). In other words, carbon contamination on a substrate may not directly cause the nucleation of APBs, but regions with higher amounts of residual contamination will have a greater density of single-steps and thus a greater APB density. Further study is needed to investigate the Si(001) surface at different stages of the pre-growth processing, i.e. after the Siconi[TM] clean and after the pre-growth bake.

3.4 Summary

The effect of interfacial contamination on APB density was examined for GaAs grown on Si(001) by MOCVD. The pre-clean was varied across the substrate to affect the amount of residual contamination from the wafer center to the wafer edge. SIMS analysis confirmed an increase in both interfacial oxygen and carbon from center to edge. It was shown that there is a quantitative correlation between the APB density and the amount of interfacial contamination. Over a range of interfacial carbon dose determined by SIMS of 1.9×10^{14} atoms/cm^2 to 1.7×10^{15} atoms/cm^2 from center to edge, the APB density increased from 0.14 to 3.2 µm^{-1}. Examination of the GaAs/Si interface with XTEM showed the physical association of APBs with amorphous interfacial particles. The particles are likely carbon based, such as SiC. It is unclear if the higher

78

APB densities are an effect of contaminant particles directly nucleating APBs or an indirect effect from agglomerated carbon passivating single-steps on the Si surface. The results of this study demonstrate the importance of reducing residual contamination on Si substrates prior to GaAs epitaxy. If the APB density is minimized, then the complete suppression of antiphase disorder via APB self-annihilation can be achieved with minimal GaAs layer thickness. In addition, this study shows that if the pre-clean is not effective, the antiphase disorder will still be significant regardless of a pre-growth bake of the substrate. When the same pre-clean procedure is used, but no pre-growth bake, the APB density is also relatively high (Figure 3-1). Therefore, the combination of an effective substrate clean and the pre-growth bake is critical for reducing the density of nucleated APBs in GaAs-on-Si films.
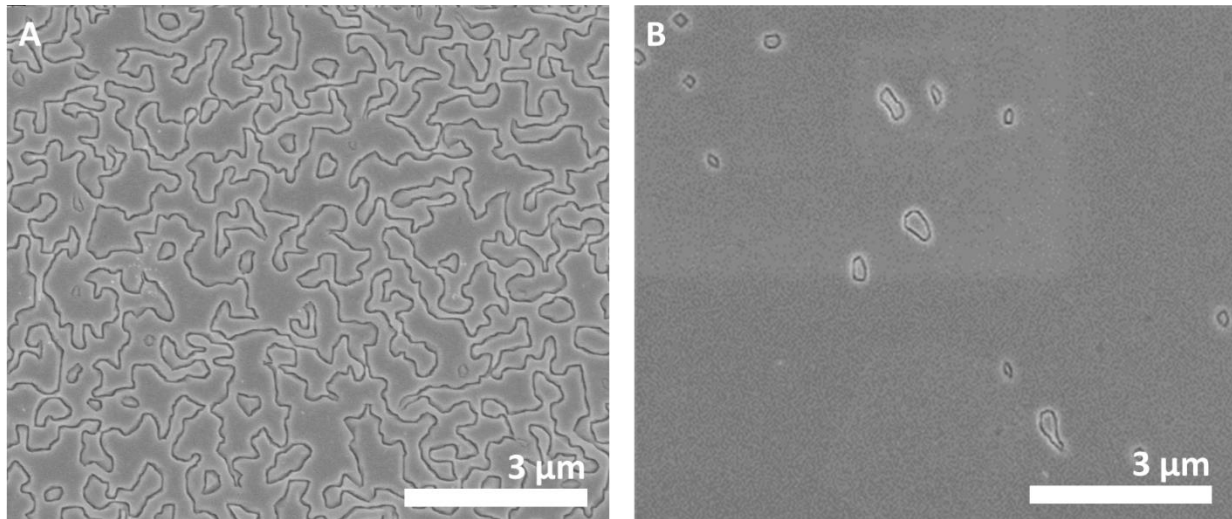
Figure 3-1. Representative plan view SEM images of GaAs film grown on Si(001) with varying pre-growth conditions. A) Without a pre-growth bake and B) with a pre-growth bake at 900 °C. APBs are visible as linear features with dark contrast after selective etching.
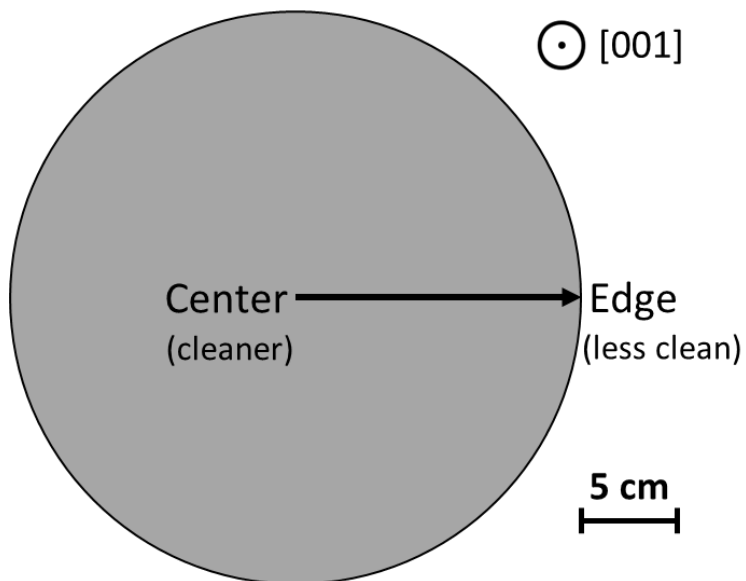
Figure 3-2. Illustration showing the variation in pre-cleaning procedure to affect the amount of residual contamination across the Si(001) wafer from center to edge.
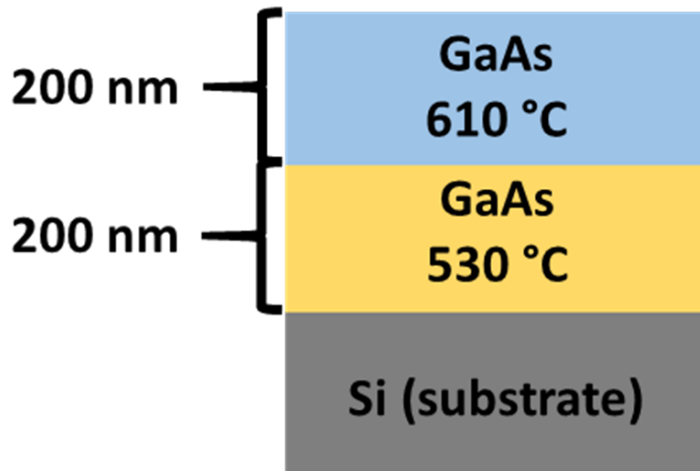
Figure 3-3. Diagram of the GaAs layer structure. Initial layer of 200 nm is first grown at a low temperature of 530 °C followed by 200 nm at 610 °C. The two-step growth process is commonly used for III-V epitaxial films to improve crystal quality.
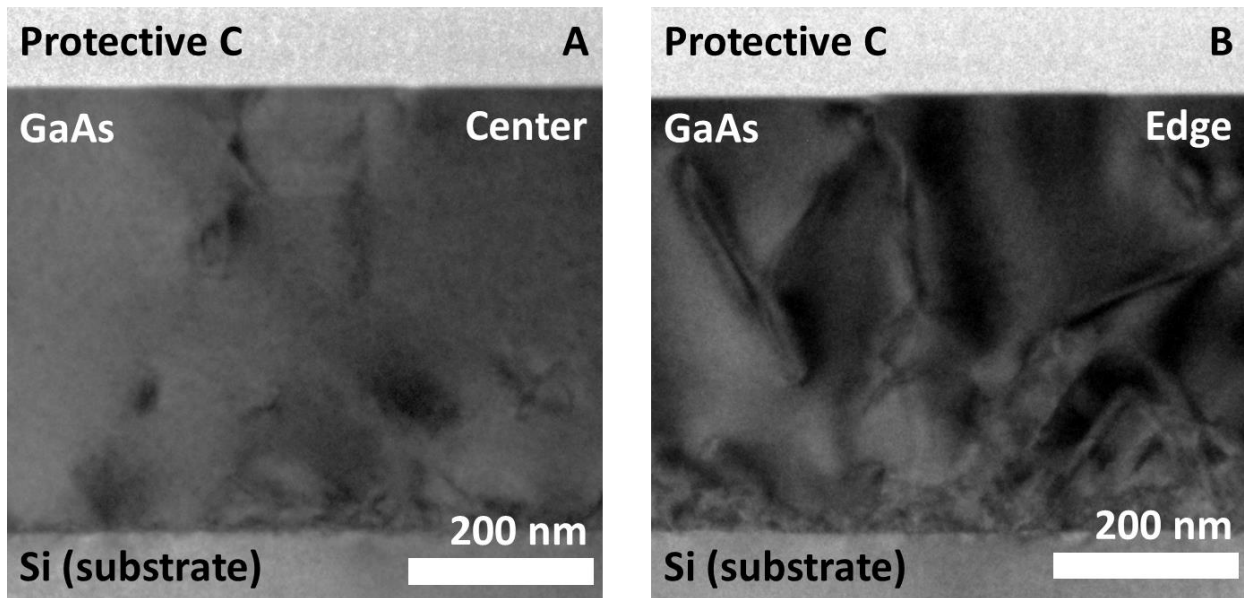
Figure 3-4. BF XTEM images of GaAs layer at different wafer positions. A) At the center of the wafer and B) at the edge of the wafer. There is a ~10 nm decrease in film thickness from center to edge and defect density is qualitatively higher at the edge.
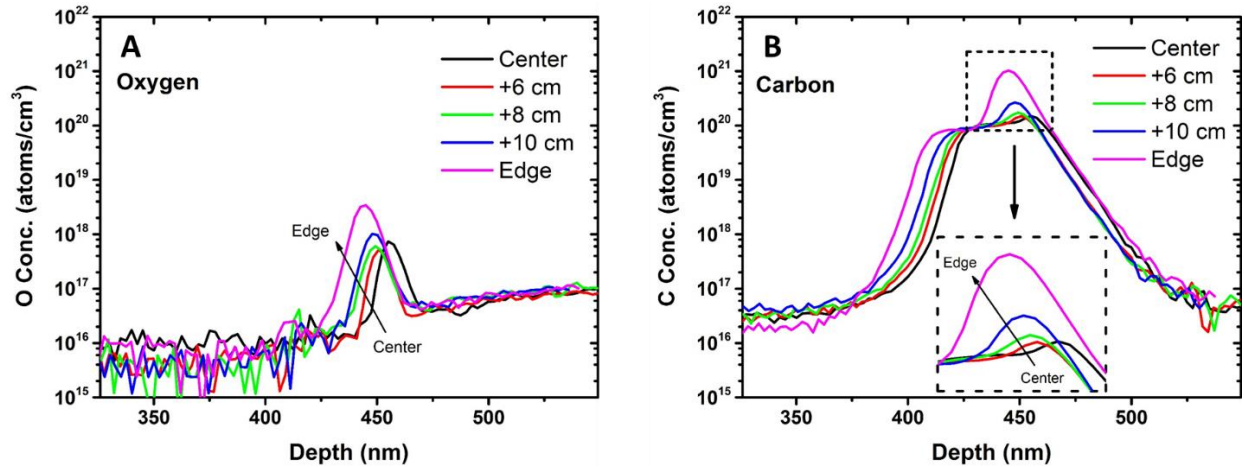
Figure 3-5. SIMS profiles of contamination sources at the GaAs/Si interface with varying wafer position. A) Oxygen interfacial contamination. B) Carbon interfacial contamination. There is an overall trend of increasing interfacial oxygen and carbon from center to edge. The carbon profile has a large shoulder, likely from incorporation of MOCVD precursor reaction products; however, there is still a distinguishable interfacial peak shown in the inset.
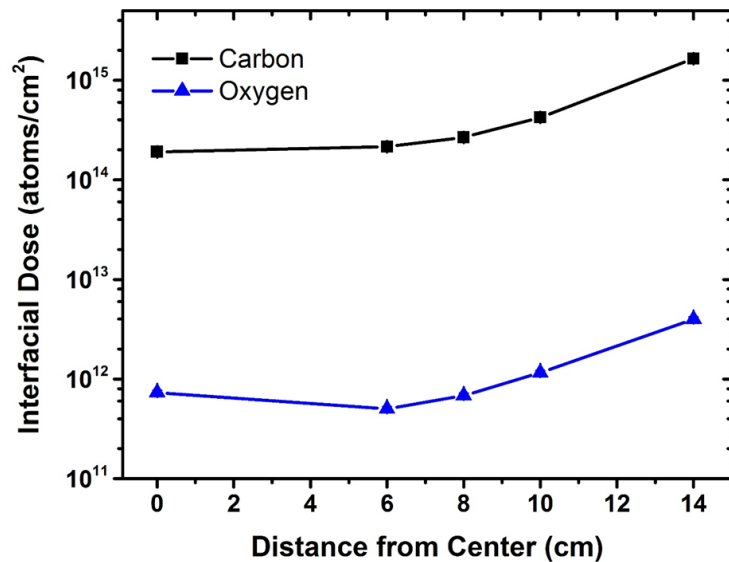
Figure 3-6. Interfacial oxygen and carbon doses determined by integrating the respective interfacial peaks in SIMS as a function of wafer position. Dose tends to increase from center to edge for both oxygen and carbon. Carbon dose is over two orders of magnitude greater than oxygen dose.
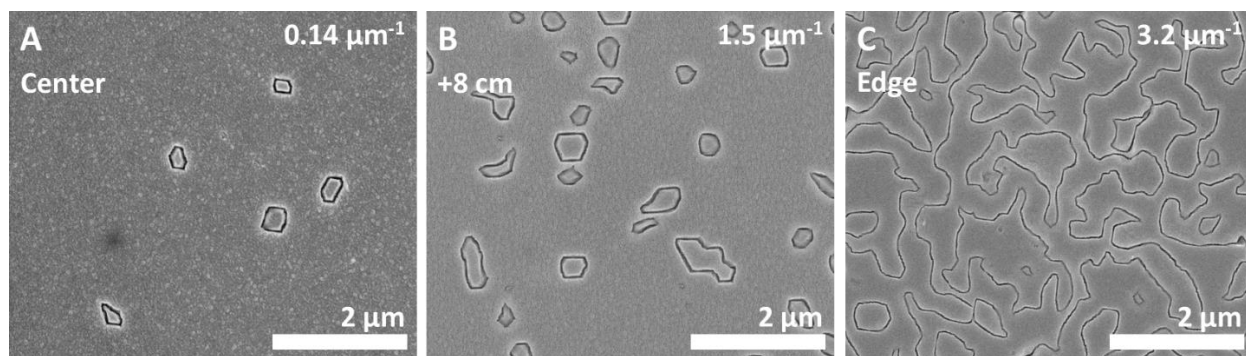
Figure 3-7. Representative plan view SEM images of the APB density in the GaAs film at different wafer positions. A) Center of the wafer, B) +8 cm from the center, and C) at the edge of the wafer. The APB density increases from 0.14 μm^{-1} to 3.2 μm^{-1} over this distance and there is a marked increase in antiphase domain size.
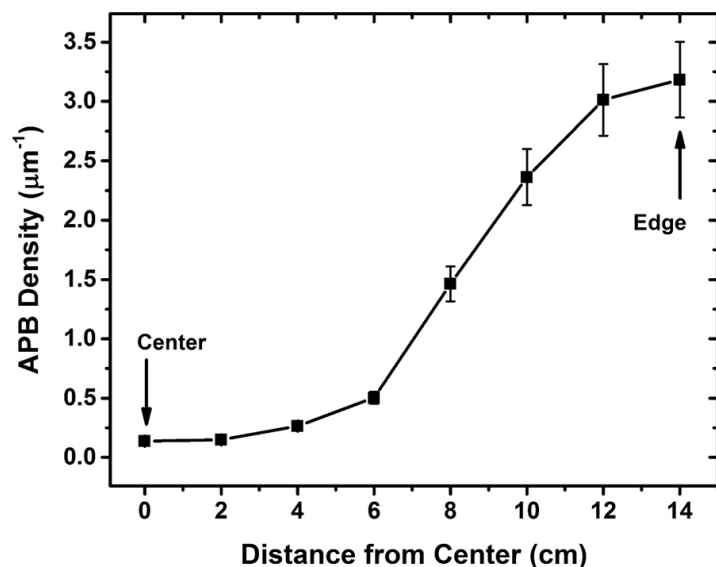
Figure 3-8. Plot of all APB density counts as a function of wafer position. There is a consistent trend of increasing APB density from center to edge that correlates with the increase in contamination. There is a large jump in APB density from +6 to +10 cm from the wafer center. The APB density appears to reach a maximum value towards the edge of the wafer.
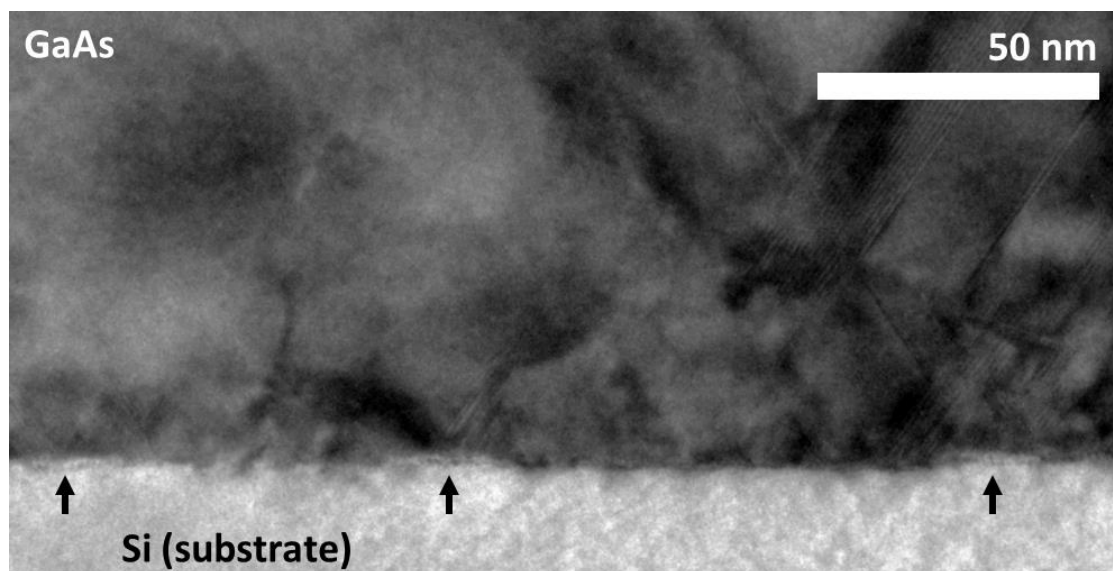
Figure 3-9. HRTEM image of GaAs/Si interface of a sample from the wafer edge. Amorphous particles are observed at the interface (marked by arrows). The particles are associated with the formation of defects including stacking faults.
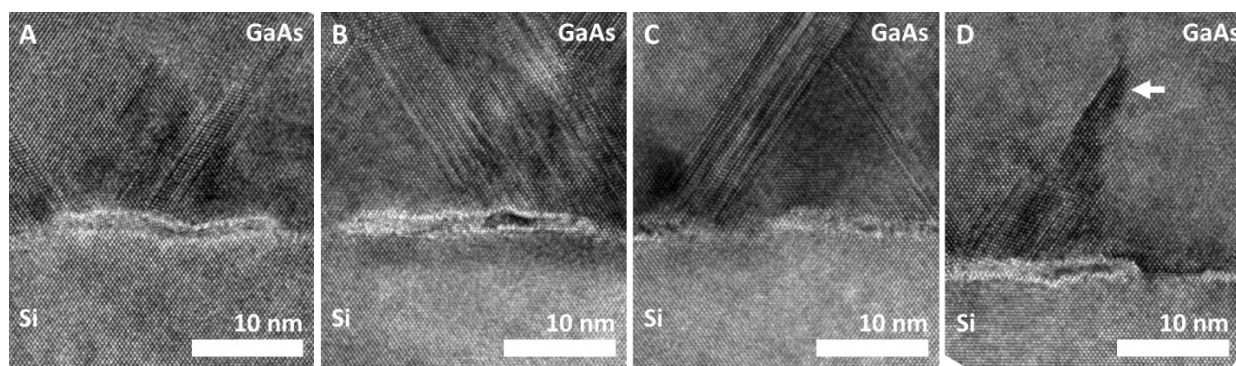
Figure 3-10. HRTEM images at higher magnification of a series of amorphous particles observed at the GaAs/Si interface. A stacking fault in D) is terminated ~15 nm away from the interface (marked by arrow) which may correspond with the presence of an APB.
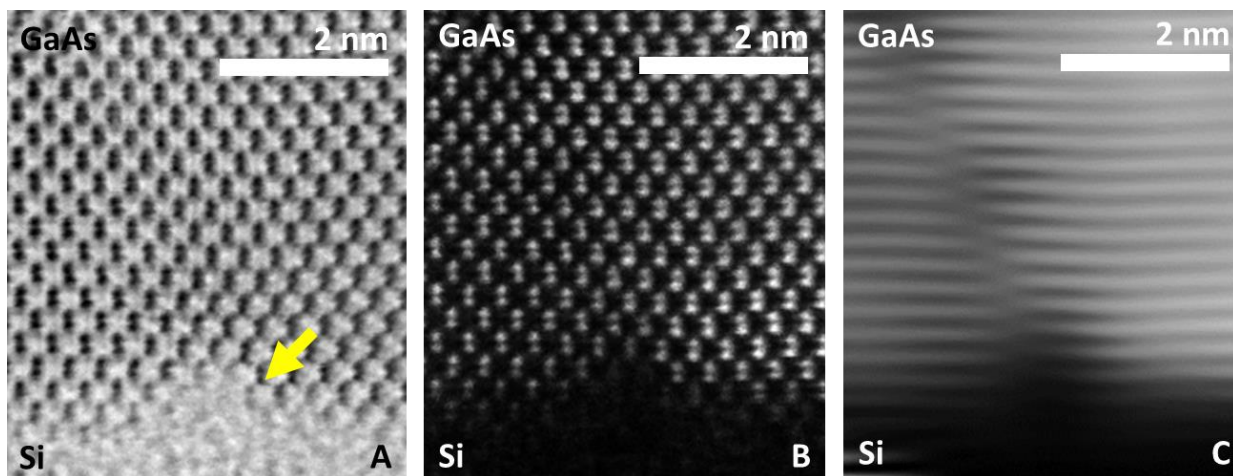
Figure 3-11. STEM images of the GaAs/Si interface in an edge sample showing an APB associated with an amorphous particle. A) ABF-STEM image with amorphous particle marked by an arrow. B) HAADF-STEM image of same area. C) The Fourier filtered HAADF image using the 002 spots reveals an APB that is directly emanating from the location of the particle, evidenced by the misordering of the (002) planes.
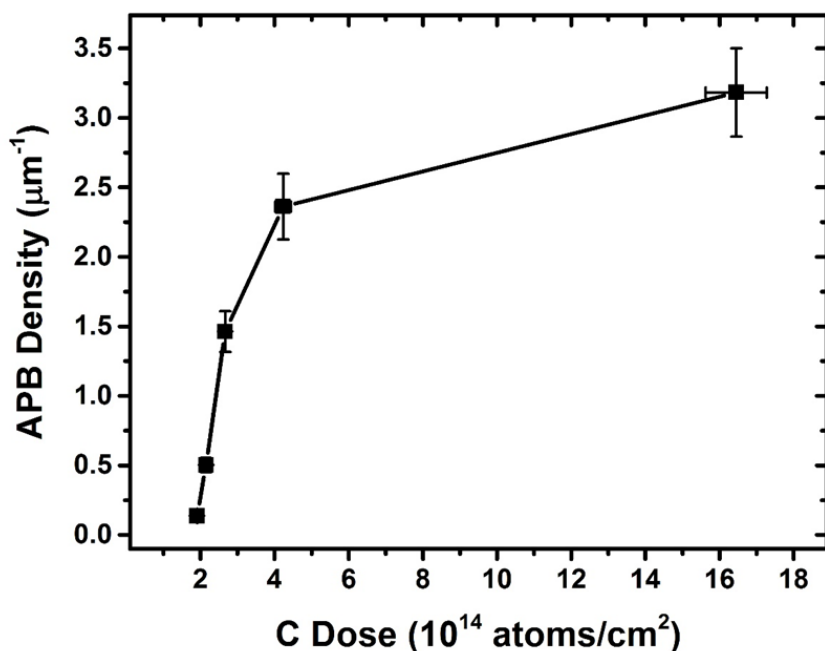
Figure 3-12. Plot of APB density as a function of interfacial carbon dose for measured samples. APB density increases linearly with carbon dose and then plateaus after ~4×10^{14} atoms/cm^2. The plateau may stem from an upper limit on the total APB density in the layer from self-annihilation.

CHAPTER 4
THE EFFECT OF GROWTH TEMPERATURE

4.1 Background

The recent drive for alternative materials to replace Si in future transistor devices has renewed interest in the III-V compound semiconductors. III-V materials such as InGaAs and InAs have much better electron transport properties than Si [6]. The long-standing barrier to the implementation of III-V materials in commercial applications has been cost. The renewed interest has prompted a need for economical integration of III-V materials on Si. Perhaps the simplest method is to epitaxially grow a layer stack on top of a Si substrate. GaAs is a good candidate as an initial buffer layer because it has an intermediate lattice constant between that of Si and InAs. Unfortunately, the epitaxy of GaAs and other III-Vs on Si is typically plagued by a number of defects such as APBs.

APBs in epitaxial GaAs films are nucleated at the site of single-steps on the Si(001) surface. These APBs tend to nucleate along {110} planes that are the lowest energy of formation [92] and thus can propagate entirely through a film. The most common strategy for reducing the density of APBs is to use an intentionally misoriented substrate along with a high temperature pre-growth anneal at 1000 °C [13, 67]. The anneal promotes the transition of single-steps into double-steps that reset the ordering of atoms in the epitaxial layer and prevent APB formation. However, the use of misoriented substrates is not practical in conventional CMOS processing because it would require a complete respecification of existing tools and procedures. High temperature anneals should also be avoided if possible to prevent unintentional effects to any other devices on the chip. Therefore, other methods of suppressing antiphase disorder in GaAs-on-Si films must be explored and understood.

It has been observed that while APBs tend to nucleate along {110} orientations, they readily change their plane of propagation in the layer during growth [82, 146]. Thus, it is possible for the antiphase disorder in a film to be completely suppressed if all nucleated APBs kink over and self-annihilate. Georgakilas et al. [11] analyzed the through-thickness APB density for a GaAs-on-Si film and found that the APB density decreased further away from the GaAs/Si interface. It can then be inferred that APBs must be self-annihilating via propagation along inclined planes, even if they are nominally higher formation energy. Possible APB habit planes that would be conducive for annihilation are {111}, {112}, and {113} planes. Figure 4-1 shows an illustration of these APBs in a GaAs-on-Si film. APBs along {111} planes are non-stoichiometric, i.e. composed of all the same type wrong bond, and have the highest relative formation energy [92]. On the other hand, APBs along {112} planes maintain stoichiometry, similar to {110} APBs, and so may be favorable for APB annihilation.

One factor that may influence the tendency of APBs to kink over from {110} type planes to higher index planes is the growth temperature of the film. Increasing the thermal energy available should help drive the system to an equilibrium configuration. APBs are high energy defects and thus their existence in a film should be energetically unfavorable. There is evidence that higher growth temperatures lead to a greater proportion of APBs propagating along higher index planes and self-annihilating. It was found for GaP films grown on Si via MOCVD that low bulk growth temperatures favored {110} APBs, but at higher bulk growth temperatures the APBs became majority {111} and {112} oriented and completely self-annihilated [113, 114]. Unfortunately, these studies did not quantify the effect of growth temperature on APB annihilation. It is also

unclear why APB propagation along orientations that are nominally higher in formation energy becomes favorable at these higher growth temperatures. It is plausible that there is a kinetic barrier to APB propagation along higher index planes, but that the process is thermodynamically favored overall due to the consequential reduction in total APB interfacial area. The goal of this work is to conclusively analyze the effect of growth temperature on APB annihilation in GaAs grown on Si(001) by MOCVD and to gain insight on the associated APB energetics. The work in this chapter has been published in Barrett et al. [147].

4.2 Experimental

The substrates used in this work were 300 mm Si(001) wafers with no intentional off-cut. The wafers were cleaned of native oxide and other contaminants using the Siconi[TM] process [118] and then transferred under vacuum to the growth chamber. Each wafer was then subjected to a ~900 °C bake to help promote the formation of double-steps. This preparation procedure reduces the APB density in GaAs films by over an order of magnitude (see Chapter 3). Starting with a low APB density is advantageous both from an engineering standpoint and for this study since it becomes easier to track changes in APB density over the thickness of the film.

GaAs film growth was performed in an Applied Materials III-V MOCVD system. Layers were grown in the conventional two-step manner to improve crystal quality [26, 75]. The precursors for Ga and As were trimethylgallium (TMGa) and tertiarybutylarsine (TBAs), respectively. The V/III ratio was in the typical process range for MOCVD and the chamber was maintained at standard reduced pressure. Figure 4-2 shows the layer structure used for the GaAs films in this study. First, an identical nucleation layer of 200 nm of GaAs was grown at 530 °C. This initial layer was important to set the same

88

approximate starting APB density across all of the samples. Next, a bulk layer of 600 nm of GaAs was grown for temperatures ranging from 530 °C to 650 °C to analyze the effect of increasing the growth temperature on APB propagation and annihilation. The sample grown completely at 530 °C is used as a control. Growth at higher temperatures was not feasible due to cracking of the GaAs film upon cooling. No other growth conditions besides growth temperature were changed, i.e. this study only investigates "turning one knob" in the MOCVD process. Therefore, actual film thicknesses for the samples varied over a small range from the nominal 800 nm thickness due to differences in the growth rate at different bulk growth temperatures.

In order to analyze the through-thickness APB density for the samples, a two part etching process was used similar to that discussed by Georgakilas et al. [11]. A non-selective $CH_3OH:H_3PO_4(85\%):H_2O_2(30\%)$ (10:1:1) solution was first used to etch the GaAs films down to different depth points. The remaining film thickness at each point was measured with a JA Woollam M88 ellipsometer. The ellipsometry measurements were compared with selected XTEM samples and found to be in good agreement with less than 10 nm of variation. Samples were then dipped in a $HF(49\%):HNO_3(69\%):H_2O$ (10:1:7) solution for 10 s to selectively etch down APBs and improve contrast in SEM. Thus, the APB density as a function of depth in the GaAs films could be determined. Plan view SEM images were collected in various areas of the samples to obtain accurate counts of APB density. APB features in SEM were traced using ImageJ software [132]. The APB density is defined as the line length of APBs per unit area, giving units of μm^{-1}. The detection limit of antiphase domains is on the order of 0.1 to

0.2 μm in circumference, based on the minimum value of APB lengths that were collected.

The evolution of APB propagation in the samples was analyzed with DF XTEM imaging using a JEOL 200CX TEM operating at 200 kV. XTEM specimens were prepared in <110> orientations using a FEI Strata DB325 dualbeam FIB/SEM instrument. DF imaging was performed with the 002 and 00-2 superlattice reflections in order to have sensitivity for crystal orientation across antiphase domains [129, 148]. The contrast in DF imaging was improved by further tilting of the samples off of the <110> zone axis to excite 115 and 11-7 type spots along with the 002 type spot. These tilting conditions increase the intensity of the 002 reflection [113]. Using these DF imaging conditions, antiphase domains will have opposing contrast relative to the main phase crystal, i.e. one will be bright and the other will be dark. This contrast allows for the direct identification of APBs and their habit planes.

4.3 Results

4.3.1 APB Density Depth Profiles

After etching the samples down to different film thickness and gathering a series of images of the APB density in SEM, it was readily apparent that number of antiphase domains visible, along with the overall APB density, began to increase with decreasing GaAs film thickness. An example of this trend can be seen in the sample with the bulk layer grown at 570 °C. Figure 4-3 shows representative plan view SEM images of the surface of this sample after selectively etching APBs at different film thicknesses. The type of discrete domains was typical for all samples. The decrease in the number of antiphase domains visible with increasing distance from the GaAs/Si interface indicates that the bounding APBs must be kinking over and self-annihilating, thereby suppressing

the domains within the film. The APB density from a film thickness of 240 nm (D) to a film thickness of 745 nm (A) decreases from 0.33 μm^{-1} to 0.047 μm^{-1}. Similar trends were observed in the other samples with different bulk growth temperatures.

The through-thickness APB density depth profiles for all samples with varied bulk growth temperature are shown in Figure 4-4. Note the logarithmic scale used for APB density. There is a marked decrease in APB density for all samples with increasing distance from the GaAs/Si interface. This decrease in APB density is facilitated by a reduction in the total line length of APBs in the (001) growth plane due to APBs kinking to inclined planes and self-annihilating. The control sample grown completely at 530 °C also experienced a moderate decrease in APB density, indicating that there is an inherent tendency for APBs to self-annihilate during growth. However, there is a variation in the magnitude of APB density reduction with GaAs film thickness that appears to be temperature dependent. Increasing the bulk growth temperature to 570, 590, and 610 °C causes an increase in the rate of APB annihilation with respect to film thickness. After this point, i.e. for the samples grown at 630 and 650 °C, the APB density depth profiles follow the same approximate curve. Thus, there is no further enhancement of APB annihilation for bulk growth temperatures greater than 610 °C.

4.3.2 APB Annihilation Rates

A quantitative measure of APB annihilation rate for the samples grown at different bulk growth temperatures can be obtained by fitting the respective APB density depth profiles in Figure 4-4. These profiles follow an approximate exponential decay, as evidenced by the linear relationships on a semi-log plot. This character allows for a trivial determination of the APB annihilation rates. Figure 4-5 shows an example of the fitting procedure for the sample with bulk growth at 610 °C. The profile is fit to a

standard exponential decay function and the APB annihilation rate is taken as the exponential decay rate. The units of APB annihilation rate are then μm^{-1}. This procedure was repeated for the depth profiles of all samples to extract the respective rates.

Figure 4-6 shows the extracted APB annihilation rates with respect to film thickness for all samples versus the bulk growth temperature. The APB annihilation rate increases by approximately a factor of four from 2.6 μm^{-1} to 10.7 μm^{-1} over a bulk growth temperature range of 530 °C to 610 °C. After 610 °C, the annihilation rate saturates at ~10-11 μm^{-1}, corresponding to the overlap of APB density depth profiles in Figure 4-4. The strong correlation between APB annihilation rate and the bulk growth temperature, combined with the knowledge that APB annihilation occurs via APBs kinking to higher-index planes, indicates that the kinking of APBs is a thermally activated process. At higher growth temperatures, a greater portion of APBs are able to change their plane of propagation and self-annihilate. The saturation of APB annihilation rate at growth temperatures above 610 °C may stem from geometric factors. The film thickness required for an APB to self-annihilate is dependent on its plane of propagation. Therefore, if a given set of planes is preferred energetically to achieve annihilation, e.g. {112} over {111}, and a majority of APBs are already kinked over to these planes, then there will be no significant change in the APB annihilation rate with respect to film thickness at higher temperatures.

An Arrhenius relationship can be used to determine the associated activation energy for APBs kinking to higher index planes during growth. Figure 4-7 is an Arrhenius plot of the APB annihilation rates for the samples with bulk growth from 530 °C to 610 °C, i.e. before the saturation of APB annihilation rate. The activation energy

92

found from fitting this plot is 1.1 eV. This activation energy likely corresponds to the energy barrier for APBs to form along a higher index plane configuration, e.g. {112}, versus a {110} configuration. APBs along {112} planes have a higher wrong bond density compared to {110} APBs [92]. It is unknown how this activation energy compares to the activation energy for the GaAs growth process, i.e. growth rate. However, based on previous literature for the MOCVD growth of GaAs using TMGa and TBAs under similar conditions, the growth rate activation energy is likely between 0.5 to 1.5 eV [29, 30, 149]. In addition, the consistency of the film thicknesses at different bulk growth temperatures indicates that the growth process is not kinetically limited. Thus, the process of APB kinking is unlikely to be affected by GaAs film growth reactions.

4.3.3 XTEM Analysis

The evolution of APBs in the GaAs layer was investigated using DF XTEM imaging. Due to the overall low density of APBs in the samples, it is difficult to capture entire domains in a single XTEM sample. However, a few examples of antiphase domains were found in the samples that were imaged. Figure 4-8 shows an antiphase domain in the sample with bulk growth at 630 °C imaged using the g_{002} reflection (A) and the $g_{00\text{-}2}$ reflection (B). The reversal of contrast in the image from Figure 4-8A to Figure 4-8B using the opposing reflections confirms that the feature is an antiphase domain. The size of the domain is on the order of those observed in plan view SEM (Figure 4-3). It can be observed that, while the domain is not completely suppressed in the film, the diameter decreases with increasing distance from the GaAs/Si interface. This observation is consistent with the quantitative trend of the APB density depth profiles (Figure 4-4). The APBs on either side of the domain appear to be faceted both along {110} planes and higher index planes leading to a net decrease in width.

93

Another example of an antiphase domain in DF XTEM is shown in Figure 4-9 for the sample with bulk growth at 610 °C. The image contrast in the GaAs layer is again reversed when using the g_{002} reflection (A) and the $g_{00\text{-}2}$ reflection (B), confirming that this is an antiphase domain. This domain is suppressed within the GaAs layer. The APBs appear to nucleate along {110} planes before eventually kinking over to what are macroscopically {112} planes and self-annihilating. This observation is consistent with the work by Volz et al. [114] and Beyer et al. [95] that showed preferential propagation along {112} planes at higher growth temperatures for APBs in GaP-on-Si grown by MOCVD. It is important to note that Figure 4-9 is not necessarily representative of typical APB annihilation for GaAs-on-Si, but it is an example of an energetically allowable pathway. The kinking of APBs from {110} planes to {112} planes as seen in Figure 4-9 is likely limited by a kinetic barrier, i.e. the 1.1 eV energy barrier found for the relationship between APB annihilation rate and growth temperature (Figure 4-7).

4.4 Discussion

4.4.1 Driving Force for Annihilation

The results of the through-thickness APB density analysis for the GaAs-on-Si films in this study demonstrate that APB annihilation during growth is dependent on the growth temperature. This relationship is not surprising given that APBs are defects with large associated energies and therefore should be inherently unstable in a crystal. The equilibrium configuration for a GaAs crystal should be free of APBs. However, APBs are forced to form because of single-steps on the Si surface. At lower growth temperatures, APBs nucleate along {110} planes that are lower formation energy. These APBs would otherwise propagate entirely through a film. Increasing the growth temperature helps to overcome a kinetic energy barrier for APBs to kink over to higher index planes, such as

94

{112}. In turn, this configuration leads to the self-annihilation of APBs and a total reduction in APB density.

The energetic driving force for APBs kinking during growth can be understood using a simple schematic diagram of atoms in the (001) growth plane, as seen in Figure 4-10. A typical annihilating antiphase domain is shown in cross-section in Figure 4-10A, similar to the domains seen in DF XTEM (Figure 4-8 and Figure 4-9). Two (001) slices are taken at a point where the APBs lie along {110} planes (B) and where they lie along inclined planes (C). Each atom depicted in Figure 4-10B and Figure 4-10C is involved in an APB. The kinking of APBs to inclined planes facilitates a reduction in the number of atoms involved in an APB with each successive monolayer of growth. A significant reduction in the contribution of APBs to the overall free energy of the crystal can then be achieved, as seen by comparing the total APB line length in Figure 4-10B versus Figure 4-10C. The domain will eventually be completely suppressed within the film.

4.4.2 Discussion of Mechanism

Another explanation for the dependence of APB annihilation rate on growth temperature is not a pure kinking of APBs to higher index planes such as {112}, but a stepwise kinking of APBs mediated by jumps to {110} planes. In addition to showing the preferential annihilation of APBs along {112} planes [95], Beyer et al. [131] observed that in similarly grown GaP-on-Si samples APBs oriented along {110} planes displayed a tendency to jump one or more atomic planes, thereby creating a finite thickness to the APB. It follows that increasing growth temperature can increase the jump probability for APB planes and enhance the annihilation rate. However, the jumping mechanism inherently forms segments of APB facets that should be energetically unfavorable, e.g. non-stoichiometric {111} or {001}. APBs along {001} also have greater wrong bond

density than {110}, {111}, or {112} [91]. It is possible that these segments are relatively small enough in length that the APB jump is still rendered favorable. Otherwise, it is unclear how a macroscopic {112} APB as observed in this study (Figure 4-9) would be manifested via the stepwise kinking mechanism. Considering the geometry of an APB in a {112} orientation, construction with {111} and {110} facets would never meet the shallow angle of a {112} plane on average. Construction with {110} and {001} facets requires that the unfavorable {001} segments must be longer than the {110} segments.

APB annihilation may also be influenced by rotation of the lattice due to the differing lengths of Ga-Ga and As-As wrong bonds versus Ga-As bonds. Vajargah et al. [130] measured phase changes HAADF-STEM images of a GaSb-on-Si layer and observed rotation of the lattice at an APB. The rotation alternated in sequential segments which allowed the APB to initially preserve a normal direction relative to the substrate before the APB eventually kinked over to inclined planes. The authors posit that faceting along higher-index planes is influenced by this lattice rotation and local relaxation at the APB and thus it will promote annihilation. However, since the alternating rotation was seen in both the curved and normal sections of the APB, it is unclear how much effect the rotation has on the actual APB kinking process. As well, the change in APB formation energies along different planes due to the lattice rotation and relaxation is unknown. There may be a relationship between the local relaxation and lattice rotation at an APB and the tendency to kink to higher index planes.

4.4.3 Comparison with Other Samples

The results of the APB density depth profiles for the samples in this study can be compared to those of samples grown at different times. Figure 4-11 shows a series of APB density depth profiles for samples with different bulk growth temperatures, along

with the profile of the sample with bulk growth at 610 °C from this work. The other samples include two proof of concept (POC) samples with bulk growth at 590 °C and 630 °C; the growth conditions are otherwise identical to the samples in this study. Another sample is shown that was grown with a 400 nm nucleation layer and 600 nm bulk layer at 610 °C for a total GaAs film thickness of 1 μm; the growth conditions are otherwise identical. Note the shifted positioning of the bulk layer demarcation for this 1 μm sample as well as the lower initial APB density prior to the onset of the bulk layer in Figure 4-11. The POC sample with bulk growth at 590 °C experiences much slower APB annihilation with respect to GaAs film thickness compared to the other samples which is consistent with the findings of this work. What is also interesting to point out is that the APB annihilation rates for the POC sample at 630 °C and the 1 μm sample at 610 °C are similar to that of the sample with 610 °C bulk growth from this study, i.e. they follow the same approximate slope of decay. The similarity of the APB annihilation rates for the samples with bulk growth at 610 °C and above demonstrate that there is a consistent saturation point for the APB annihilation rate. Further, the similarity of the rate of decay for the 1 μm sample shows that the starting APB density prior to the growth of the bulk layer does not affect the APB annihilation rate.

4.5 Summary

In conclusion, the annihilation rate of APBs with respect to film thickness for GaAs films grown on Si(001) by MOCVD has been shown to have a dependence on the bulk growth temperature. Increasing the bulk growth temperature from 530 °C to 610 °C increased the exponential decay rate of APB density with respect to GaAs film thickness from 2.6 μm^{-1} to 10.7 μm^{-1}. The annihilation rate saturated after 610 °C. Higher growth

temperatures likely remove kinetic barriers for the kinking of APBs from {110} type planes to higher index planes, such as {112}, that are nominally higher in formation energy but facilitate self-annihilation. An activation energy for the APB annihilation process during growth of 1.1 eV was found using an Arrhenius relationship. The driving force for APBs kinking to higher index planes stems from a reduction in the total line length of APBs in the (001) growth plane, i.e. a reduction in the number of adatoms involved in an APB for each subsequent monolayer of growth. DF XTEM imaging showed a tendency for antiphase domains to shrink in width during growth and that {112} is a possible habit plane for APB propagation to facilitate annihilation at higher growth temperature. These findings are consistent with prior studies showing a preference for APB propagation along {112} planes over {110} at higher growth temperatures. This work demonstrates a quantitative relationship between APB annihilation rate and growth temperature.
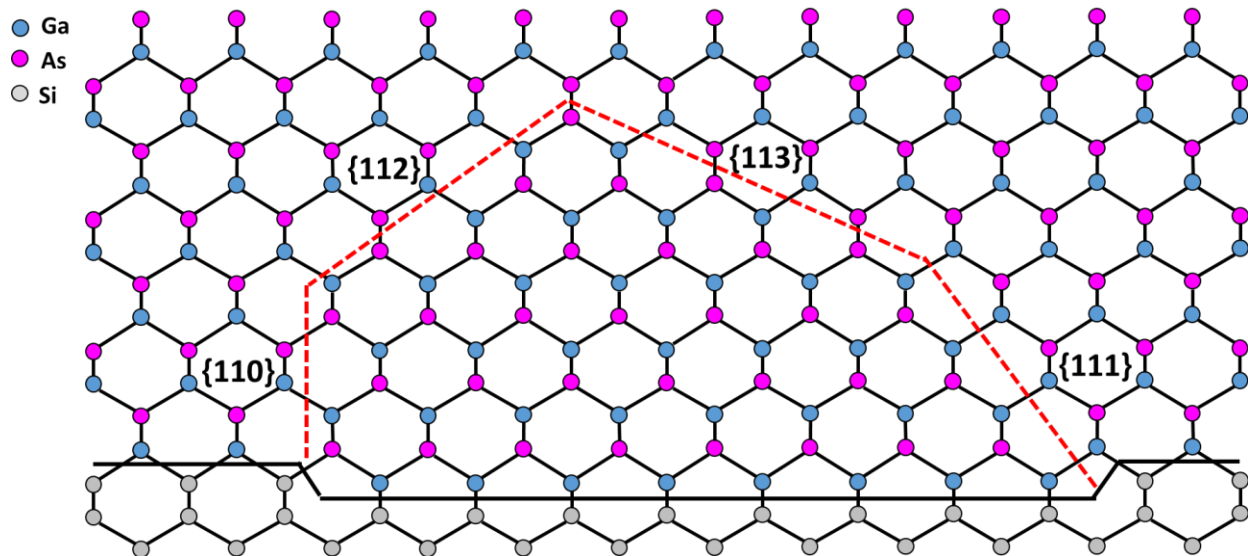
Figure 4-1. Illustration of APBs oriented along various habit planes in a GaAs-on-Si film. Inclined habit planes such as {111}, {112}, and {113} favor APB self-annihilation. Note the stoichiometric nature of {110} and {112} type APBs.
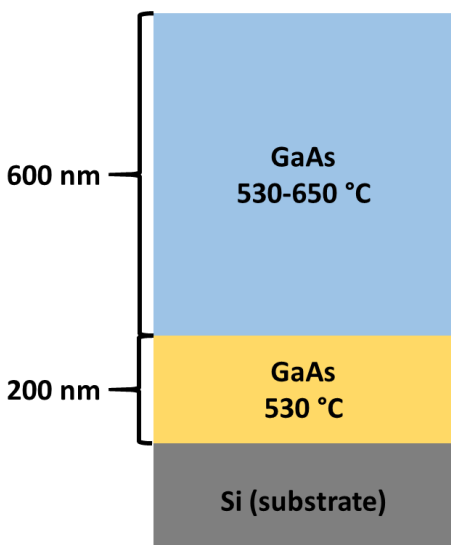
Figure 4-2. Illustration of GaAs layer structure for the growth temperature experiment. A 200 nm layer was first grown at 530 °C for all samples to set the APB density. Next a 600 nm bulk layer was grown with varying temperature from 530 to 650 °C.
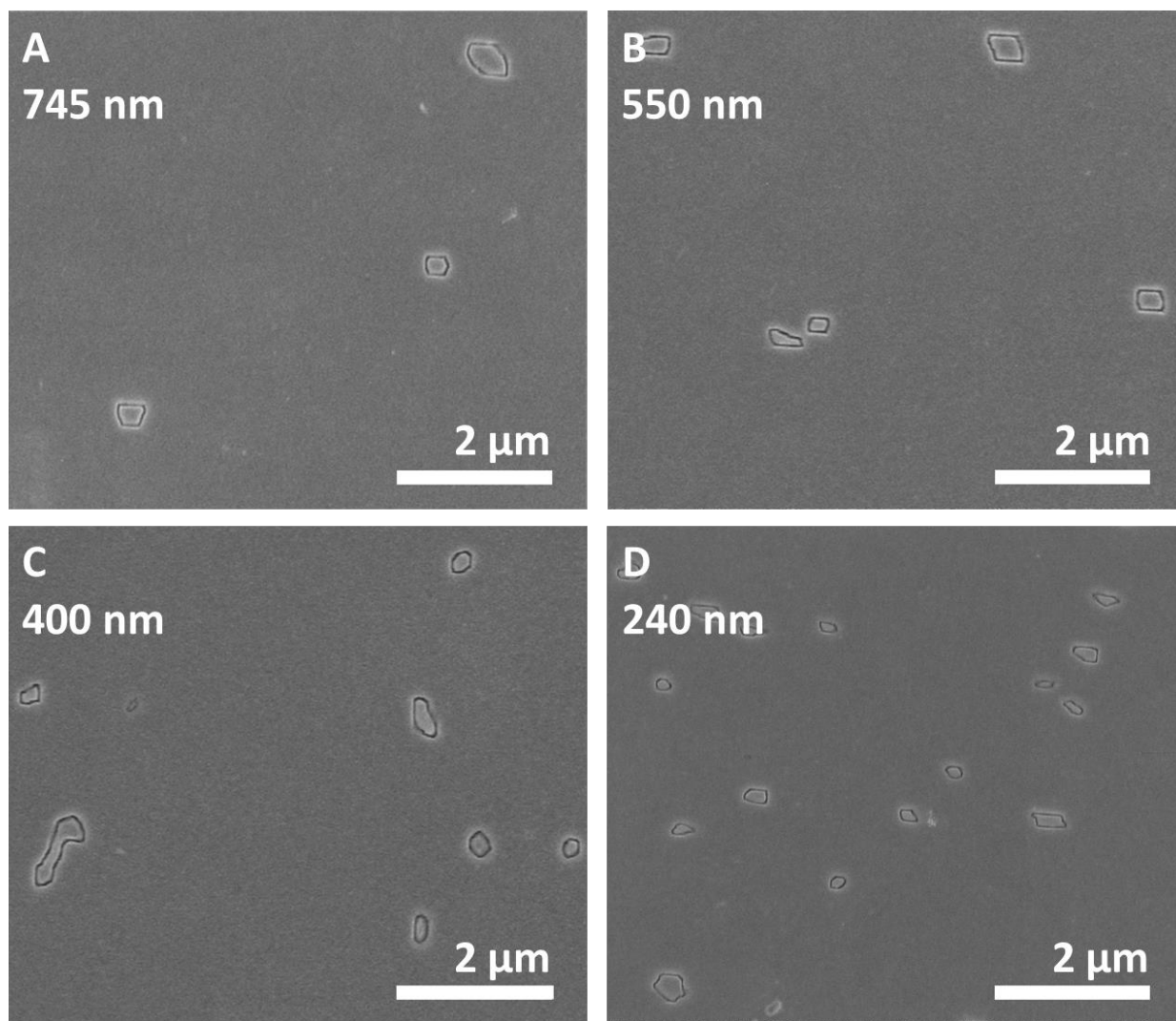
Figure 4-3. Representative plan view SEM images of the APB density in the sample with bulk growth at 570 °C at varying film thickness points: A) 745 nm, B) 550 nm, C) 400 nm, and D) 240 nm. There is a marked increase in APB density and the number of domains visible closer to the GaAs/Si interface, indicating that APBs are annihilating during growth and suppressing antiphase domains.
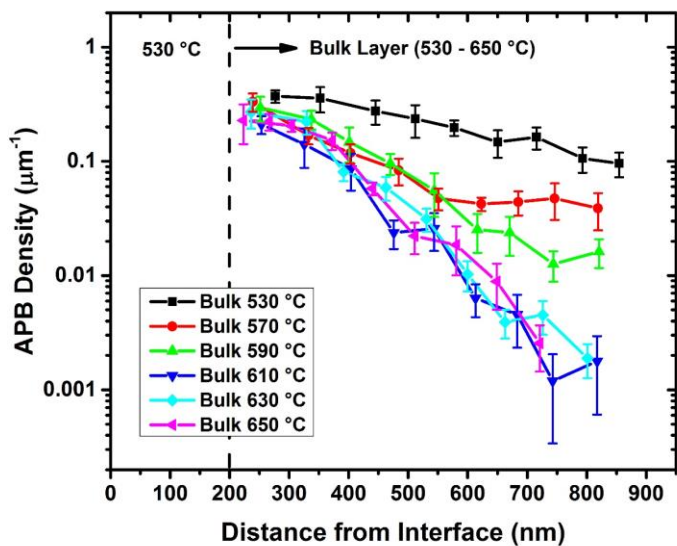
Figure 4-4. Depth profiles of APB density for all samples with varying bulk growth temperature. APB density for all samples decreases with increasing distance from the GaAs/Si interface. The rate of decrease with respect to film thickness increases with increasing bulk growth temperature, but plateaus after 610 °C.
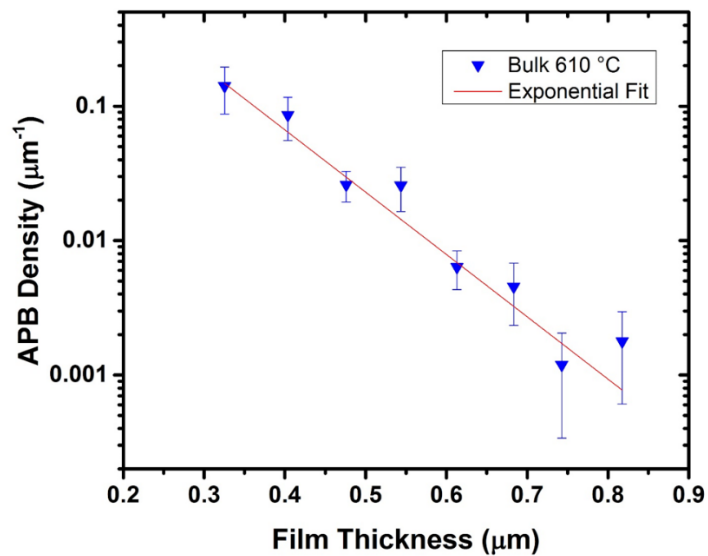
Figure 4-5. Example of fitting procedure for APB density depth profile curves for the sample with bulk growth at 610 °C. The curves follow an approximate exponential decay. The APB annihilation rate is taken as the exponential decay rate.
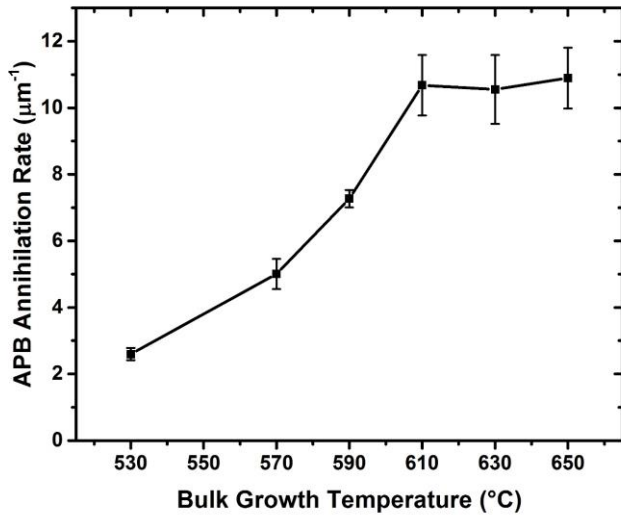
Figure 4-6. Plot of the extracted APB annihilation rates, i.e. exponential decay rate, for all samples versus the bulk growth temperature. The APB annihilation rate increases by ~4x from 530 to 610 °C before it plateaus. The annihilation rate is likely limited by the APB habit planes at higher growth temperatures.
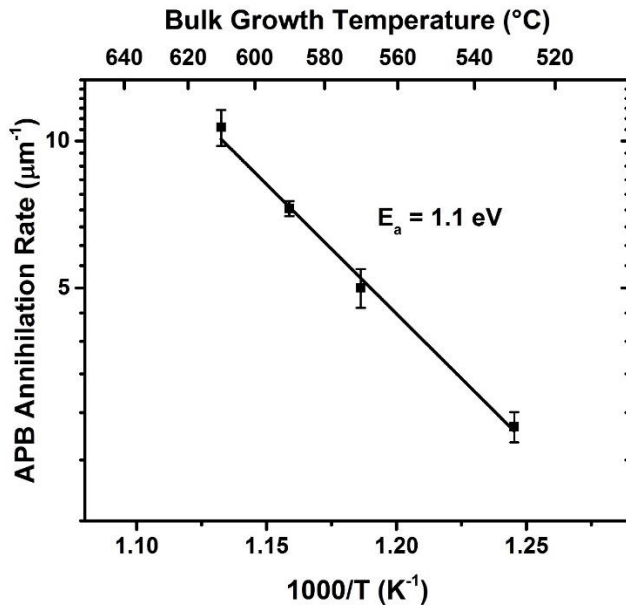
Figure 4-7. Arrhenius plot of APB annihilation rates for samples with bulk growth from 530 to 610 °C. The extracted activation energy is 1.1 eV which likely corresponds to the energy barrier for APBs to kink to inclined habit planes during growth and self-annihilate.

102
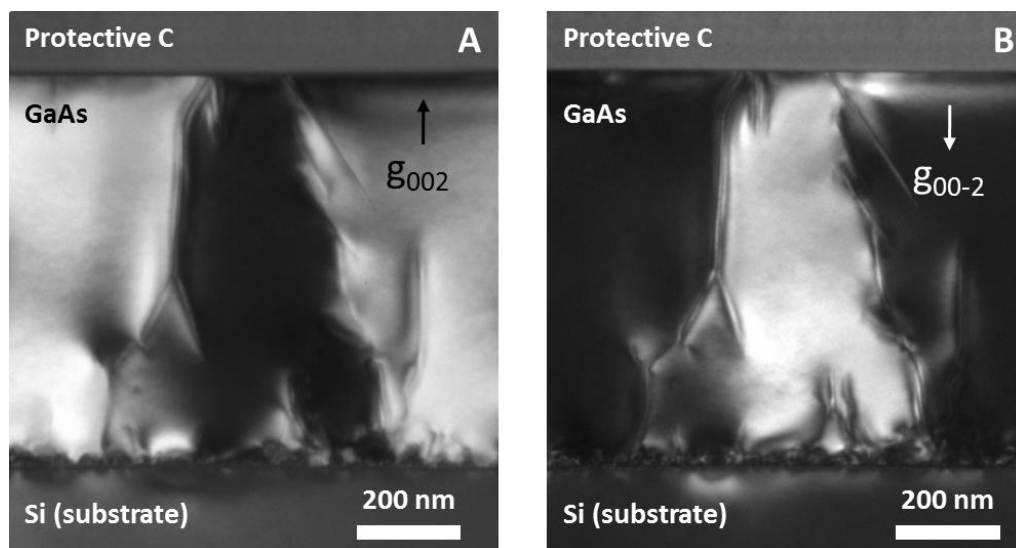
Figure 4-8. Pair of DF XTEM images showing an antiphase domain in a sample with bulk growth at 630 °C. A) DF image using the g_{002} reflection and B) DF image using the $g_{00\text{-}2}$ reflection. The reversal of contrast from A to B demonstrates that this feature is an antiphase domain. There is a net decrease in domain width with increasing GaAs film thickness.
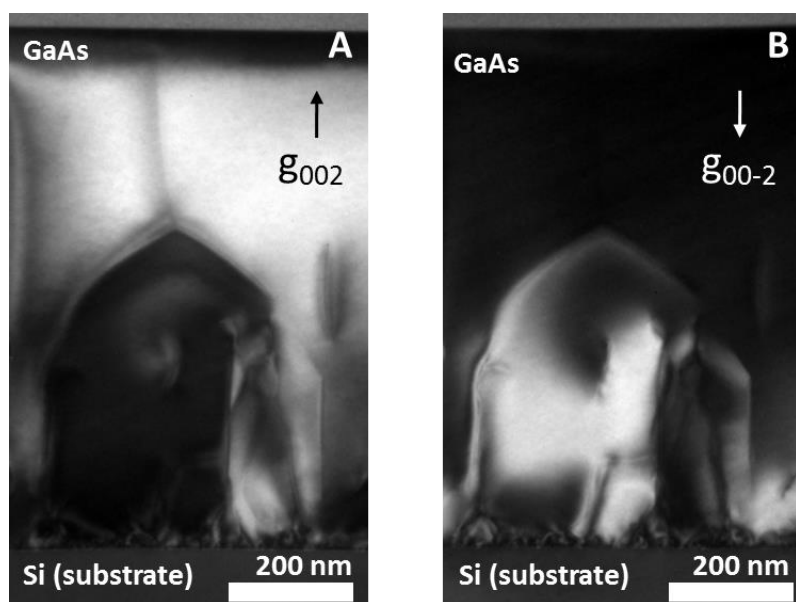
Figure 4-9. Pair of DF XTEM images showing an antiphase domain in the sample with bulk growth at 610 °C. A) DF image using the g_{002} reflection and B) DF image using the $g_{00\text{-}2}$ reflection. The reversal of contrast from A to B demonstrates that this feature is an antiphase domain. The domain is suppressed within the film due to the self-annihilation of APBs along {112} planes.

103
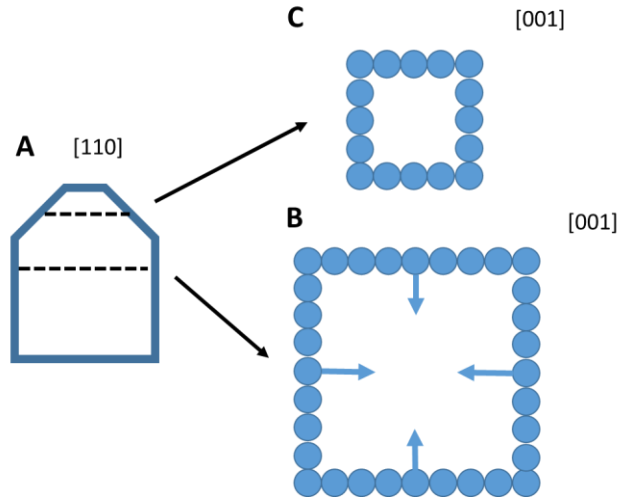
Figure 4-10. Illustration of an annihilating antiphase domain. A) Cross-section of the domain, B) arbitrary (001) section of APBs in the bulk of the domain, and C) arbitrary (001) section of APBs in the annihilating portion of the domain. The kinking of APBs leads to a net reduction in the number of atoms involved in an APB for (001) sections from B to C.
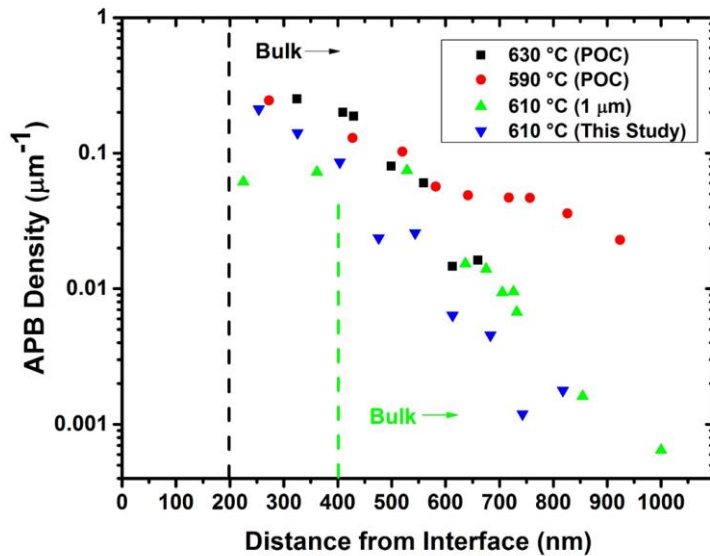
Figure 4-11. Comparison of APB density depth profiles for samples grown at different times with similar conditions as a proof of concept (POC) and with different layer thicknesses (1 µm sample) compared to data from this study. The APB annihilation rates for the high temperature bulk growth samples (≥ 610 °C) are qualitatively similar which demonstrates that there is a consistent saturation point for the annihilation rate, likely stemming from geometric factors.

CHAPTER 5
THE EFFECT OF POST-GROWTH ANNEALING

The following chapter discusses the effect of post-growth annealing on APBs in GaAs films grown on Si. The chapter is broken down into four major sections. The first section discusses the main experiment regarding the annealing effects on APBs in GaAs-on-Si samples with standard preparation and growth conditions, i.e. Siconi^{TM} clean, pre-growth bake, and two-step growth process. The second section discusses the results of annealing samples with varying substrate preparation and growth procedures. The third section discusses the results of varying the annealing conditions on APBs, specifically the type of surface protection used. The fourth and final section will discuss the effect of APB density on Si diffusion from the substrate during annealing.

Samples for annealing were first encapsulated with Al_2O_3 deposited by ALD. Unless otherwise stated, the recipe for Al_2O_3 deposition was a hybrid exposure/plasma mode using water as the precursor for oxygen for the first 0.5 nm (5 cycles) and then oxygen plasma as the oxygen source for the remainder of film growth. The full recipe is given in Appendix A.2. Films thicker than 10 nm made using water as the precursor for the entirety of film growth are prone to having trapped hydrogen [150–152]. The trapped hydrogen can bubble and cause blistering and delamination of the film at elevated temperatures, i.e. during annealing.

5.1 Dissolution of Antiphase Domains by Annealing

5.1.1 Background

GaAs-on-Si will play a vital role in the implementation of III-V materials in future electronic devices. Unfortunately, the crystal quality of GaAs layers grown epitaxially on

Si is typically much worse than bulk GaAs. Threading dislocations from the lattice mismatch and APBs from single-steps on the Si surface degrade the electronic and optical properties of the GaAs layer. Bulk GaAs wafers are too expensive and too small relative to Si wafers for use in large-scale commercial applications. There are avenues for reducing the density of these defects during the growth of the GaAs layers. For threading dislocations, strained-layer superlattices [46–51] and growth on patterned substrates [52–59], known as aspect ratio trapping, have been shown to be effective. For APBs, careful preparation of the Si substrate can reduce the nucleated density [143] and further tuning of the growth temperature can encourage self-annihilation [113, 147]. In addition to changing the growth conditions, defect densities can be reduced via post-growth processing.

Annealing is a common method to reduce defect densities in epitaxial layers, including GaAs on Si, and to improve the overall crystal quality. Post-growth annealing by furnace or RTA has seen extensive use in the semiconductor research field and industry. RTA is used most often over conventional furnace annealing when there are thermal budget restrictions for processing, such as for the activation of dopants without excessive diffusion of the dopant species. However, both techniques can be equally effective in the reduction of grown-in defects for GaAs grown on Si by MBE or MOCVD. The elevated temperatures allow for threading dislocations and atoms in stacking faults and twins to become mobile. These defects add to the free energy of the crystal, so their elimination should be thermodynamically favorable. Furnace annealing in the range of 800 to 850 °C for 10 to 30 min leads to lower densities of dislocations, stacking

faults, and twins in GaAs-on-Si layers [153–156]. RTA is able to accomplish similar decreases in defect densities for treatments at 800 to 950 °C for 10 s [83, 157, 158].

Further studies on the activation energy for threading dislocation reduction has also been performed for GaAs-on-Si. Yamaguchi et al. [159] interrupted the GaAs growth and performed in situ anneals, i.e. in the growth chamber, at 700 to 900 °C under As overpressure and found an activation energy for dislocation density reduction of 1.35 eV. Ayers et al. [138] performed post-growth in situ anneals from 675 to 900 °C under As overpressure and found an associated activation energy for threading dislocation density reduction of 1.91 eV.

The effect of annealing on APBs in III-V films, including GaAs, on Si is not as well studied. Chu et al. [115] found that antiphase domains grew, i.e. APB density was reduced, for highly defective GaAs-on-Si films for furnace anneals from 700 to 800 °C for 2 hrs. No attempt at calculating an activation energy for APB migration was made. Guo et al. [116] investigated the evolution of APBs in GaP films grown on Si using X-ray methods for a single anneal at 600 °C for 10 min. The effect of anneal temperature on APB density was not quantified. The authors concluded that APBs reconstructed from grown-in {111} type orientations to {110} planes. However, this result would indicate that APBs can never be eliminated in III-V films. The goal of this study is to systematically examine the effect of post-growth annealing on APBs in GaAs grown on Si and determine the associated energetics of APB mobility.

5.1.2 Experimental

Samples for this study were taken from a single GaAs-on-Si wafer to ensure that all had experienced similar growth conditions prior to annealing. A 300 mm Si(001) wafer with no intentional misorientation was used as the substrate for GaAs growth. The

Si wafer was cleaned using the Siconi^{TM} process [118] prior to transfer to the growth chamber. A pre-growth bake at ~900 °C was then performed in the growth chamber to help promote the formation of double-steps. This substrate preparation procedure is effective in reducing the density of nucleated APBs [143].

GaAs growth was performed in an Applied Materials III-V MOCVD reactor. The precursors for Ga and As were trimethylgallium (TMGa) and tertiarybutylarsine (TBAs), respectively. The V/III ratio was within the standard MOCVD process range and the chamber was maintained at typical reduced pressure ambient during film growth. GaAs was grown in a standard two-step process. The layer structure is similar to that shown in Figure 3-3. An initial layer of 200 nm of GaAs was grown at 530 °C followed by an additional 200 nm grown at 610 °C. The higher growth temperature layer has the added benefit of accelerating APB annihilation via kinking of APBs to inclined planes [147].

For the annealing treatments, samples were encapsulated with 20 nm of Al_2O_3 deposited at 200 °C by ALD to protect against surface degradation. Figure 5-1 shows a BF XTEM image of a GaAs-on-Si sample annealed at 600 °C for 30 min using this encapsulant. The surface is still very smooth and free of any visible pits after annealing and removing the cap. Anneals for this study were performed at temperatures from 550 to 700 °C for a range of times. Longer anneals (> 5 min) were performed in a tube furnace with Ar ambient and shorter anneals (< 5 min) were performed in RTA with Ar ambient. Test anneals with overlapping times were done to ensure consistency between the furnace and RTA. After annealing, the Al_2O_3 caps were removed by dipping the samples in concentrated pure HF(49%) for 30 s.

The APB densities in as-grown and annealed samples were determined by selective etching of APBs using HF(49%):HNO$_3$(69%):H$_2$O (20:1:7) for 10 s and then imaging in SEM. APB features in SEM images were traced using ImageJ software [132]. The APB density is defined as the total APB line length measured of the total observed surface area, giving units of μm^{-1}. Depth profiling of APB density was also conducted. Samples for depth profiling were simultaneously annealed side-by side for each anneal condition. After removing the Al$_2$O$_3$ caps, a non-selective etchant of CH$_3$OH:H$_3$PO$_4$(85%):H$_2$O$_2$(30%) (10:1:1) was used to etch the GaAs layer in the samples down to various thicknesses. The remaining GaAs film thickness was measured using a JA Woollam M88 ellipsometer. Ellipsometry measurements were in good agreement with select film thickness measurements by XTEM with less than 10 nm of variation. The selective HF/HNO$_3$ was then used to delineate the APBs for imaging in SEM.

5.1.3 Results and Discussion

Annealing treatments had a noticeable effect on the density of APBs at the surface of the GaAs layer. Figure 5-2 shows representative plan view SEM images of the GaAs surface after etching with the APB-selective HF/HNO$_3$ solution for an as-grown sample (A) and a 650 °C, 7.5 min furnace annealed sample (B). The APB density is reduced from 0.10 μm^{-1} to 0.014 μm^{-1} after annealing and there is also a clear decrease in the number of antiphase domains present in a given area. The corresponding histograms of domain size, i.e. APB loop length for a domain, for all domains counted in the as-grown sample and the sample annealed at 650 °C for 7.5 min are shown in Figure 5-2C and Figure 5-2D, respectively. There is a significant

decrease in the average domain size after annealing. It can then be inferred that the APBs must be mobile during the anneal and that the net motion is towards their centers of curvature. This motion eventually leads to self-annihilation.

Figure 5-3 shows the surface APB densities of the GaAs-on-Si samples for all annealing conditions. There is a clear and consistent trend of decreasing APB density with increasing anneal time and temperature. For the higher temperature anneals at 650 °C and 700 °C the APB density decreases very rapidly but plateaus at a nonzero value. These low densities represent an average of one to two antiphase domains present in a given SEM image of approximately 200 μm^2. It is unclear why some domains are still present for relatively long and high temperature anneals. Regardless, over 90% of domains at the surface are eliminated and the APB density is reduced by an order of magnitude.

In order to gain further insight on the evolution of APBs during post-growth anneals, depth profiles of the APB density in GaAs-on-Si samples were obtained for selected anneal conditions of varying time and temperature. Figure 5-4 shows the APB density depth profiles for these annealed samples along with an as-grown sample. In the as-grown sample, the APB density starts very high near the GaAs/Si interface but then drops significantly with the onset of the higher temperature bulk growth layer. This decrease is consistent with the tendency of APBs to kink over from vertical {110} type planes to inclined higher-index planes, e.g. {111} or {112}, and self-annihilate at higher growth temperatures [114, 147]. After annealing at 600 °C for 10 min, it is observed that the APB density closer to the surface of the GaAs layer begins to decrease relative to the as-grown sample. In the middle of the GaAs layer, the APB density remains

110

approximately the same. Thus, it is hypothesized that APBs begin self-annihilating from the surface down during annealing. Further annealing for longer time (30 min) or at a higher temperature (650 °C) reduces the APB density throughout the GaAs layer.

The thermally activated motion and subsequent annihilation of APBs observed for GaAs-on-Si in this study is similar to the motion of APBs that has been investigated in metals and metal oxides. According to the theory established by Allen and Cahn [110], APBs in binary alloys evolve to reduce their curvature and the density of APBs changes with annealing time as $t^{-1/2}$. This time dependence of APB density with annealing has been observed experimentally for epitaxial Fe_3O_4 films grown on MgO [112] and for bulk Cu-Pd alloys [160]. A similar treatment of the APB density evolution data in this study is applied to determine the activation energy of APB motion in GaAs-on-Si. For simplicity, the inverse square of the surface APB density (see Figure 5-3) is plotted against the annealing time. The rate constant for APB motion, k, for the Arrhenius equation $k=k_0*exp(-E_a/k_BT)$ is extracted from the slope and has units of $\mu m^2/s$. Figure 5-5A shows this procedure for the APB density versus annealing time data at 700 °C. This procedure was repeated for the surface APB density data for all other annealing temperatures. Figure 5-5B shows the Arrhenius plot of the natural log of the extracted rate constants versus inverse annealing temperature. From the slope of this curve, the activation energy is determined to be 3.8 eV.

While it is not immediately clear what atomic exchange process facilitates the movement of an APB during annealing, a plausible mechanism can be proposed. The requirements for APB motion involve the breaking of the original antisite bond, either Ga-Ga or As-As, and then the diffusion of the Ga or As atom to an adjacent antisite.

111

This process must also occur nearly simultaneously for numerous antisite bonds for the entire APB plane to move. The activation energy of 3.8 eV determined in this study is very close to the activation energy that has been reported for Ga self-diffusion via Ga vacancies in GaAs of ~4 eV [161–163]. The self-diffusion of As in GaAs is not as well studied, but is also believed to occur via vacancies [164]. Correspondingly, there is a greater thermal equilibrium concentration of vacancies at elevated temperatures. It follows that the motion of an APB during annealing is likely enabled by the presence of nearby vacancies and that the rate limiting step is the diffusion of Ga atoms. The APBs will have a tendency to migrate towards their centers of curvature in order to reduce the total APB interfacial area in the GaAs layer and consequently lower the overall free energy of the system. Figure 5-6 illustrates the possible mechanism for the movement of an APB segment from a {110} configuration to {111} from the diffusion of a Ga vacancy.

It should also be noted that this activation energy for APB diffusion in GaAs-on-Si is much higher than the activation energy previously determined for APB kinking during growth of 1.1 eV [147]. Thus, the reduction of APB density during film growth is expected to be dominated by APB kinking from adatoms aligning along higher-index planes, rather than the diffusive motion of existing APBs. Both processes have a large energetic driving force to reduce the APB interfacial area and decrease the proportion of antiphase to main phase in the GaAs layer. These findings illustrate the need for additional computational analysis of APB systems in GaAs and other III-V materials. Future work should also investigate the effect of in situ annealing with an As overpressure and whether a similar reduction in APB density would occur.

5.1.3 Summary

In summary, it was shown that APBs in GaAs grown on planar Si(001) can be removed by ex situ post-growth annealing. APB evolution at the surface of the GaAs layer followed the $t^{-1/2}$ time dependence established by Allen and Cahn [110]. At annealing temperatures of 650 °C and above, the surface APB density was decreased by an order of magnitude in less than 10 min. The activation energy for APB migration at the surface during annealing was determined to be 3.8 eV. The motion of APBs is believed to be limited by Ga diffusion via vacancies. Depth profiles of APB density for annealed samples confirmed that the dissolution process starts at the surface and that the APBs were being removed throughout the GaAs layer. The energetic driving force for the migration of APBs can be understood by a reduction in the total APB interfacial area. Since it is difficult to prevent the nucleation of APBs on Si(001) wafers with no intentional off-cut or high temperature pre-growth treatments, the ability to greatly reduce the grown-in APB density with relatively little additional processing is advantageous.

5.2 Effect of Sample Conditions

5.2.1 Background

The results discussed in section 5.1 are considered to be for a low starting APB density sample with standard growth conditions, i.e. high temperature bulk growth. This section will discuss the results of annealing samples with varying starting APB densities and growth conditions. The samples include two samples with high starting APB densities, one with large domains and extended APBs and one with mostly discrete domains, and a low density sample with low temperature bulk growth.

5.2.2 Experimental

All additional samples were grown on 300 mm Si(001) wafers with no intentional off-cut in an Applied Materials III-V MOCVD system. The growth conditions, unless otherwise stated, are identical to those stated in section 5.1.2. All samples were cleaned using the Siconi^{TM} process prior to growth. The layer structure for the two high density samples is the same as that shown in Figure 3-3, i.e. 200 nm grown at 530 °C followed by 200 nm grown at 610 °C. The high APB density in these samples was caused by changing the pre-growth bake conditions. The layer structure for the low density, low temperature bulk growth sample is similar to that shown in Figure 4-2 except that the total ~800 nm of growth was completed at 530 °C. A standard pre-growth bake at ~900 °C was used for this sample.

The processing conditions for annealing and characterization are also identical to those stated in section 5.1.2. Briefly, samples were encapsulated with 20 nm of Al_2O_3 by ALD and annealed in a tube furnace with Ar ambient. APBs were selectively etched for imaging in SEM using the HF/HNO_3 solution. Non-selective etching with H_3PO_4/H_2O_2 was used for depth profiling of APB density.

5.2.3 Results

5.2.3.1 High density samples

Figure 5-7 shows representative plan view SEM images of the high starting APB density sample with the largest domains as-grown (A) and then after annealing at 700 °C for 30 min (B) and 4 hrs (C). The APB density decreases in these images from the as-grown value of 3.3 μm^{-1} to 2.6 μm^{-1} to 2.4 μm^{-1}, respectively. Along with the overall decrease in APB density, the APBs appear to become more rounded with annealing compared to as-grown. This observation is not surprising if the evolution of APBs is

driven by a reduction in curvature, following the Allen-Cahn theory [110]. The APBs that loop around an antiphase domain should follow a much less tortuous path and smooth out over time. Figure 5-8 shows the surface APB density results of all anneals for this sample at 650 and 700 °C for various times. The largest decrease occurs within the first 30 min of annealing which agrees with the qualitative observations in the SEM images. The APB density appears to plateau after this point. This appearance of a plateau is likely due to the annihilation of smaller domains within the first 30 min of annealing and the comparatively much slower annihilation of larger domains since the APBs must diffuse over a longer distance to annihilate the domains.

Anneals performed on separate occasions for this high density sample led to much more noticeable rounding of APBs. Figure 5-9 shows representative plan view SEM images of the APB density after annealing at 700°C for 2 hrs (A) and 750 °C for 1 hr (B). Some domains appear to be nearly circular in shape. It should be noted that these specific specimens were encapsulated with Al_2O_3 entirely with water as the oxygen precursor. Therefore, it is possible that there was a cap failure that led to disparate annealing conditions. However, it is interesting that this degree of rounding is possible. Also, this rounding again would be consistent with Allen-Cahn theory for the minimization of free energy. If annealing was extended for infinite time and temperature, it is expected that the antiphase domains would all decrease in diameter and eventually become circular before completely annihilating.

Representative plan view SEM images of the second high density sample with more discrete domains are shown in Figure 5-10 for the sample as-grown (A) and then after annealing at 700 °C for 1 hr (B) and 4 hrs (C). The decrease in APB density with

115

annealing is noticeable along with the decrease in number of antiphase domains visible. The APBs also become more rounded with annealing, similar to the previous high density sample. Figure 5-11 shows a plot of the surface APB densities for all of the annealing conditions for this sample. There is a consistent trend of decreasing APB density with increasing anneal time and temperature. However, the APB density decrease appears to slow after ~1 hr of annealing time. To test whether this was an effect of smaller domains being eliminated initially and slower annihilation of larger domains, counts of domain size versus annealing were made for select conditions. Figure 5-12A shows a graph of domain counts for as-grown and after annealing at 700 °C for 30 min and 4 hrs. The domain counts are separated into categories of small domains for those less than 2 μm in APB loop length and large domains for those greater than 2 μm in APB loop length. Figure 5-12B shows how the ratio of small to large domains changes with annealing conditions. From these two plots, it can be concluded that small domains are in fact annihilated much more rapidly than large domains. This result is intuitive based on the longer distance APBs looping around a larger domain would have to diffuse in order to annihilate the domain. The much quicker annihilation of smaller domains leads to plateaus in APB density decreases for extended annealing times.

5.2.3.2 Low temperature bulk growth sample

The low starting APB density sample with low temperature bulk growth is the same sample used in the growth temperature study in Chapter 4 with bulk growth at 530 °C. Figure 5-13 shows a representative plan view SEM image of the as-grown surface APB density for this sample. Anneals were performed on this sample in order to

determine whether a similar decrease in APB density as seen by raising the bulk growth temperature could be replicated through post-growth annealing. To this end, analysis of this sample focused on through-thickness APB density.

Figure 5-14 shows the through-thickness APB density depth profiles for the low temperature bulk growth sample as-grown and after annealing up to 30 min at 600 to 650 °C. At first glance, it is apparent that the APB density for the annealed samples is always lower compared to the as-grown sample and the degree of decrease correlates with increasing anneal time and temperature. However, the profiles do not indicate a steady decrease in APB density, i.e. APB annihilation from the surface down, as was seen for the annealed sample in section 5.1.3 (Figure 5-4), nor do they match the profiles for samples grown at higher bulk growth temperatures in section 4.3.1 (Figure 4-4). In some cases for the annealed profiles, e.g. 650 °C for 30 min, the APB density is markedly lower towards the GaAs/Si interface than at the surface of the film. This unusual trend indicates that APBs may be being pinned at the GaAs/Al_2O_3 interface for this sample and antiphase domains are being pinched off in the bulk of the GaAs film.

Further investigation of APB evolution in this sample after annealing was performed with XTEM. Figure 5-15 shows a pair of DF XTEM images of the low temperature growth sample after annealing at 600 °C for 30 min under a g_{002} condition (A) and a g_{00-2} condition (B). A domain can be observed near the surface of the GaAs film. The reversal of contrast from the g_{002} to g_{00-2} condition indicates this feature is an antiphase domain. The antiphase domain is terminated towards the middle of the GaAs film. This occurrence can only be an effect of the anneal, as the spontaneous nucleation of an APB during growth would be highly energetically unfavorable. The shape of this

117

domain, particularly the wider diameter at the GaAs surface, indicates that the APBs

may have been pinned at the GaAs/Al$_2$O$_3$ interface during the anneal. At the GaAs/Si

interface, another domain-like feature is observed directly under the pinched-off portion

of the previously mentioned antiphase domain. This domain is likely indicative of where

the first antiphase domain nucleated. The antiphase domain was then pinched-off

during the anneal, leaving two separate portions of antiphase domains in the GaAs

layer. These observations support the results of the APB density depth profiles.

5.2.4 Discussion

The evolution of the high APB density samples during annealing was consistent

with the results from section 5.1 for the low density sample with standard growth

conditions. The surface APB density decreased with increasing annealing time and

temperature. APBs were observed to smooth out with annealing, i.e. forming less

tortuous loops around antiphase domains, indicating that they were evolving to reduce

their curvature. This reduction in curvature and in turn the reduction in APB density

lowers the free energy of the system. Eventually, antiphase domains are eliminated due

to APB self-annihilation.

The evolution of APB density in the low density sample with low temperature bulk

growth was more curious. Through-thickness APB density depth profiles showed that

APB annihilation occurred more rapidly and efficiently in the bulk of the GaAs film,

rather than from the surface down. The XTEM analysis supports a conclusion that APBs

are being pinned at the GaAs/Al$_2$O$_3$ during annealing leading to pinched-off domains.

The results indicate that the grown-in character of APBs and the surface conditions

during annealing may play a role in APB mobility and annihilation. APBs for this sample

with growth completely at a low temperature should tend to {110} type configurations,

rather than the inclined habit planes that are preferred at higher growth temperatures [114, 147] (see Chapter 4). It is possible that {110} APBs are more difficult to diffuse, i.e. they are more energetically stable, with high temperature post-growth treatments compared to higher index plane APBs, e.g. {112}. This hypothesis is supported by the lower formation energy of {110} APBs over higher index planes [92]. Thus, it may be required for more efficient annihilation of APBs with annealing for the APBs to already be configured along relatively energetically unstable planes, i.e. higher index planes, due to high bulk growth temperatures. The effect of the surface conditions during annealing will be expanded upon in section 5.3; briefly, {110} APBs may be even more stable at the surface of the GaAs film during annealing compared to the bulk, leading to the appearance of APB pinning at the surface.

5.2.5 Summary

APBs are driven to annihilation with increasing annealing time and temperature regardless of the starting APB density for GaAs films grown on Si. The APB density in high starting density samples decrease with increasing annealing time and temperature. The results support the notion that the equilibrium state for the film should be APB-free. The driving force for APB evolution with annealing is a reduction in curvature and a corresponding decrease in the total APB interfacial area. It was also observed that the sample growth conditions, particularly the growth temperature, appear to affect the nature of APB annihilation with post-growth annealing. That is, APB annihilation occurs with annealing more readily if the APBs are already configured along higher index planes, e.g. {112}, rather than {110} planes. Through-thickness APB density depth profiles of a sample with low temperature bulk growth indicated that APBs were being pinned at the surface of the GaAs film. XTEM analysis supported this theory and

showed an antiphase domain that had the appearance of propagating from the surface down and was terminated in the middle of the film. The surface conditions during annealing may also play a role in this pinning effect.

5.3 Effect of Annealing Conditions

5.3.1 Background

Protecting the surface against degradation is an important aspect of annealing GaAs films or substrates. Arsenic has a relatively high vapor pressure and is prone to leave the surface, leading to the formation of pits [120]. The Al_2O_3 films used in this study provide a diffusion barrier against As outgassing. An As overpressure can also be provided to prevent the loss of As during annealing by flowing As vapor or gas. A more practical means of providing an As overpressure is to use a proximity cap, i.e. place another piece of GaAs on top of the sample. The loss of As is limited by outdiffusion from between the two contacted surfaces which leads to a local As overpressure [165]. Proximity capping has the additional advantage over depositing encapsulant materials of reducing the processing time needed for preparing samples for annealing. The effect of the surface conditions during annealing, i.e. the type of cap used, on the stability of APBs in GaAs films grown on Si was investigated in this experiment.

5.3.2 Experimental

Two separate samples were used for this experiment. The first sample was the low temperature bulk growth sample from Chapter 4, the growth temperature study. This low temperature bulk growth sample has the layer structure shown in Figure 4-2. Growth was conducted completely at 530 °C for a nominal film thickness of ~800 nm. The second sample for this experiment was the same used in section 5.1 for the annealing study. This high temperature bulk growth sample has the layer structure

shown in Figure 3-3. Bulk growth for 200 nm was conducted at 610 °C and the total film thickness was ~400 nm. These samples will henceforth be referred to as the low temperature sample and high temperature sample, respectively. The samples were chosen because they have comparable surface APB densities after growth.

Surface protection during annealing was provided either by a 20 nm Al_2O_3 cap deposited by ALD or a proximity cap. The proximity cap was a sacrificial GaAs coupon from a semi-insulating GaAs wafer. The presence of native oxide on the GaAs proximity cap and the sample was found to not have a significant effect on APB density after annealing. Therefore, the native oxide was not stripped from the samples or the cap prior to the anneals discussed here.

APB density after annealing was analyzed using the selective HF/HNO_3 etchant and SEM. Anneals were performed at 600 for times up to 30 min in a tube furnace with flowing Ar ambient.

5.3.3 Results

Figure 5-16 shows representative plan view SEM images of the APB density in the low temperature sample as-grown (A) and then after annealing at 600 °C for 30 min with a proximity cap (B) and an Al_2O_3 cap (C). There is a large disparity in the APB density and the number of domains visible at the surface after annealing this sample with the different caps. The APB density in the proximity capped sample is nearly the same as the as-grown sample. On the other hand, significant reduction in APB density is observed for the sample that was capped with Al_2O_3 during the anneal. Therefore, the proximity cap conditions appear to worsen the pinning of APBs at the GaAs surface during annealing. This APB pinning was already suspected for this sample when an Al_2O_3 cap was used (see section 5.2). The surface APB densities after the full series of

121

anneals at 600 °C for the low temperature sample with different caps is shown in Figure 5-17. The APB density for an Al_2O_3 cap experiences a steady decay with increasing annealing time, while the APB density for the proximity cap does not change. In other words, there is negligible mobility of APBs at the surface of the GaAs film during annealing for the low temperature sample when a proximity cap is used.

The effect of the proximity cap on APB dissolution during annealing was also examined for the high temperature sample. Figure 5-18 shows the results of the surface APB densities for this sample after annealing compared to the low temperature sample under the same conditions. The APBs in the high temperature sample are clearly still mobile at the surface even with a proximity cap. This result provides further evidence that the grown-in nature of the APBs, i.e. the APB habit planes, affects their stability during annealing. In fact, the difference in grown-in APB habit planes can be seen by directly comparing the as-grown samples. Figure 5-19 shows representative plan view SEM images of antiphase domains in the low temperature sample (A) and the high temperature sample (B). The APBs in the low temperature sample have a tendency to facet along {110} orientations which is expected at low growth temperatures due to the low formation energy of these APB planes. On the other hand, the APBs in the high temperature sample are not as obviously faceted, giving the appearance of antiphase domains with rounder shapes. These APBs in the high temperature sample are likely already propagating on higher index planes when they reach the GaAs surface.

5.3.4 Discussion

The surface conditions during the anneal appear to have an effect on the mobility of APBs. The surface conditions of a GaAs film annealed with a proximity cap can be considered to be As-rich due to the local As overpressure. Self-diffusion in GaAs is

known to be affected by whether the local conditions are intrinsic, Ga-rich, or As-rich [163, 166]. This effect arises from the relative stability of Ga vacancies that are the primary mediators of diffusion. As-rich conditions in particular support the formation of Ga vacancies [161]. The stability of antisite defects, which are the constituents of APBs, is also affected by the local conditions. Recent DFT calculations by Chroneos et al. [99] showed that the formation energy of As_{Ga} and Ga_{As} antisite defects change whether the conditions are Ga-rich, As-rich, or stoichiometric. As conditions become more As-rich the formation energy of As_{Ga} is lowered and for more Ga-rich conditions the formation energy of Ga_{As} is lowered. Thus, it is logical to conclude that the relative stability of point defects, i.e. vacancies and antisite defects, under given annealing conditions will affect the mobility and subsequent annihilation of APBs. The magnitude of this effect is also apparently influenced by the grown-in nature of APBs, i.e. the APB habit planes.

5.3.5 Summary

The mobility and subsequent dissolution of APBs in GaAs-on-Si films during annealing is affected by the surface conditions. APB pinning at the GaAs surface was exacerbated when a proximity cap was used compared to an Al_2O_3 cap. This effect likely stems from the influence of the local As overpressure with the proximity cap conditions on the relative formation energy and stability of point defects, such as the antisite defects that compose APBs. A secondary effect on APB mobility is the grown-in APB habit plane. These results demonstrate that the most efficient APB dissolution for post-growth annealing will occur for samples grown at a high bulk growth temperature and that are processed with Al_2O_3 encapsulating films instead of proximity caps.

5.4 Effect of APB Density on Si Diffusion

5.4.1 Background

The growth of GaAs on Si by definition creates a diffusion couple. There is a nonzero diffusivity of Ga and As atoms into Si and for Si atoms into GaAs at elevated temperatures [167]. In particular, the diffusion of Si atoms into the GaAs layer from the substrate can be enhanced by the presence of extended defects stemming from the GaAs/Si interface, e.g. grain boundaries and dislocations [13, 44]. Si concentration in GaAs epitaxial layers grown on Si has been correlated to the dislocation density in the layers [168]. Further, the diffusion coefficient of Si in GaAs for annealed GaAs-on-Si layers is enhanced for thinner films, i.e. those with higher defect densities [169]. Impurity atoms are known to be preferentially segregated to APBs in order to decrease the degree of crystal distortion and total free energy [11]. It follows that the APB density in epitaxial GaAs layers may have an effect on the diffusion of Si from the substrate during annealing treatments.

5.4.2 Experimental

Two GaAs-on-Si samples with varying APB density were chosen to compare the effect of APBs on Si diffusion from the substrate. Both samples were grown on 300 mm (001) oriented Si wafers with no intentional off-cut. The wafers were cleaned using the Siconi^{TM} process [118] prior to GaAs growth. After transferring the wafers to the growth chamber, the pre-growth bake at 900 °C was varied to affect the step doubling, and thus the nucleated APB density. GaAs films with a nominal thickness of 400 nm were grown in an Applied Materials III-V MOCVD system. The growth conditions for both samples were identical to those stated in section 5.1.2. The layer structure is the same as that

shown in Figure 3-3. First, 200 nm of GaAs is grown at 530 °C followed by 200 nm of GaAs grown at 610 °C.

Annealing was performed in a tube furnace at 650 °C for 15 min and 2 hrs with flowing Ar ambient. Annealed samples were capped with 20 nm of Al_2O_3 deposited by ALD. The APB density in the samples was analyzed using the selective HF/HNO_3 etchant and SEM. The GaAs layers were compared in XTEM after cutting out samples in a FIB and imaging with a JEOL 2010F TEM operating at 200 kV. SIMS was performed to determine the amount of Si diffusion in the layers as a function of annealing time. Samples for SIMS were sputtered with Cs^+ ions. XRD was performed with a Panalytical Xpert MRD system to compare the structural quality of the layers.

5.4.3 Results and Discussion

Figure 5-20 shows the as-grown surface APB densities in the low density (A) and high density (B) samples. The low density sample has a starting APB density of 0.10 μm^{-1} and the high density sample has a starting APB density of 2.8 μm^{-1}. Figure 5-21 shows BF XTEM images of the low density sample (A) and the high density sample (B). There is no apparent difference in the density of defects besides for APBs. The GaAs layer thicknesses are also approximately the same. The difference in APB density is large enough to analyze the effect of APBs on Si diffusion from the substrate.

The SIMS profiles of Si concentration in the GaAs layers is shown in Figure 5-22 for the low density sample (A) and the high density sample (B) for as-grown conditions and after annealing at 650 °C for 15 min and 2 hrs. For the low density sample, it is difficult to differentiate the Si concentration profiles for each condition. The effect of annealing is most obvious for the sample annealed for 2 hrs. At the location of the

GaAs/Si interface (depth of ~400 nm) for the low density sample, there is an apparent shoulder in the Si concentration profile after annealing at 650 °C for 2 hrs. The total Si concentration in the GaAs layer near the interface tends to increase with increasing annealing time. The effect of annealing is more pronounced for the high density sample. The total Si concentration in the GaAs layer increases with increasing annealing time. Figure 5-23 compares the Si concentration profiles after annealing at 650 °C for 2 hrs for the low density and high density samples. It is apparent that Si diffusion from the substrate is enhanced for the sample with higher APB density compared to the sample with low APB density.

To further rule out the effect of other defects on the enhanced Si diffusion from the substrate, XRD analysis was performed. Figure 5-24 shows the (002) (A) and (004) (B) rocking curves for the low and high density samples. The (002) rocking curve should be sensitive to the degree of antiphase disorder in the samples. However, the profiles are very similar for both samples. It is likely that most of the antiphase domains in the high density sample are too large to be detected by XRD (>300 nm) [13, 116]. The (004) peak is sensitive to defect density and the overall crystalline order in the GaAs layer without contribution from antiphase domains. The (004) profiles for both samples are also very similar in peak intensity and shape. The similarity between these two profiles indicates that the defect density (other than antiphase domains) and crystal quality is also very similar. Thus, the difference in Si diffusion from the substrate (Figure 5-23) is less likely to be from factors other than the difference in APB density between the samples.

The caveat to these results is that APBs are simultaneously being dissolved during annealing while Si is diffusing into the GaAs layer from the substrate along APBs. Based on the results of the annealing experiments previously discussed in sections 5.1 and 5.2, it can be assumed that APBs are still prevalent in the high density sample, while they are likely most dissolved in the low density sample after 2 hrs of annealing at 650 °C. It is unclear what role this effect plays on Si diffusion, although it would likely lead to an even greater difference in Si diffusion for the high versus low APB density samples.

5.4.4 Summary

The diffusion of Si from the substrate for GaAs-on-Si films is enhanced during annealing treatments by the presence of APBs. SIMS analysis showed that after annealing at 650 °C for 2 hrs, there was markedly higher Si concentration in the GaAs layer for the sample with a starting APB density of 2.8 μm^{-1} compared to the sample with a starting APB density of 0.10 μm^{-1}. XRD analysis indicated that the difference in Si diffusion from the substrate between the two samples is more likely to be from the difference in APB density than from any other defects, e.g. threading dislocations.

5.5 Summary of Findings for the Chapter

It is possible to annihilate APBs in GaAs layers grown on Si through post-growth annealing treatments. APBs diffuse in order to reduce their curvature and minimize the total APB interfacial area. It is unclear what the exact atomic mechanism is that facilitates the motion of an APB. However, APBs are clearly energetically unstable in GaAs and there is an energetic driving force for their dissolution. The stability of APBs in GaAs is affected by the grown-in nature of the APBs, i.e. the APB habit planes, and

the surface conditions during annealing, i.e. when an Al_2O_3 cap is used versus a proximity cap. Si diffusion from the substrate is enhanced during annealing by the presence of APBs. The Si-Ga and Si-As bonds are energetically preferred over the wrong Ga-Ga and As-As bonds at an APB.
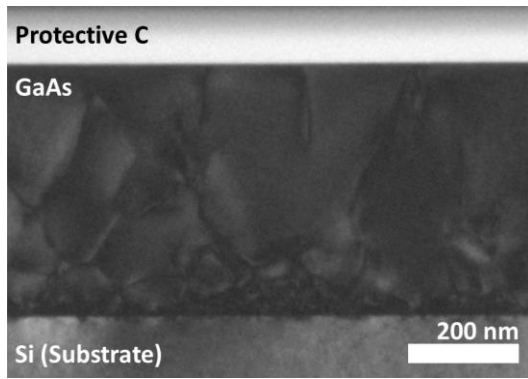
Figure 5-1. BF XTEM image of of a GaAs-on-Si sample annealed at 600 °C for 30 min with 20 nm of Al$_2$O$_3$ as a capping layer. There are no visible signs of surface degradation.
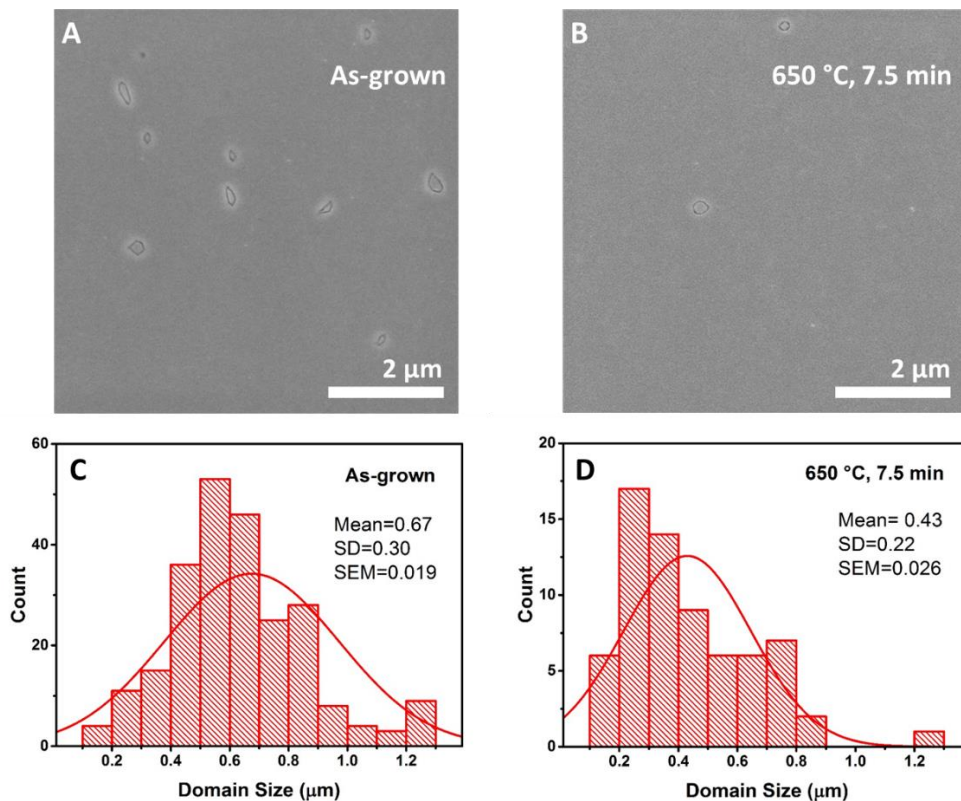
Figure 5-2. Evolution of APB density and domain size with annealing. Representative plan view SEM images of the surface APB density in the GaAs layer A) as-grown and B) after annealing at 650 °C for 7.5 min. There is a clear reduction in the number of antiphase domains visible after annealing. The corresponding histograms of domain size C) as-grown and D) after annealing show that the average domain size is also decreasing.
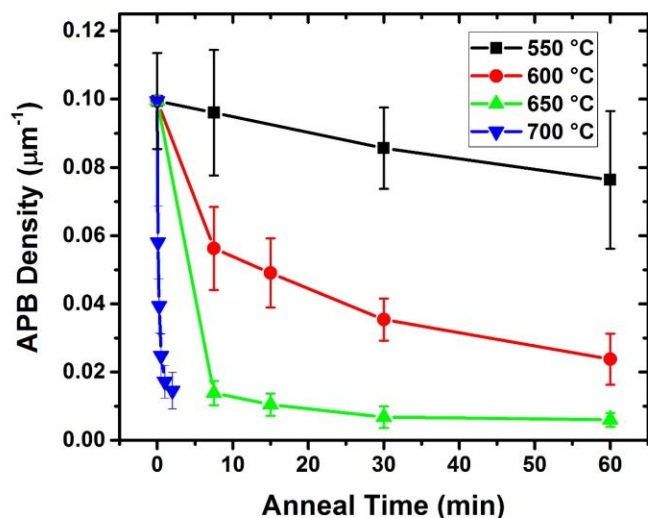
Figure 5-3. Plot of surface APB densities for samples with varying annealing times and temperatures. There is a consistent trend of decreasing APB density and increasing annealing time and temperature.
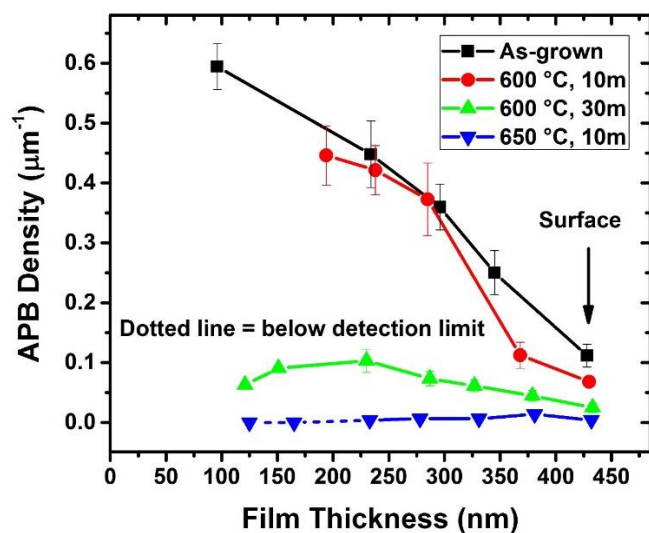
Figure 5-4. Depth profiles of APB density for samples as-grown and with varying annealing conditions. After annealing at 600 °C for 10 min, there is a noticeable decrease in APB density towards the GaAs surface. After annealing for longer time or at higher temperature, the APB density decreases throughout the GaAs layer. The annihilation of APBs during annealing may propagate from the surface down.
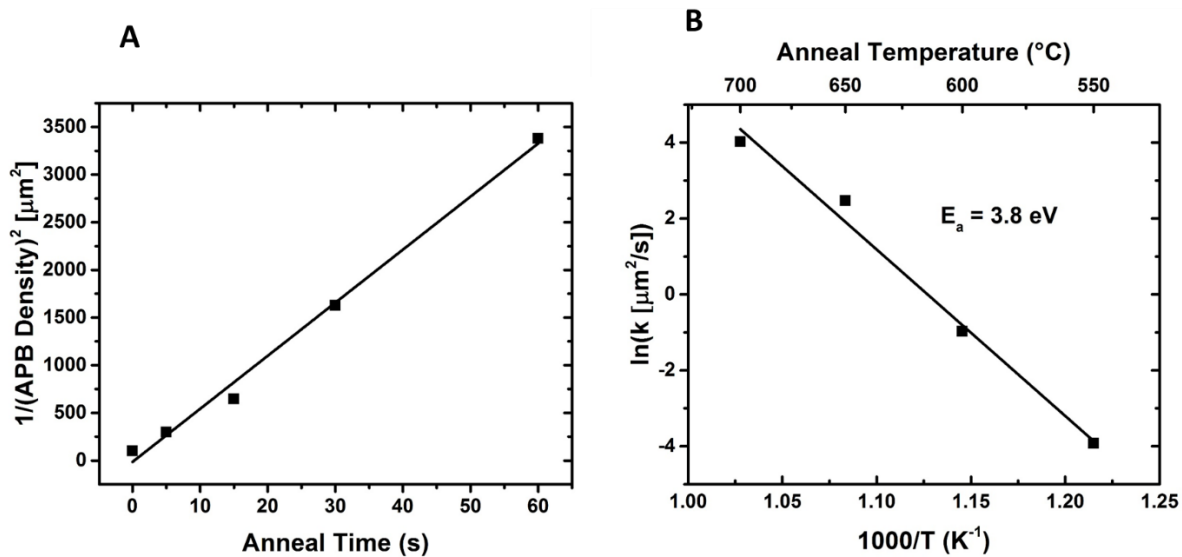
Figure 5-5. Example of the fitting procedure for APB density versus annealing time. A) Data for sample annealed at 700 °C. The rate, k, is extracted from the slope. B) The Arrhenius plot of all extracted rates for varying anneal temperature is shown. The corresponding activation energy is 3.8 eV.
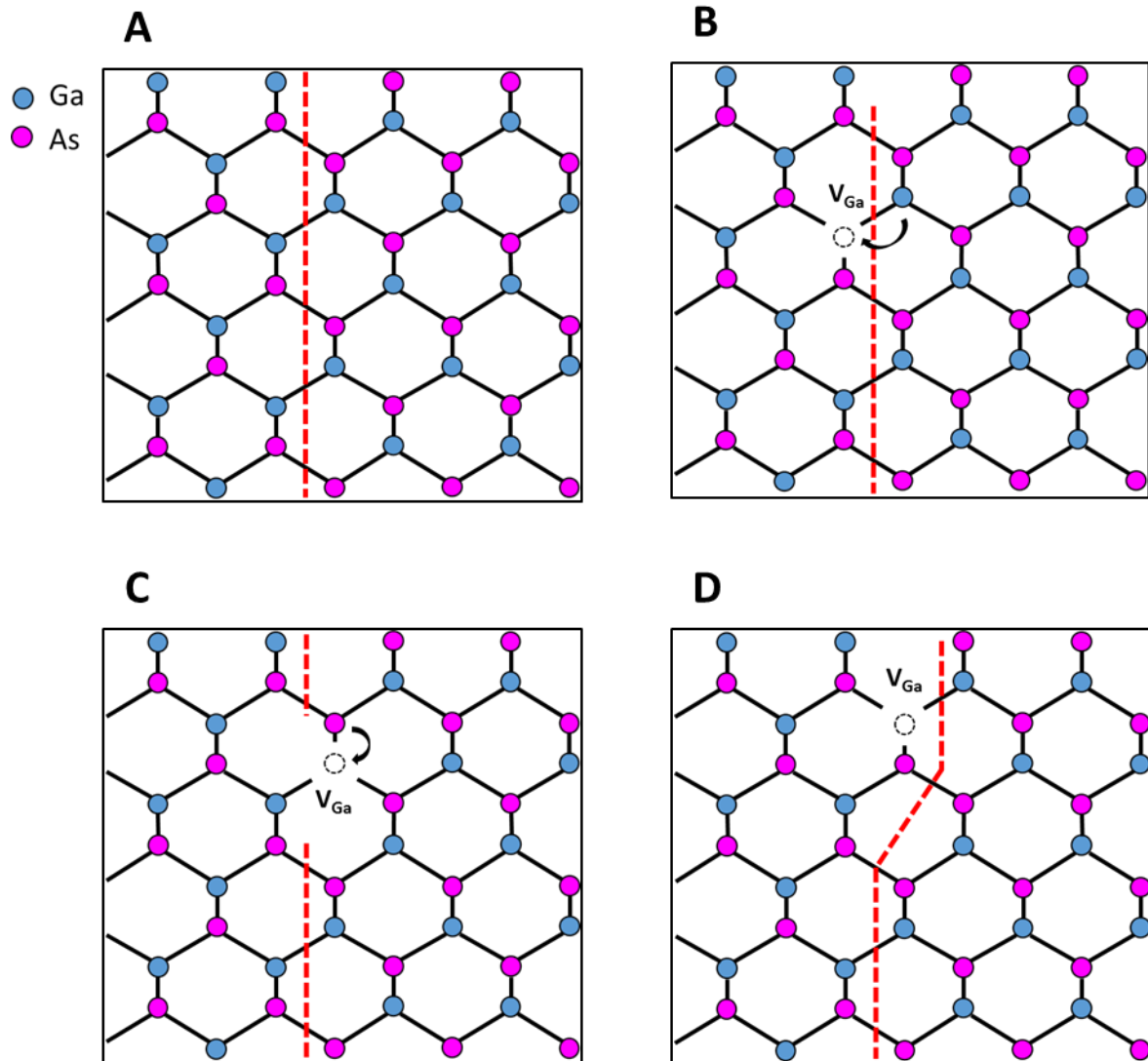
Figure 5-6. Illustration of a possible mechanism for the movement of an APB segment from a {110} configuration to a {111} configuration via the diffusion of a Ga vacancy (V_{Ga}). A) Original structure with {110} APB, B) generation of Ga vacancy, C) diffusion of Ga vacancy to neighboring site, and D) further diffusion of Ga vacancy and consequential development of a {111} kink.
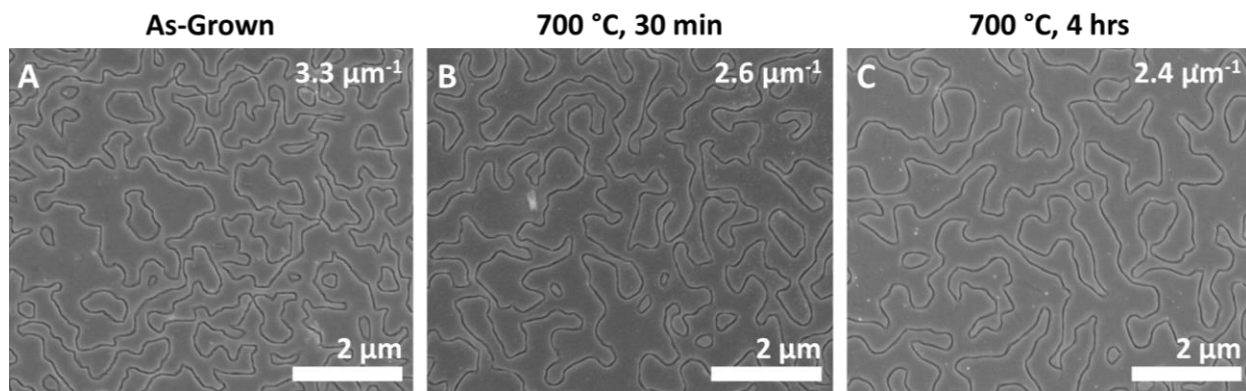
Figure 5-7. Representative plan view SEM images of APB density in highly defective
         sample as-grown and after annealing. A) Sample as-grown, B) after
         annealing at 700 °C for 30 min, and C) after annealing at 700 °C for 4 hrs.
         The APB density decreases from 3.3 μm^{-1} to 2.6 μm^{-1} to 2.4 μm^{-1},
         respectively, and APBs become noticeably rounder with annealing.
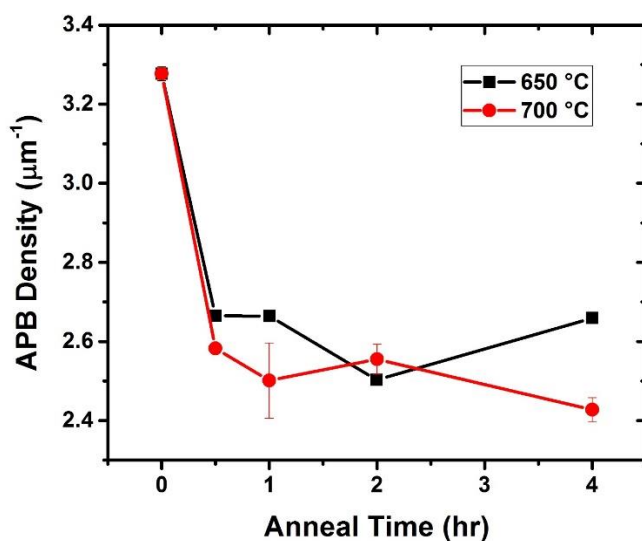
Figure 5-8. Plot of surface APB densities for high starting APB density sample for
         various annealing conditions. There is a large decrease in APB density after
         annealing for 30 min, but then the density plateaus. The plateau is likely an
         artifact of smaller domains being annihilated from 0-30 min of annealing and
         the slower motion and annihilation of large APBs and domains.

133

700 °C, 2 hrs   **750 °C, 1 hr**
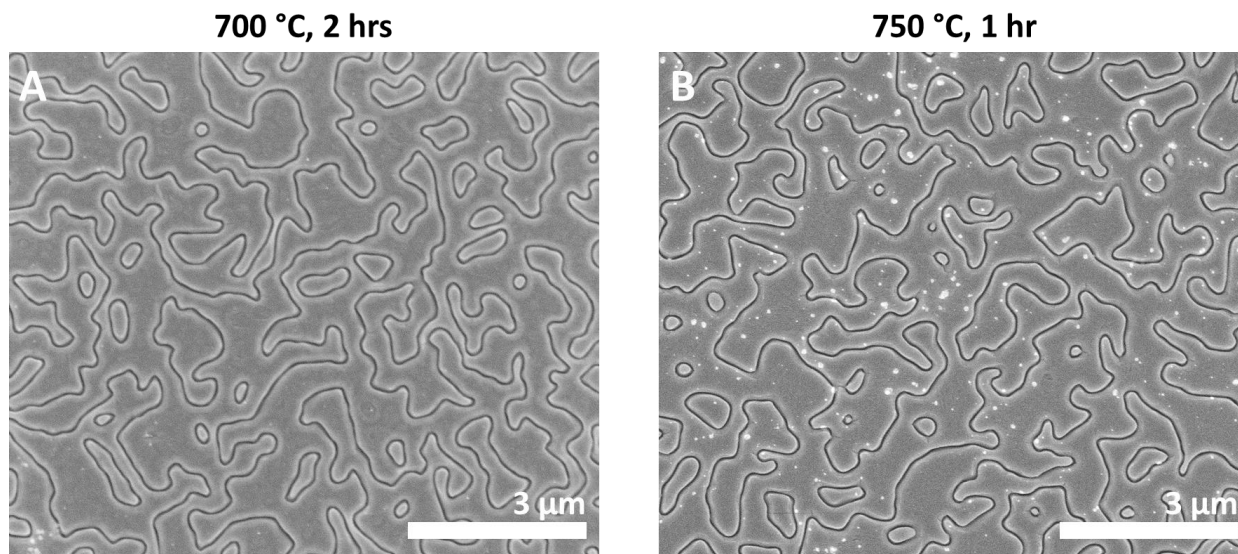
Figure 5-9. Representative plan view SEM images of high starting APB density sample after annealing at 700 °C for 2 hrs A) and 750 °C for 1 hr B). There is much more noticeable rounding of APBs after annealing for these samples and some domains even appear circular. The rounding demonstrates the evolution of APBs to minimize free energy in accordance with Allen-Cahn theory.

As-Grown   **700 °C, 1 hr**   **700 °C, 4 hrs**
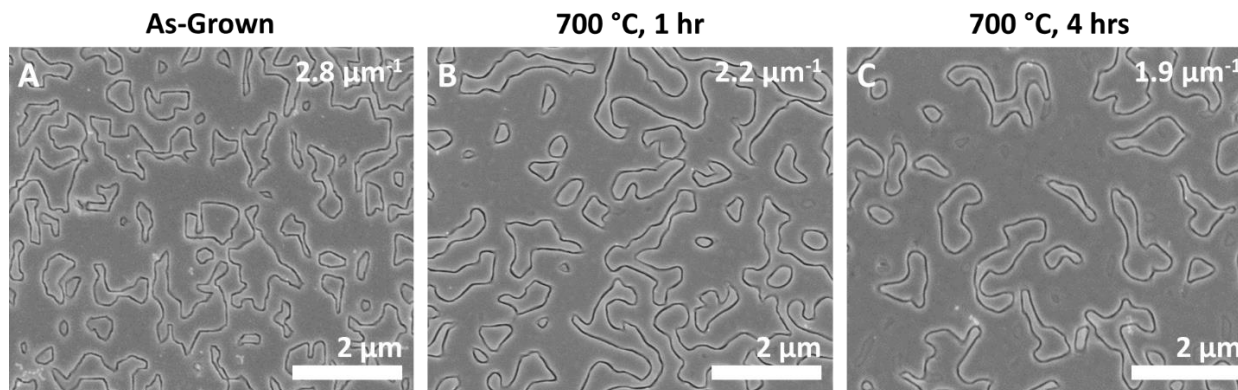
Figure 5-10. Representative plan view SEM images of the APB density in a highly defective sample with more discrete domains as-grown A), after annealing at 700 °C for 1 hr B) and then 4 hrs C). There is a noticeable rounding of APBs and an overall decrease in APB density.
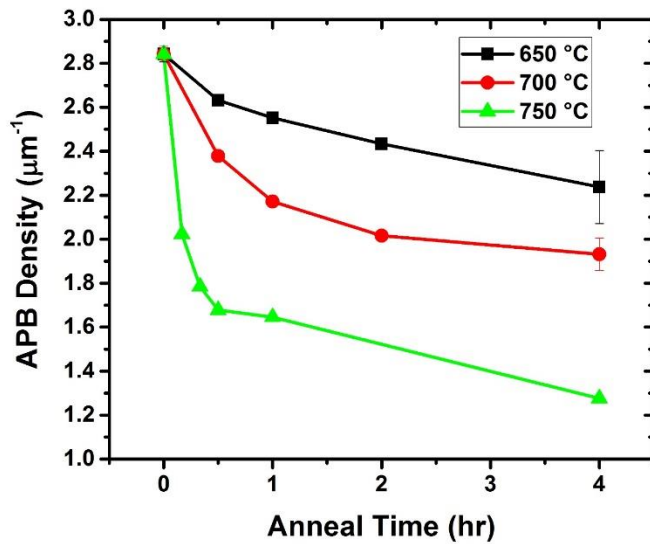
Figure 5-11. Plot of surface APB densities for sample with high starting density and discrete domains after various annealing treatments. There is a consistent trend of decreasing APB density with increasing annealing time and temperature. The rate of APB density decrease appears to slow after ~1 hr of annealing time likely from the faster elimination of smaller domains.
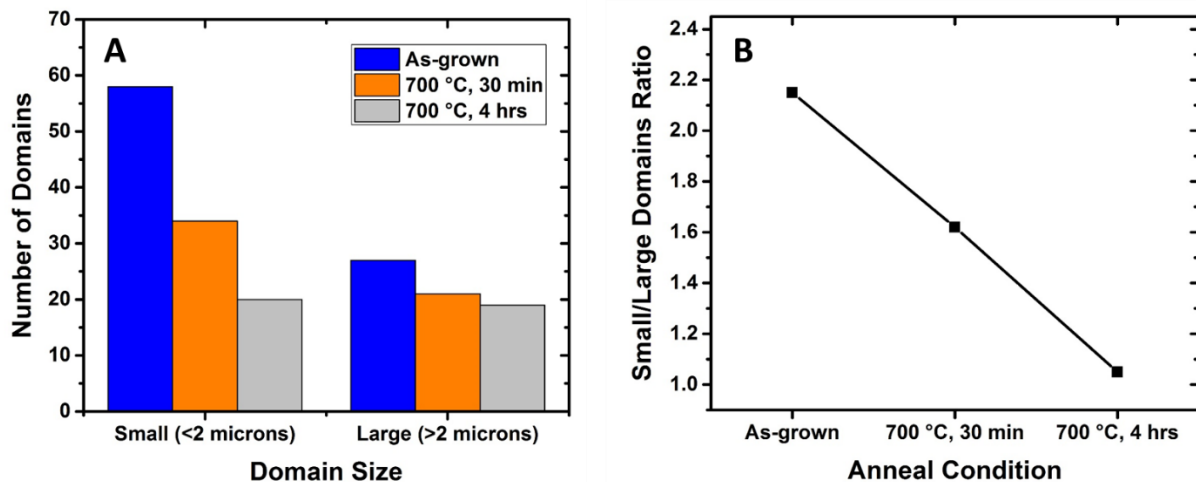

Figure 5-12. Evolution of large and small antiphase domains in high density sample with annealing. A) Histogram of domain size as-grown and after annealing separated into categories of small and large domains. B) The ratio of small to large domains decreases with annealing indicating that small domains are in fact annihilated much more rapidly than large domains. This difference leads to apparent plateaus in APB density for extended annealing times.
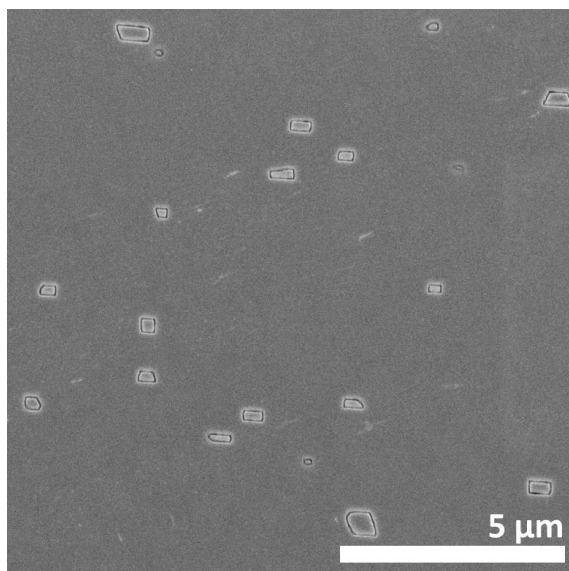
Figure 5-13. Representative plan view SEM image of APB density in a sample grown entirely at a low temperature of 530 °C.
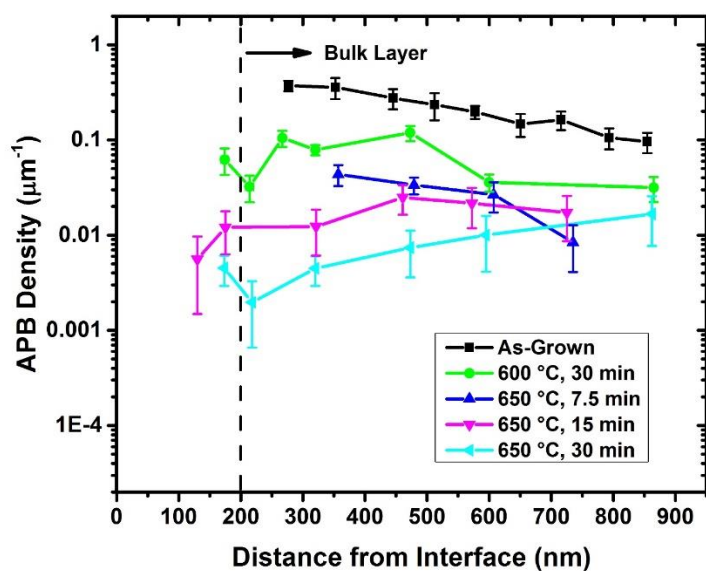
Figure 5-14. APB density depth profiles for the low temperature growth sample as-grown and after various annealing treatments. The APB density in annealed samples is consistently lower compared to the as-grown profile, but there is not a steady decrease in density from the surface down. The APB density is sometimes higher towards the surface indicating that APBs may be being pinned at the GaAs/Al$_2$O$_3$ interface during annealing.

136
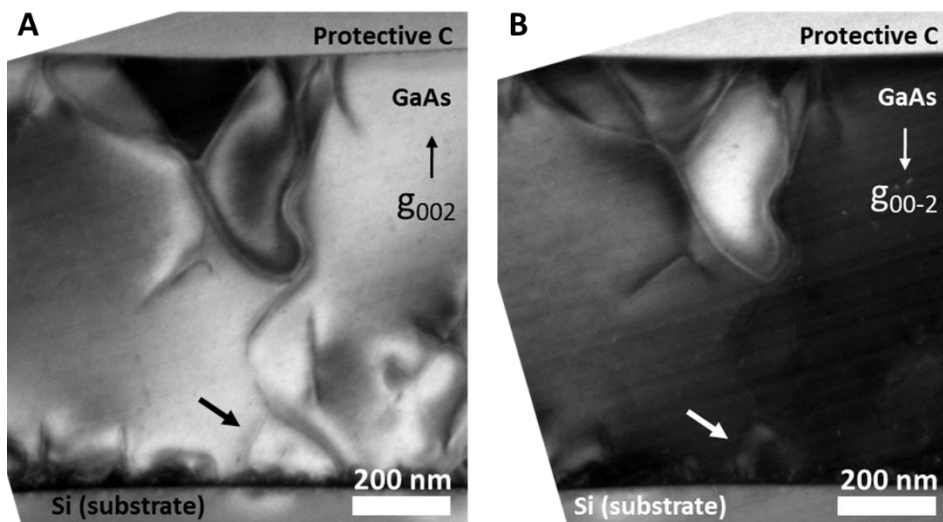
Figure 5-15. Pinched-off antiphase domain in the low temperature growth sample after annealing at 600 °C for 30 min. A) DF image using the g_{002} reflection and B) DF image using the $g_{00\text{-}2}$ reflection. The antiphase domain is visible near the surface of the GaAs film and is terminated towards the middle of the film. Another possible domain is observed near the GaAs/Si interface (marked by arrow) that may have been connected to the domain near the surface prior to annealing.
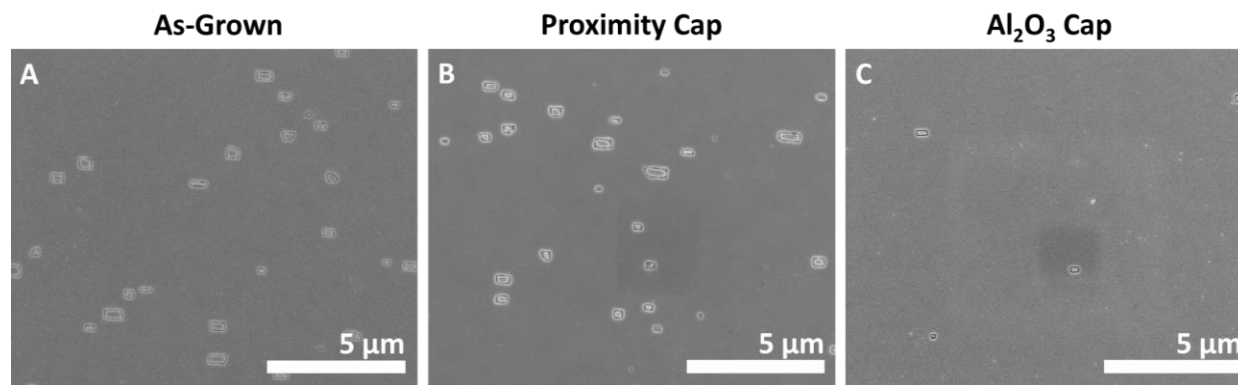
Figure 5-16. Representative plan view SEM images of the APB density in the low temperature growth sample after annealing with different capping conditions. A) Sample as-grown, B) after annealing at 600 °C for 30 min with a proximity cap, and C) after annealing at 600 °C for 30 min with an Al_2O_3 cap. There is no apparent difference in APB density after annealing with the proximity cap which indicates that the pinning of APBs at the GaAs surface is greater under these conditions. There is a noticeable decrease in APB density when using the Al_2O_3 cap.

137
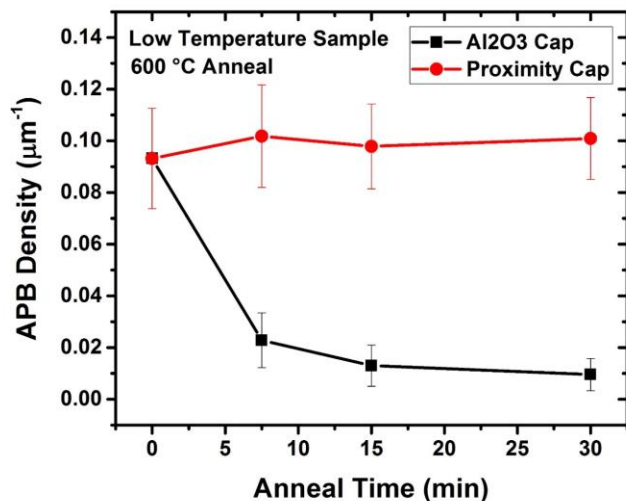
Figure 5-17. Plot of surface APB densities for the low temperature sample after annealing with a proximity cap and Al_2O_3 cap at 600 °C for various times. There is a steady decrease in APB density when using the Al_2O_3 cap and no decrease when using the proximity cap supporting the notion that APB pinning at the GaAs surface is affected by the surface conditions.
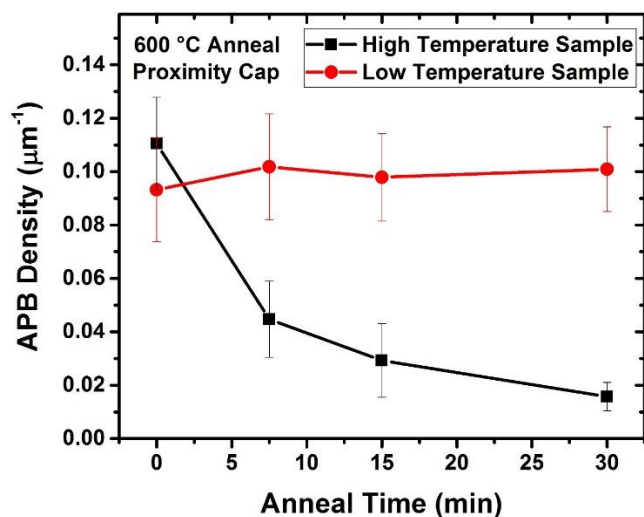
Figure 5-18. Plot of surface APB densities for the low temperature growth sample compared with a high temperature growth sample (610 °C) for similar annealing conditions with a proximity cap. APB density decreases for the high temperature growth sample even with a proximity cap. Therefore, the stability of APBs during annealing may also be affected by the grown-in nature of APBs, i.e. {110} versus inclined habit planes.

138
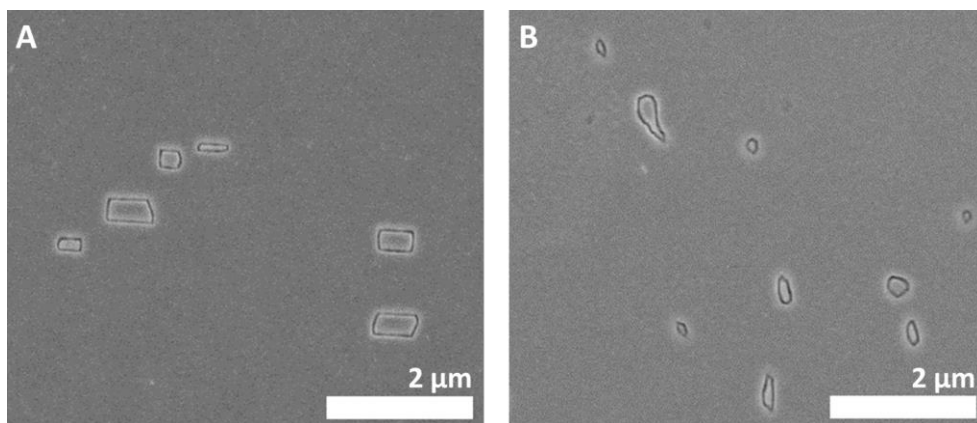
Figure 5-19. Representative plan view SEM images showing the grown-in nature of APBs as a function of growth temperature. A) APBs in the low temperature growth sample and B) APBs in the high temperature growth sample. The APBs in the low temperature growth sample tend to be faceted along {110} orientations while the APBs in the high temperature growth sample tend to be more rounded.
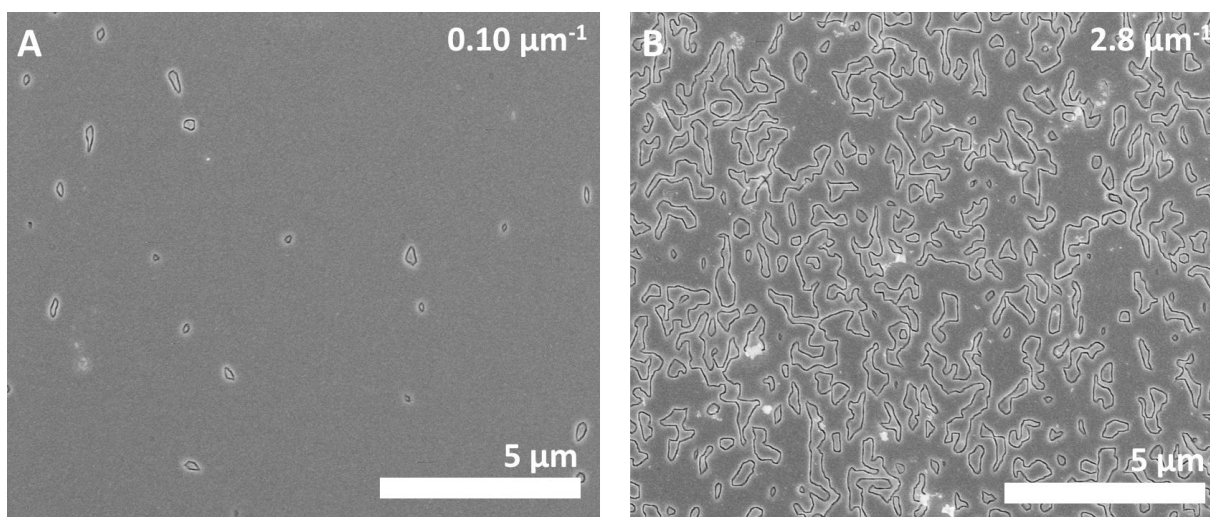
Figure 5-20. Representative plan view SEM images of the as-grown surface APB densities in the samples for the Si diffusion study. A) Low density sample and B) high density sample. The APB densities are 0.10 μm^{-1} and 2.8 μm^{-1}, respectively.
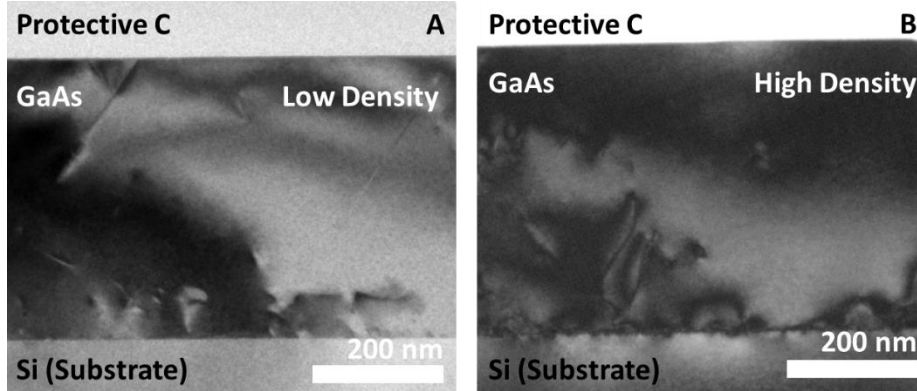
Figure 5-21. BF XTEM images of samples for the Si diffusion study. A) Low APB density sample and B) high APB density sample. There is no apparent difference in defect densities besides that of APBs and the GaAs layer thicknesses are approximately the same.
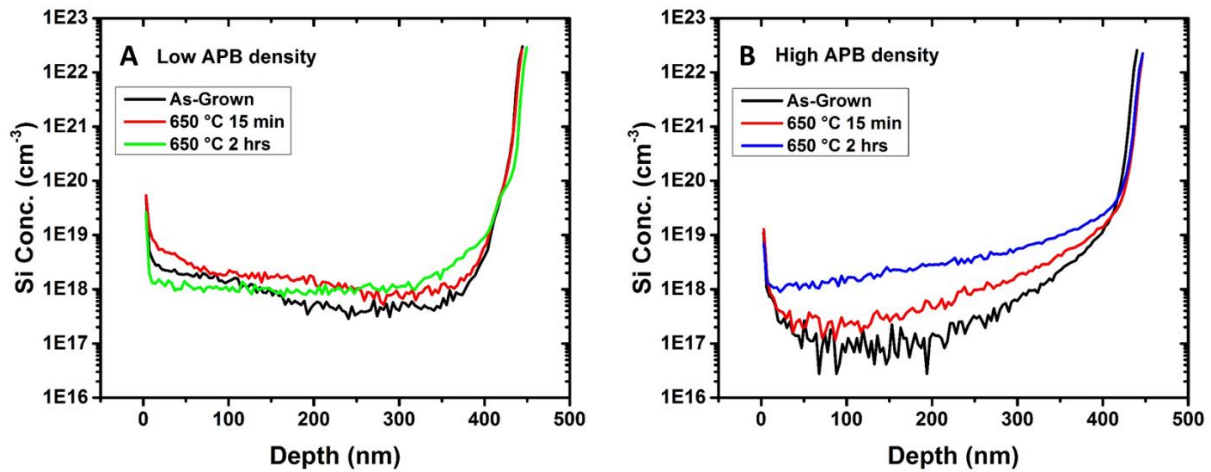
Figure 5-22. SIMS profiles of Si concentration in the GaAs layers for samples with different starting APB densities as-grown and after annealing. A) Low APB density sample and B) high APB density sample. Si profiles are shown for as-grown conditions and after annealing at 650 °C for 15 min and 2 hrs.
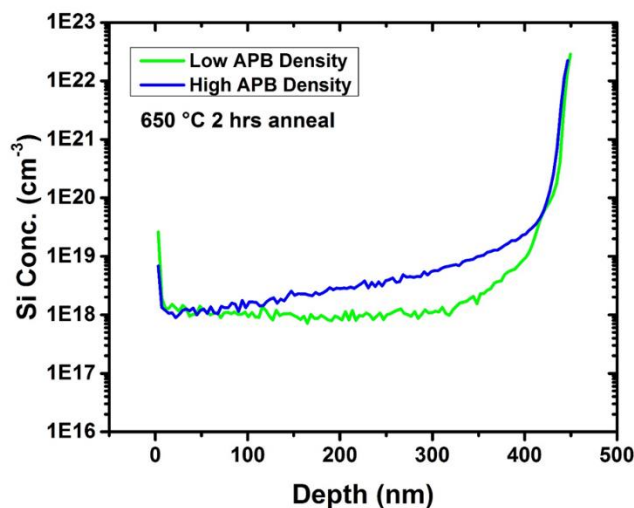
Figure 5-23. Comparison of Si concentration profiles for the low and high APB density samples after annealing at 650 °C for 2 hrs. There is noticeably more diffusion of Si from the substrate for the high APB density sample compared to the low APB density sample.
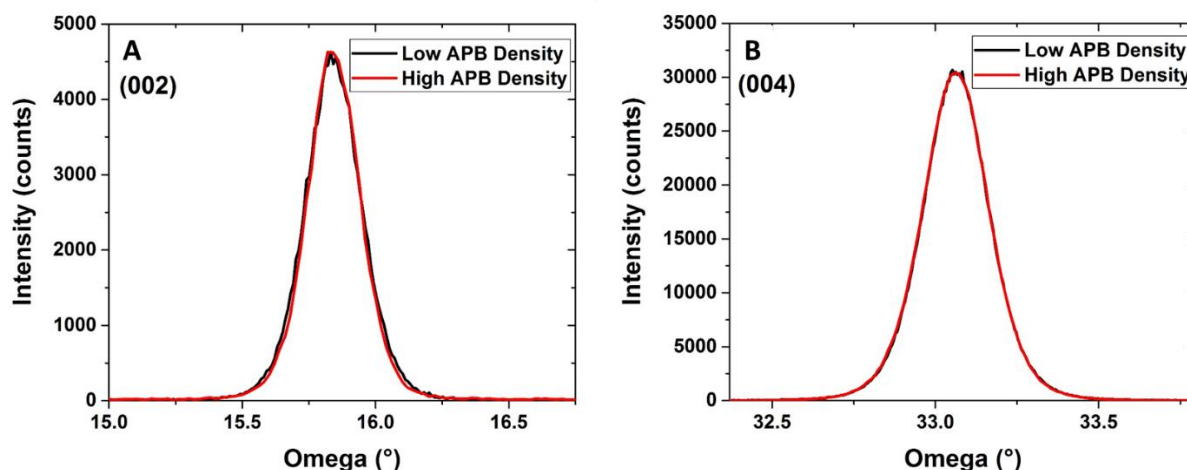
Figure 5-24. XRD rocking curves of the low and high APB density samples as-grown. A) Profiles for the (002) peak and B) profiles for the (004) peak. There is no difference in the (002) peaks that should be sensitive to antiphase disorder likely because the domains in the high density sample are larger than the XRD detection limit (~300 nm). There is also no apparent difference in the (004) peaks which indicates that the density of defects other than APBs, e.g. dislocations, and the overall crystalline quality are similar between the two samples.

CHAPTER 6
THE EFFECT OF DOPING

6.1 Background

The electrical and optical properties of GaAs layers grown epitaxially on Si(001) are degraded by the formation of APBs. These APBs nucleate at single-steps on the Si surface and form planar defects composed entirely of antisite bonds, i.e. Ga-Ga and As-As. The inherent formation of antisite bonds contributes to the large formation energy of APBs [92]. The presence of APBs in a GaAs layer should be energetically unfavorable. It has been demonstrated that higher growth temperatures lead enhanced annihilation of APBs [114, 147] and that post-growth annealing is capable of dissolving antiphase domains (see Chapter 5). These results indicate that the kinetic stability of APBs can be affected and overcome by increasing the thermal energy available. The lowest energy configuration for a GaAs layer should be free of APBs.

It may be possible to affect the energetic stability of APBs either during growth or during post-growth thermal treatments through other avenues. One option is to alter the relative stability of the antisite defects that constitute APBs. Walukiewicz [97] hypothesized that p-type or n-type shifts in the Fermi level for GaAs, i.e. doping, will favor the formation of antisite defects and vacancies to compensate the charge from the dopant species. The formation energy of Ga_{As} antisite defects (and Ga vacancies) is lowered as the Fermi level approaches the conduction band edge and the formation energy of As_{Ga} antisite defects (and As vacancies) is lowered towards the valence band edge. The work by Walukiewicz was corroborated later on by DFT studies by Chroneos et al. [99]. The authors focused on the formation energy of Ga_{As} and As_{Ga} antisite defects as a function of the Fermi level. The formation energy of As_{Ga} defects is

decreased near either the valence or conduction band edge. The formation energy of Ga_{As} decreases moving from the valence band edge to the conduction band edge, at which point it is lower overall in energy compared to As_{Ga}. It follows from the effect of Fermi level shifts on antisite formation energies that doping may also change the energetic stability of APBs in GaAs. This section investigates the effect of doping on the grown-in APB density for GaAs films grown on Si. In situ doping was chosen to avoid any possible effects of damage and regrowth from ex situ doping, i.e. ion implantation, on APBs.

6.2 Experimental

All samples in this experiment were grown on 300 mm lightly p-doped Si(001) wafers with no intentional off-cut. The wafers were cleaned prior to GaAs growth using the Siconi™ process [118]. The wafers were then transferred under vacuum to an Applied Materials III-V MOCVD system. A ~900 °C bake was performed to promote the formation of double-steps on the Si surface. GaAs film growth proceeded in the standard two-step process with a low temperature nucleation layer and high temperature bulk layer. The layer structure is similar to that depicted in Figure 3-3 with 200 nm of GaAs grown at 530 °C followed by 200 nm of GaAs grown at 610 °C. The precursors for Ga and As were trimethylgallium (TMGa) and tertiarybutylarsine (TBAs), respectively. The V/III ratio was within the standard MOCVD process range and the chamber was maintained at typical reduced pressure ambient during film growth. P-doping was accomplished by the addition of diethylzinc (DEZn) flow during growth and n-doping was accomplished by the addition of disilane flow. One sample was p-doped, one was n-doped, and one was nominally undoped for the control.

As-grown layer thickness measurements for the samples were obtained using ellipsometry. Electrical characterization of the samples was performed using Hall effect measurements. Contacts were made using pressed-on In wire. The nominally undoped sample was further annealed at 425 °C for 2 min in a tube furnace with Ar ambient to make good electrical contact. The APB density in the samples was measured using the selective HF(49%):HNO$_3$(69%):H$_2$O (20:1:7) etchant and SEM. APB features in SEM images were traced using ImageJ software [132].

6.3 Results

The sheet number, i.e. areal density, of active charge carriers in the GaAs films was first measured by Hall effect. The sheet number was then converted to a volumetric density by dividing the sheet number by the GaAs layer thickness. The n-type sample was determined to possess 2.7×10^{18} electrons/cm^3, the p-type sample had 2.5×10^{18} holes/cm^3, and the undoped sample had 4.3×10^{16} electrons/cm^3. Unintentional doping from background contamination in MOCVD, e.g. carbon or silicon, is unavoidable. Therefore, even the nominally undoped sample has some amount of extrinsic doping. It is important to reiterate that the undoped sample was measured after annealing the In contacts and so the sheet number measurement may be unreliable. The charge carrier concentration can be used to determine the Fermi level of each sample through the relation [170]:

$$E_F - E_{Fi} = kT ln\left(\frac{N_d}{n_i}\right) \tag{6-1}$$

where E_F is the extrinsic Fermi level, E_{Fi} is the intrinsic Fermi level, N_d is the concentration of donors (or acceptors), n_i is the intrinsic carrier concentration, k is Boltzmann's constant, and T is temperature. The n-type and p-type samples are both

~0.7 eV deviated from the intrinsic Fermi level, placing the extrinsic Fermi level for these samples near the conduction band edge and valence band edge, respectively, for GaAs. The extrinsic Fermi level of the nominally undoped sample is calculated to be ~0.6 eV above the intrinsic Fermi level; however, this calculation has a large dependence on the accuracy of the sheet number measurement from Hall effect.

Figure 6-1 shows representative plan view SEM images of the surface APB densities for the p-type sample (A), undoped sample (B), and n-type sample (C). The APB densities are 0.33 μm^{-1}, 0.50 μm^{-1}, and 1.2 μm^{-1}, respectively. The APB density of the n-type sample is noticeably higher than that of the p-type or undoped samples simply from comparing the SEM images. Figure 6-2 plots the APB density of the samples versus the dopant type (A) and the calculated Fermi level (B). There is a clear trend of increasing APB density with increasing n-type character. The jump in APB density is much more sudden on Figure 6-2B when representing the data against the calculated Fermi level. This difference may arise from inaccurate determination of the undoped sample Fermi level. Regardless, the n-type sample APB density is much higher (~4x) that of the p-type sample, indicating that the Fermi level does have an effect on the stability of APBs during growth.

6.4 Discussion

The substrate surface preparation procedure was identical for all samples, so they can be presumed to have the same nucleated APB density. The growth conditions for the samples in this work were also identical except for the addition of the dopant precursors. Further, Zn and Si are both preferentially dissolved on the Ga sublattice [163], so there is no disparity in the physical incorporation of the dopant atoms on lattice

sites. Therefore, the difference in surface APB densities most likely arises from an effect of the dopant precursor molecule reaction on the APB kinetic stability or from the Fermi level shift due to the incorporation of dopant atoms on lattice sites. It would difficult to decouple these two possible effects experimentally, unless a precursor for Si with similar number and structure of alkyl groups to DEZn can be used.

The trend of increasing APB density with increasing n-type character in the samples correlates with the decrease in antisite formation energies from the work of Walukiewicz [97] and Chroneos et al. [99]. Therefore, it is plausible that the decrease in antisite formation energies stabilizes APBs during growth instead of facilitating APBs kinking to inclined planes and self-annihilating. Previous work showed that at the growth temperature for the GaAs films in this study that APB propagation along inclined planes should be preferred for nominally undoped conditions [147]. P-type doping may have a small effect on enhancing APB annihilation, i.e. making APBs less energetically stable.

6.5 Summary

In situ doping in MOCVD affects the grown-in APB density for GaAs films grown on Si. N-type doping with Si caused a >2x increase in surface APB density compared to a nominally undoped sample. P-type doping with Zn led to a slight decrease in APB density compared to the undoped sample. The results indicate that the lowering of antisite defect formation energies with more n-type Fermi level shifts works to stabilize APBs during growth. Therefore, fewer APBs kink to inclined planes and self-annihilate. The results of this work also show that intentional n-type doping should be avoided in GaAs layers grown on Si for the purposes of reducing grown-in APB density. Rather, intentional p-type doping may be optimal for the lowest APB density.
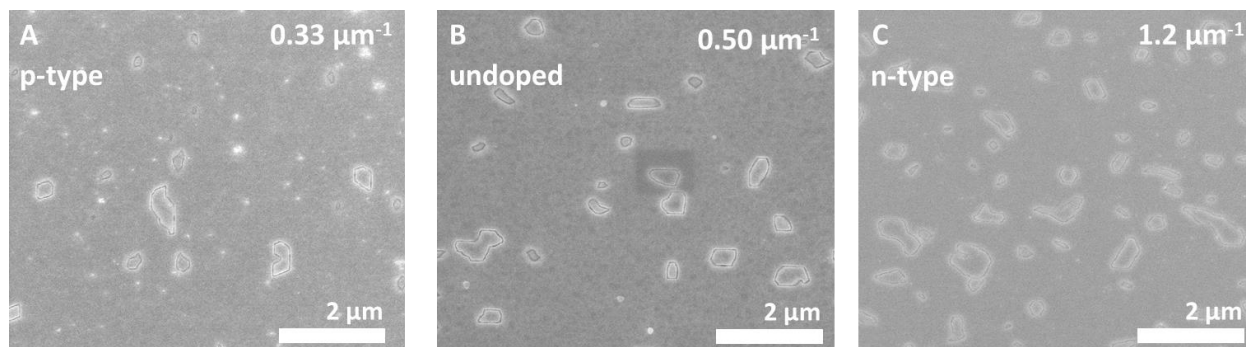
Figure 6-1. Representative plan view SEM samples of the APB density in doped and undoped samples as-grown. A) p-type sample, B) nominally undoped sample, and C) n-type sample. The measured carrier concentrations are 2.5×10^{18} holes/cm^3, 4.3×10^{16} electrons/cms^3, and 2.7×10^{18} electrons/cm^3, respectively. APB density is significantly higher for the n-type sample compared to either the p-type or undoped samples.
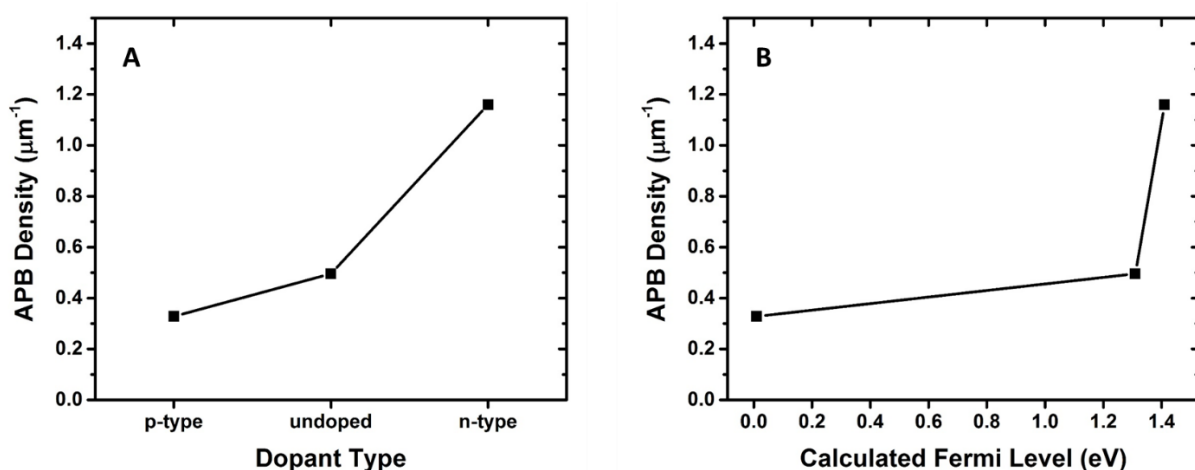
Figure 6-2. Plots of APB density as a function of doping conditions and Fermi level for the p-type, undoped, and n-type samples. A) APB density versus dopant type and B) APB density versus calculated Fermi level. APB density increases with increasing n-type character.

CHAPTER 7
CONCLUSIONS AND FUTURE WORK

7.1 Major Findings

The results of the experiments in this work support the conclusion that APBs in GaAs-on-Si are inherently unstable defects. APBs are forced to nucleate in epitaxial GaAs films because of single-steps on the Si surface. The elimination of APBs is only feasible through processes that are kinetically unfavorable, e.g. kinking of APBs to inclined planes during growth and the diffusive motion of APBs post-growth. However, there is a significant thermodynamic driving force for the elimination of APBs due to their large associated energies. Therefore, the kinetic barriers to APB annihilation can be overcome by increasing the thermal energy available and affecting the APB energetics. The GaAs-on-Si system approaches its lowest energy configuration which is free of APBs.

Growth temperature in MOCVD was found to play a large role in the tendency of APBs in GaAs films to kink to inclined planes and self-annihilate during growth. APB nucleation along {110} planes is favored energetically. Self-annihilation can only occur if APBs propagate along higher index planes such as {111} or {112} that are nominally higher in formation energy. Increasing the growth temperature from 530 to 610 °C increased the APB annihilation rate with respect to film thickness by a factor of four. An associated activation energy of 1.1 eV was found. APBs along {112} planes and other higher index plane configurations were observed in DF XTEM. The higher growth temperatures likely remove kinetic barriers for the propagation of APBs along these planes and facilitate annihilation. The kinking of APBs to inclined planes allows for a reduction in the total line length of APBs in the (001) growth plane with each

consecutive monolayer of growth. The rate of APB annihilation with respect to film thickness is ultimately limited by the preferred habit plane for APB kinking.

It was found that APB annihilation and suppression of antiphase domains can be achieved with post-growth annealing. Diffusive motion of APBs occurred at annealing temperatures as low as 550 °C and had an Arrhenius dependence up to 700 °C. The activation energy for APB diffusion was determined to be 3.8 eV. The motion of an APB is likely mediated by the presence of vacancies and the rate limiting step may be Ga self-diffusion. Decreases in APB density with annealing were observed regardless of the initial starting density. The evolution of APBs during annealing is qualitatively similar to the well-known phenomenon of grain growth and appears to be governed by similar kinetics. The energetic driving force for APB diffusion is a reduction in curvature and total interfacial area which, in turn, allows for the elimination of the antiphase "grains," or domains. Annealing brings the GaAs layer closer to an equilibrium structure that is APB-free and not with {110} oriented APBs. The grown-in structure of APBs, i.e. their grown-in habit planes, as well as the surface conditions during annealing may affect the energetics of APB diffusion.

The energetics of APB propagation during growth can also be affected by in situ doping. The APB density in GaAs-on-Si samples grown with identical conditions, besides the addition of dopant precursors, varied based on the calculated Fermi level. Heavy n-type doping (>10^{18} electrons/cm^3) led to a more than 2x increase in APB density compared to a nominally undoped reference sample. Conversely, heavy p-type doping (>10^{18} holes/cm^3) led to a slight decrease in APB density compared to the undoped sample. The increase in APB density with more n-type Fermi level shifts

correlates to decreases in antisite formation energies in GaAs. The decrease in antisite formation energy has a broader effect of stabilizing APBs during growth and hindering self-annihilation.

The effect of interfacial contamination on nucleated APB density in GaAs films grown on Si was also studied in depth. Carbon was determined to be the primary source of contamination. Oxygen was also a source of contamination but was not present in as much quantity. It was found that the APB density increased with increasing interfacial carbon dose. Amorphous contaminant particles were observed at the GaAs/Si interface in XTEM and were directly associated with the formation of APBs as well as other crystalline defects. It is possible that there is a direct nucleation effect of amorphous particles for APBs. However, it is more likely that residual contamination essentially passivates single-steps on the Si surface and prevents their reconstruction to double-steps during high temperature pre-growth anneals. Therefore, areas of the substrate surface with more contamination are associated with greater number of single-steps which in turn lead to higher nucleated APB densities.

7.2 Future Work

The future experimental work for this investigation of APB energetics in GaAs-on-Si centers on the effect of doping. Ideally, it would be better to grow a full series of doped samples with varying p-type and n-type doping levels to develop a more quantitative relationship of the effect on grown-in APB density. Further, annealing experiments of the doped samples can be performed to study the effect of Fermi level shifts on the energetics of APB diffusion. It would be interesting to see if there is a change in the activation energy for APB diffusion during annealing. These experiments

would provide greater insight on how antisite defects and their respective formation energies play a role in APB motion.

There is an additional need for computational work to support the experimental findings presented here and gain insight on the atomic mechanisms that facilitate APB annihilation. The most recent DFT studies on APB energetics in GaAs only investigated simple systems of parallel APB planes [92]. More complex APB systems should be modeled, e.g a {110} APB with a {112} kink, to determine which configurations are energetically feasible for APB propagation and annihilation during growth. The diffusion process of APBs during annealing should also be modeled. It is not clear what atomic exchange process allows for the net diffusive motion of an APB and would also be energetically favorable. An additional nuance to these computational studies would be to add the effect of Fermi level shifts on the APB energetics.

APPENDIX
SUPPLEMENTARY INFORMATION

A.1 Particle Distribution Calculation

Assume cylindrical particles
Radius = 10 nm
Height = 2 nm
Volume = $\pi r^2 h$ = 6.3×10^{-19} cm^3

If particles are SiC
Want atoms/cm^3
Density = 3.21 g/cm^3
Molar mass = 40.1 g/mol
Avogadro's # = 6.02×10^{23} atoms/mol
=> 9.6×10^{22} atoms/cm^3

One half are C atoms in SiC
=> 4.8×10^{22} C atoms/cm^3

Want atoms/particle
$(4.8 \times 10^{22}$ C atoms/cm$^3)*(6.3 \times 10^{-19}$ cm^3 [volume per particle])
=> 3.0×10^4 C atoms/particle

Want areal density of interfacial particles
$(1.7 \times 10^{15}$ C atoms/cm^2 [SIMS dose])/(3.0×10^4 atoms/particle)
=> 5.7×10^{10} particles/cm^2 = 5.7×10^{-4} particles/nm^2

Assume lamella thickness of 50 nm
(50 nm)*(5.7×10^{-4} particles/nm^2)
=> 0.028 particles/nm
=> 1 particle every ~36 nm

If particles are SiO$_2$
Want atoms/cm^3
Density = 2.65 g/cm^3
Molar mass = 60.1 g/mol
Avogadro's # = 6.02×10^{23} atoms/mol
=> 8.0×10^{22} atoms/cm^3

Two thirds are O atoms in SiO$_2$
=> 5.3×10^{22} C atoms/cm^3

Want atoms/particle
$(5.3 \times 10^{22}$ O atoms/cm$^3)*(6.3 \times 10^{-19}$ cm^3 [volume per particle])
=> 3.3×10^4 O atoms/particle

Want areal density of interfacial particles

$(4.0 \times 10^{12}$ O atoms/cm^2 [SIMS dose])/(3.3×10^4 atoms/particle)

$\Rightarrow 1.2 \times 10^8$ particles/cm$^2 = 1.2 \times 10^{-6}$ particles/nm^2

Assume lamella thickness of 50 nm

$(50$ nm$)*(1.2 \times 10^{-6}$ particles/nm$^2)$

$\Rightarrow 6.0 \times 10^{-5}$ particles/nm

$\Rightarrow 1$ particle every ~17000 nm or 17 μm

A.2 Hybrid Al$_2$O$_3$ ALD Recipe

Step	Intruction	#	Value	Units/Comment
1	flow	0	20	sccm
2	flow	1	40	sccm
3	heater	16	150	C
4	heater	17	150	C
5	stabilize	16		
6	stabilize	17		
7	heater	12	195	C
8	heater	13	195	C
9	heater	14	195	C
10	heater	15	200	C
11	stabilize	12		
12	stabilize	13		
13	stabilize	14		
14	stabilize	15		
15	wait		600	sec
16	flow	0	20	sccm
17	flow	1	60	sccm
18	wait		5	sec
19	stopvalve		0	closed
20	wait		1	sec
21	pulse	Al	0.3	sec
22	wait		60	sec
23	stopvalve		1	open
24	flow	0	40	sccm
25	flow	1	140	sccm
26	wait		90	sec
27	flow	0	20	sccm
28	flow	1	60	sccm
29	wait		5	sec
30	stopvalve		0	closed
31	wait		1	sec
32	pulse	0	0.3	sec

33	wait		60	sec
34	stopvalve		1	open
35	flow	0	40	sccm
36	flow	1	140	sccm
37	wait		90	sec
38	flow	0	20	sccm
39	flow	1	60	sccm
40	wait		5	sec
41	goto	18	5	cycles//end of exposure mode 0.5nm
42	wait		30	sec
43	flow	0	20	sccm//go to has to come back here42
44	flow	1	60	sccm
45	wait		30	sec
46	stopvalve		0	closed//start hybrid exposure
47	wait		1	sec
48	pulse	Al	0.3	sec
49	wait		60	sec
50	stopvalve		1	open
51	flow	0	40	sccm//purge cycle after Al pulse
52	flow	1	140	sccm
53	wait		90	sec//end purge cycle
54	flow	0	60	sccm
55	flow	1	200	sccm
56	MFCvalve	3	1	
57	wait		5	sec
58	flow	3	20	sccm
59	wait		5	sec
60	plasma		300	Watts
61	wait		60	sec
62	plasma		0	Watts
63	flow	3	0	sccm
64	wait		2	sec
65	MFCvalve	3	0	
66	wait		60	sec
67	goto	42	200	cycles//end of hybrid exposure
68	flow	0	20	sccm
69	flow	1	40	sccm
70	wait		30	sec
71	heater	12	195	C

72	heater	13	195	C
73	heater	14	195	C
74	heater	15	200	C
75	wait		5	sec
76	flow	0	0	sccm
77	flow	1	0	sccm
78	wait		10	sec
79	doorpurge		0	
80	wait		5	sec

LIST OF REFERENCES

[1]   G. E. Moore, "Cramming more components onto integrated circuits," *Electronics*, vol. 38, no. 8, p. 56, 1965.

[2]   R. H. Dennard, V. L. Rideout, E. Bassous, and A. R. LeBlanc, "Design of ion-implanted MOSFET's with very small physical dimensions," *IEEE J. Solid-State Circuits*, vol. 9, no. 5, pp. 256–268, Oct. 1974.

[3]   D. J. Frank, R. H. Dennard, E. Nowak, et al., "Device scaling limits of Si MOSFETs and their application dependencies," *Proc. IEEE*, vol. 89, no. 3, pp. 259–288, Mar. 2001.

[4]   N. S. Kim, T. Austin, D. Baauw, et al., "Leakage current: Moore's law meets static power," *Computer*, vol. 36, no. 12, pp. 68–75, 2003.

[5]   J. Warnock, "Circuit and PD Challenges at the 14Nm Technology Node," in *Proceedings of the 2013 ACM International Symposium on International Symposium on Physical Design*, New York, NY, USA, 2013, pp. 66–67.

[6]   J. A. del Alamo, "Nanometre-scale electronics with III–V compound semiconductors," *Nature*, vol. 479, no. 7373, pp. 317–323, Nov. 2011.

[7]   J. E. Bowers, J. T. Bovington, A. Y. Liu, et al., "A path to 300 mm hybrid silicon photonic integrated circuits," in *Optical Fiber Communication Conference. Optical Society of America*, 2014.

[8]   D. W. Shaw, "Epitaxial GaAs on Si: Progress and Potential Applications," *MRS Proc.*, vol. 91, Jan. 1987.

[9]   S. E. Grillo, M. Ducarroir, M. Nadal, E. Tournié, and J.-P. Faurie, "Nanoindentation of Si, GaP, GaAs and ZnSe single crystals," *J. Phys. Appl. Phys.*, vol. 36, no. 1, p. L5, 2003.

[10]   J. S. Harris, S. M. Koch, and S. J. Rosner, "The Nucleation and Growth of GaAs on Si," *MRS Proc.*, vol. 91, Jan. 1987.

[11]   A. Georgakilas, J. Stoemenos, K. Tsagaraki, et al., "Generation and annihilation of antiphase domain boundaries in GaAs on Si grown by molecular beam epitaxy," *J. Mater. Res.*, vol. 8, no. 8, pp. 1908–1921, 1993.

[12]   M. Heyns and W. Tsai, "Ultimate Scaling of CMOS Logic Devices with Ge and III–V Materials," *MRS Bull.*, vol. 34, no. 7, pp. 485–492, Jul. 2009.

[13]   S. F. Fang, K. Adomi, S. Iyer, et al., "Gallium arsenide and other compound semiconductors on silicon," *J. Appl. Phys.*, vol. 68, no. 7, pp. R31–R58, Oct. 1990.

[14] S. Takagi, R. Zhang, J. Suh, et al., "III–V/Ge channel MOS device technologies in nano CMOS era," *Jpn. J. Appl. Phys.*, vol. 54, no. 6S1, p. 06FA01, Jun. 2015.

[15] H. Temkin and J. C. M. Hwang, "Undoped, semi-insulating GaAs layers grown by molecular beam epitaxy," *Appl. Phys. Lett.*, vol. 42, no. 2, pp. 178–180, Jan. 1983.

[16] H. Welker, "Semiconducting intermetallic compounds," *Physica*, vol. 20, no. 7, pp. 893–909, Jan. 1954.

[17] W. R. Wisseman and W. R. Frensley, "GaAs Technology Perspective," *VLSI Electron. Microstruct. Sci.*, vol. 11, pp. 1–39, Jan. 1985.

[18] P. H. Holloway and G. E. McGuire, *Handbook of Compound Semiconductors: Growth, Processing, Characterization, and Devices*. Elsevier, 1996.

[19] R. Pelzel, "A comparison of MOVPE and MBE growth technologies for III-V epitaxial structures," in *CS MANTECH Conference, USA*, 2013, pp. 105–108.

[20] W. I. Wang, "Molecular beam epitaxial growth and material properties of GaAs and AlGaAs on Si (100)," *Appl. Phys. Lett.*, vol. 44, no. 12, pp. 1149–1151, Jun. 1984.

[21] M. Akiyama, Y. Kawarada, and K. Kaminishi, "Growth of GaAs on Si by MOVCD," *J. Cryst. Growth*, vol. 68, no. 1, pp. 21–26, Sep. 1984.

[22] T. Li, M. Mastro, and A. Dadgar, *III–V Compound Semiconductors: Integration with Silicon-Based Microelectronics*. CRC Press, 2011.

[23] E. Tournié and K. H. Ploog, "Surface stoichiometry, epitaxial morphology and strain relaxation during molecular beam epitaxy of highly strained InAs/Ga0.47In0.53As heterostructures," *J. Cryst. Growth*, vol. 135, no. 1–2, pp. 97–112, Jan. 1994.

[24] J. E. Ayers, *Heteroepitaxy of Semiconductors: Theory, Growth, and Characterization*. CRC Press, 2007.

[25] W. D. Callister and D. G. Rethwisch, *Fundamentals of materials science and engineering: an integrated approach*. John Wiley & Sons, 2008.

[26] D. K. Biegelsen, F. A. Ponce, A. J. Smith, and J. C. Tramontana, "Initial stages of epitaxial growth of GaAs on (100) silicon," *J. Appl. Phys.*, vol. 61, no. 5, pp. 1856–1859, Mar. 1987.

[27] D. K. Biegelsen, F. A. Ponce, B. S. Krusor, J. C. Tramontana, and R. D. Yingling, "Graded-thickness samples for molecular beam epitaxial growth studies of GaAs/Si heteroepitaxy," *Appl. Phys. Lett.*, vol. 52, no. 21, pp. 1779–1781, May 1988.

[28] Y. B. Bolkhovityanov and O. P. Pchelyakov, "GaAs epitaxy on Si substrates: modern status of research and engineering," *Phys.-Uspekhi*, vol. 51, no. 5, pp. 437–456, May 2008.

[29] C. A. Larsen, N. I. Buchan, S. H. Li, and G. B. Stringfellow, "GaAs growth using tertiarybutylarsine and trimethylgallium," *J. Cryst. Growth*, vol. 93, no. 1–4, pp. 15–19, 1988.

[30] G. B. Stringfellow, *Organometallic Vapor-Phase Epitaxy: Theory and Practice*. San Diego, CA: Academic Press, 1989.

[31] S. J. Rosner, S. M. Koch, J. S. Harris, and S. Laderman, "Microstructure of thin layers of MBE-grown GaAs on Si substrates," *MRS Proc.*, vol. 67, Jan. 1986.

[32] A. E. Blakeslee, M. M. Al-Jassim, and S. E. Asher, "Origin of Defects in MOCVD Growth of GaP on Silicon," *MRS Proc.*, vol. 91, Jan. 1987.

[33] Z. Liliental-Weber, E. R. Weber, L. Parechanian-Allen, and J. Washburn, "On the use of convergent-beam electron diffraction for identification of antiphase boundaries in GaAs grown on Si," *Ultramicroscopy*, vol. 26, no. 1–2, pp. 59–63, 1988.

[34] H. Kawanami, "Heteroepitaxial technologies of III–V on Si," *Sol. Energy Mater. Sol. Cells*, vol. 66, no. 1–4, pp. 479–486, Feb. 2001.

[35] R. C. Henderson, "Silicon Cleaning with Hydrogen Peroxide Solutions: A High Energy Electron Diffraction and Auger Electron Spectroscopy Study," *J. Electrochem. Soc.*, vol. 119, no. 6, pp. 772–775, Jun. 1972.

[36] A. Ishizaka and Y. Shiraki, "Low Temperature Surface Cleaning of Silicon and Its Application to Silicon MBE," *J. Electrochem. Soc.*, vol. 133, no. 4, pp. 666–671, Apr. 1986.

[37] S. M. Koch, S. J. Rosner, D. Schlom, and J. S. Harris, "The Growth of GaAs on Si by Molecular Beam Epitaxy," *MRS Proc.*, vol. 67, Jan. 1986.

[38] P. Demeester, A. Ackaert, G. Coudenys, et al., "Relaxed lattice-mismatched growth of III–V semiconductors," *Prog. Cryst. Growth Charact. Mater.*, vol. 22, no. 1–2, pp. 53–141, 1991.

[39] H. Döscher, S. Brückner, A. Dobrich, et al., "Surface preparation of Si(100) by thermal oxide removal in a chemical vapor environment," *J. Cryst. Growth*, vol. 315, no. 1, pp. 10–15, Jan. 2011.

[40] S. L. Wright, M. Inada, and H. Kroemer, "Polar-on-nonpolar epitaxy: Sublattice ordering in the nucleation and growth of GaP on Si(211) surfaces," *J. Vac. Sci. Technol.*, vol. 21, no. 2, pp. 534–539, Jul. 1982.

[41]   S. L. Wright, H. Kroemer, and M. Inada, "Molecular beam epitaxial growth of GaP on Si," *J. Appl. Phys.*, vol. 55, no. 8, pp. 2916–2927, Apr. 1984.

[42]   P. N. Uppal and H. Kroemer, "Molecular beam epitaxial growth of GaAs on Si(211)," *J. Appl. Phys.*, vol. 58, no. 6, pp. 2195–2203, Sep. 1985.

[43]   H. Kroemer, "MBE Growth of GaAs on Si: Problems and Progress," *MRS Proc.*, vol. 67, Jan. 1986.

[44]   D. B. Holt and B. G. Yacobi, *Extended Defects in Semiconductors: Electronic Properties, Device Effects and Structures*. Cambridge University Press, 2007.

[45]   F. Glas, "A simple calculation of energy changes upon stacking fault formation or local crystalline phase transition in semiconductors," *J. Appl. Phys.*, vol. 104, no. 9, p. 93520, Nov. 2008.

[46]   L. Goldstein, F. Glas, J. Y. Marzin, M. N. Charasse, and G. L. Roux, "Growth by molecular beam epitaxy and characterization of InAs/GaAs strained-layer superlattices," *Appl. Phys. Lett.*, vol. 47, no. 10, pp. 1099–1101, Nov. 1985.

[47]   T. Soga, S. Hattori, S. Sakai, M. Takeyasu, and M. Umeno, "Characterization of epitaxially grown GaAs on Si substrates with III-V compounds intermediate layers by metalorganic chemical vapor deposition," *J. Appl. Phys.*, vol. 57, no. 10, pp. 4578–4582, May 1985.

[48]   H. Okamoto, Y. Watanabe, Y. Kadota, and Y. Ohmachi, "Dislocation Reduction in GaAs on Si by Thermal Cycles and InGaAs/GaAs Strained-Layer Superlattices," *Jpn. J. Appl. Phys.*, vol. 26, no. 12A, p. L1950, Dec. 1987.

[49]   N. El-Masry, J. C. L. Tarn, T. P. Humphreys, et al., "Effectiveness of strained-layer superlattices in reducing defects in GaAs epilayers grown on silicon substrates," *Appl. Phys. Lett.*, vol. 51, no. 20, pp. 1608–1610, Nov. 1987.

[50]   N. A. El-Masry, J. C. Tarn, and N. H. Karam, "Interactions of dislocations in GaAs grown on Si substrates with InGaAs-GaAsP strained layered superlattices," *J. Appl. Phys.*, vol. 64, no. 7, pp. 3672–3677, Oct. 1988.

[51]   M. Yamaguchi, T. Nishioka, and M. Sugo, "Analysis of strained-layer superlattice effects on dislocation density reduction in GaAs on Si substrates," *Appl. Phys. Lett.*, vol. 54, no. 1, pp. 24–26, Jan. 1989.

[52]   J. Z. Li, J. Bai, J.-S. Park, et al., "Defect reduction of GaAs epitaxy on Si (001) using selective aspect ratio trapping," *Appl. Phys. Lett.*, vol. 91, no. 2, p. 21114, 2007.

[53]   J. Z. Li, J. Bai, C. Major, et al., "Defect reduction of GaAs/Si epitaxy by aspect ratio trapping," *J. Appl. Phys.*, vol. 103, no. 10, p. 106102, May 2008.

[54]   M. Paladugu, C. Merckling, R. Loo, et al., "Site Selective Integration of III–V Materials on Si for Nanoscale Logic and Photonic Devices," *Cryst. Growth Des.*, vol. 12, no. 10, pp. 4696–4702, Oct. 2012.

[55]   R. Loo, G. Wang, T. Orzali, et al., "Selective area growth of InP on On-Axis Si (001) substrates with low antiphase boundary formation," *J. Electrochem. Soc.*, vol. 159, no. 3, pp. H260–H265, 2012.

[56]   C. Merckling, N. Waldron, S. Jiang, et al., "Heteroepitaxy of InP on Si(001) by selective-area metal organic vapor-phase epitaxy in sub-50 nm width trenches: The role of the nucleation layer and the recess engineering," *J. Appl. Phys.*, vol. 115, no. 2, p. 23710, Jan. 2014.

[57]   W. Guo, L. Date, V. Pena, et al., "Selective metal-organic chemical vapor deposition growth of high quality GaAs on Si(001)," *Appl. Phys. Lett.*, vol. 105, no. 6, p. 62101, Aug. 2014.

[58]   T. Orzali, A. Vert, B. O'Brien, et al., "GaAs on Si epitaxy by aspect ratio trapping: Analysis and reduction of defects propagating along the trench direction," *J. Appl. Phys.*, vol. 118, no. 10, p. 105307, Sep. 2015.

[59]   T. Orzali, A. Vert, B. O'Brian, et al., "Epitaxial growth of GaSb and InAs fins on 300 mm Si (001) by aspect ratio trapping," *J. Appl. Phys.*, vol. 120, no. 8, p. 85308, Aug. 2016.

[60]   D. B. Holt, "Antiphase boundaries in semiconducting compounds," *J. Phys. Chem. Solids*, vol. 30, no. 6, pp. 1297–1308, Jun. 1969.

[61]   K. Morizane, "Antiphase domain structures in GaP and GaAs epitaxial layers grown on Si and Ge," *J. Cryst. Growth*, vol. 38, no. 2, pp. 249–254, May 1977.

[62]   J. A. Appelbaum and D. R. Hamann, "Theory of reconstruction induced subsurface strain — application to Si(100)," *Surf. Sci.*, vol. 74, no. 1, pp. 21–33, May 1978.

[63]   D. J. Chadi, "Atomic and Electronic Structures of Reconstructed Si(100) Surfaces," *Phys. Rev. Lett.*, vol. 43, no. 1, pp. 43–47, Jul. 1979.

[64]   H. Kroemer, "Polar-on-nonpolar epitaxy," *J. Cryst. Growth*, vol. 81, no. 1–4, pp. 193–204, Feb. 1987.

[65]   D. J. Chadi, "Stabilities of single-layer and bilayer steps on Si(001) surfaces," *Phys. Rev. Lett.*, vol. 59, no. 15, pp. 1691–1694, Oct. 1987.

[66]   M. Henzler and J. Clabes, "Structural and Electronic Properties of Stepped Semiconductor Surfaces," *Jpn. J. Appl. Phys.*, vol. 13, no. S2, p. 389, Jan. 1974.

[67]   R. Kaplan, "LEED study of the stepped surface of vicinal Si (100)," *Surf. Sci.*, vol. 93, no. 1, pp. 145–158, Mar. 1980.

[68]   P. E. Wierenga, J. A. Kubby, and J. E. Griffith, "Tunneling images of biatomic steps on Si(001)," *Phys. Rev. Lett.*, vol. 59, no. 19, pp. 2169–2172, Nov. 1987.

[69]   O. L. Alerhand, A. N. Berker, J. D. Joannopoulos, et al., "Finite-temperature phase diagram of vicinal Si(100) surfaces," *Phys. Rev. Lett.*, vol. 64, no. 20, pp. 2406–2409, May 1990.

[70]   E. Pehlke and J. Tersoff, "Phase diagram of vicinal Si(001) surfaces," *Phys. Rev. Lett.*, vol. 67, no. 10, pp. 1290–1293, Sep. 1991.

[71]   T. Sakamoto and G. Hashiguchi, "Si(001)-2×1 Single-Domain Structure Obtained by High Temperature Annealing," *Jpn. J. Appl. Phys.*, vol. 25, no. 1A, p. L78, Jan. 1986.

[72]   D. E. Aspnes and J. Ihm, "Biatomic Steps on (001) Silicon Surfaces," *Phys. Rev. Lett.*, vol. 57, no. 24, pp. 3054–3057, Dec. 1986.

[73]   A. R. Laracuente and L. J. Whitman, "Step structure and surface morphology of hydrogen-terminated silicon: (0 0 1) to (1 1 4)," *Surf. Sci.*, vol. 545, no. 1–2, pp. 70–84, Nov. 2003.

[74]   K. Volz, W. Stolz, A. Dadgar, and A. Krost, "31 - Growth of III/Vs on Silicon: Nitrides, Phosphides, Arsenides and Antimonides," in *Handbook of Crystal Growth (Second Edition)*, T. F. Kuech, Ed. Boston: North-Holland, 2015, pp. 1249–1300.

[75]   M. Akiyama, Y. Kawarada, T. Ueda, S. Nishi, and K. Kaminishi, "Growth of high quality GaAs layers on Si substrates by MOCVD," *J. Cryst. Growth*, vol. 77, no. 1–3, pp. 490–497, Sep. 1986.

[76]   T. Soga, S. Hattori, S. Sakai, and M. Umeno, "Epitaxial growth and material properties of GaAs on Si grown by MOCVD," *J. Cryst. Growth*, vol. 77, no. 1–3, pp. 498–502, Sep. 1986.

[77]   H. Noge, H. Kano, T. Kato, M. Hashimoto, and I. Igarashi, "Molecular beam epitaxial growth of a GaAs layer free from antiphase domains on an exactly (100)-oriented Si substrate preheated at 1000°C," *J. Cryst. Growth*, vol. 83, no. 3, pp. 431–436, Jun. 1987.

[78]   Y. Takagi, Y. Furukawa, A. Wakahara, and H. Kan, "Lattice relaxation process and crystallographic tilt in GaP layers grown on misoriented Si(001) substrates by metalorganic vapor phase epitaxy," *J. Appl. Phys.*, vol. 107, no. 6, p. 63506, Mar. 2010.

[79] A. C. Lin, M. M. Fejer, and J. S. Harris, "Antiphase domain annihilation during growth of GaP on Si by molecular beam epitaxy," *J. Cryst. Growth*, vol. 363, pp. 258–263, Jan. 2013.

[80] Y. Wang, Q. Wang, Z. Jia, et al., "Three-step growth of metamorphic GaAs on Si(001) by low-pressure metal organic chemical vapor deposition," *J. Vac. Sci. Technol. B*, vol. 31, no. 5, p. 51211, Sep. 2013.

[81] C. B. Carter, N.-H. Cho, S. Mckernan, and D. K. Wagner, "Characterization of APBs in GaAs Grown on Si and Ge," *MRS Proc.*, vol. 91, Jan. 1987.

[82] O. Ueda, T. Soga, T. Jimbo, and M. Umeno, "Direct evidence for self-annihilation of antiphase domains in GaAs/Si heterostructures," *Appl. Phys. Lett.*, vol. 55, no. 5, pp. 445–447, Jul. 1989.

[83] Z. Liliental-Weber, "Methods to Decrease Defect Density in GaAs/Si Heteroepitaxy," *MRS Proc.*, vol. 148, Jan. 1989.

[84] A. Georgakilas, P. Panayotatos, J. Stoemenos, J.-L. Mourrain, and A. Christou, "Achievements and limitations in optimized GaAs films grown on Si by molecular-beam epitaxy," *J. Appl. Phys.*, vol. 71, no. 6, p. 2679, 1992.

[85] N.-H. Cho and C. B. Carter, "Formation, faceting, and interaction behaviors of antiphase boundaries in GaAs thin films," *J. Mater. Sci.*, vol. 36, no. 17, pp. 4209–4222, Sep. 2001.

[86] V. Alberts, J. H. Neethling, and A. W. Leitch, "Correlation between structural, optical, and electrical properties of GaAs grown on (001) Si," *J. Appl. Phys.*, vol. 75, no. 11, pp. 7258–7265, Jun. 1994.

[87] V. K. Yang, M. Groenert, C. W. Leitz, et al., "Crack formation in GaAs heteroepitaxial films on Si and SiGe virtual substrates," *J. Appl. Phys.*, vol. 93, no. 7, p. 3859, 2003.

[88] H. Huang, X. Ren, J. Lv, et al., "Crack-free GaAs epitaxy on Si by using midpatterned growth: Application to Si-based wavelength-selective photodetector," *J. Appl. Phys.*, vol. 104, no. 11, p. 113114, Dec. 2008.

[89] R. Jia and E. A. Fitzgerald, "Parameters influencing interfacial morphology in GaAs/Ge superlattices grown by metal organic chemical vapor deposition," *J. Cryst. Growth*, vol. 435, pp. 50–55, Feb. 2016.

[90] P. M. Petroff, "Nucleation and growth of GaAs on Ge and the structure of antiphase boundaries," *J. Vac. Sci. Technol. B*, vol. 4, no. 4, pp. 874–877, Jul. 1986.

[91] D. Vanderbilt and C. Lee, "Energetics of antiphase boundaries in GaAs," *Phys. Rev. B*, vol. 45, no. 19, pp. 11192–11201, May 1992.

[92] O. Rubel and S. D. Baranovskii, "Formation Energies of Antiphase Boundaries in GaAs and GaP: An ab Initio Study," *Int. J. Mol. Sci.*, vol. 10, no. 12, pp. 5104–5114, Nov. 2009.

[93] N.-H. Cho, B. C. D. Cooman, C. B. Carter, R. Fletcher, and D. K. Wagner, "Antiphase boundaries in GaAs," *Appl. Phys. Lett.*, vol. 47, no. 8, pp. 879–881, Oct. 1985.

[94] D. Cohen and C. B. Carter, "Structure of the (110) antiphase boundary in gallium phosphide," *J. Microsc.*, vol. 208, no. 2, pp. 84–99, 2002.

[95] A. Beyer, I. Németh, S. Liebich, et al., "Influence of crystal polarity on crystal defects in GaP grown on exact Si (001)," *J. Appl. Phys.*, vol. 109, no. 8, p. 83529, Apr. 2011.

[96] M. Grundmann, *The physics of semiconductors: an introduction including devices and nanophysics*. Berlin ; New York: Springer, 2006.

[97] W. Walukiewicz, "Amphoteric native defects in semiconductors," *Appl. Phys. Lett.*, vol. 54, no. 21, p. 2094, 1989.

[98] W. Walukiewicz, "Mechanism of Fermi-level stabilization in semiconductors," *Phys. Rev. B*, vol. 37, no. 9, pp. 4760–4763, Mar. 1988.

[99] A. Chroneos, H. A. Tahini, U. Schwingenschlögl, and R. W. Grimes, "Antisites in III-V semiconductors: Density functional theory calculations," *J. Appl. Phys.*, vol. 116, no. 2, p. 23505, Jul. 2014.

[100] A. G. Lind, "Dopant-Defect Interactions in Si Doped InGaAs," University of Florida, Gainesville, Fla., 2015.

[101] W. L. Bragg and E. J. Williams, "The Effect of Thermal Agitation on Atomic Arrangement in Alloys," *Proc. R. Soc. Lond. Ser. Contain. Pap. Math. Phys. Character*, vol. 145, no. 855, pp. 699–730, 1934.

[102] W. Shockley, "Theory of Order for the Copper Gold Alloy System," *J. Chem. Phys.*, vol. 6, no. 3, pp. 130–144, Mar. 1938.

[103] W. L. Bragg, "The structure of a cold-worked metal," *Proc. Phys. Soc.*, vol. 52, no. 1, p. 105, 1940.

[104] A. B. Glossop and D. W. Pashley, "The Direct Observation of Anti-Phase Domain Boundaries in Ordered Copper-Gold (CuAu) Alloy," *Proc. R. Soc. Lond. Math. Phys. Eng. Sci.*, vol. 250, no. 1260, pp. 132–146, Feb. 1959.

[105] M. J. Marcinkowski and R. M. Fisher, "Direct Observation of Antiphase Domain Boundaries in the AuCu3 Superlattice," *J. Appl. Phys.*, vol. 31, no. 9, pp. 1687–1687, Sep. 1960.

[106] S. Yamaguchi, D. Watanabe, and S. Ogawa, "Study on Anti-Phase Domains in Cu3Au by Means of Electron Diffraction and Electron Microscopy," *J. Phys. Soc. Jpn.*, vol. 17, no. 6, pp. 1030–1041, Jun. 1962.

[107] A. J. Ardell, N. Mardesich, and C. N. J. Wagner, "Antiphase domain growth in Cu3Au: Quantitative comparison between theory and experiment," *Acta Metall.*, vol. 27, no. 7, pp. 1261–1269, Jul. 1979.

[108] A. Putnis, *An Introduction to Mineral Sciences*. Cambridge University Press, 1992.

[109] D. A. Porter, K. E. Easterling, and M. Sherif, *Phase Transformations in Metals and Alloys, Third Edition (Revised Reprint)*. CRC Press, 2009.

[110] S. M. Allen and J. W. Cahn, "A microscopic theory for antiphase boundary motion and its application to antiphase domain coarsening," *Acta Metall.*, vol. 27, no. 6, pp. 1085–1095, Jun. 1979.

[111] A. V. Ramos, J.-B. Moussy, M.-J. Guittet, et al., "Magnetotransport properties of Fe3O4 epitaxial thin films: Thickness effects driven by antiphase boundaries," *J. Appl. Phys.*, vol. 100, no. 10, p. 103902, Nov. 2006.

[112] W. Eerenstein, T. T. M. Palstra, T. Hibma, and S. Celotto, "Diffusive motion of antiphase domain boundaries in ${\mathrm{Fe}}_{3}{\mathrm{O}}_{4}$ films," *Phys. Rev. B*, vol. 68, no. 1, p. 14428, Jul. 2003.

[113] I. Németh, B. Kunert, W. Stolz, and K. Volz, "Heteroepitaxy of GaP on Si: Correlation of morphology, anti-phase-domain structure and MOVPE growth conditions," *J. Cryst. Growth*, vol. 310, no. 7–9, pp. 1595–1601, Apr. 2008.

[114] K. Volz, A. Beyer, W. Witte, et al., "GaP-nucleation on exact Si (0 0 1) substrates for III/V device integration," *J. Cryst. Growth*, vol. 315, no. 1, pp. 37–47, Jan. 2011.

[115] S. N. G. Chu, S. Nakahara, S. J. Pearton, T. Boone, and S. M. Vernon, "Antiphase domains in GaAs grown by metalorganic chemical vapor deposition on silicon-on-insulator," *J. Appl. Phys.*, vol. 64, no. 6, p. 2981, 1988.

[116] W. Guo, A. Bondi, C. Cornet, et al., "Thermodynamic evolution of antiphase boundaries in GaP/Si epilayers evidenced by advanced X-ray scattering," *Appl. Surf. Sci.*, vol. 258, no. 7, pp. 2808–2815, Jan. 2012.

[117] Y. Bogumilowicz, J. M. Hartmann, R. Cipro, et al., "Anti-phase boundaries–Free GaAs epilayers on 'quasi-nominal' Ge-buffered silicon substrates," *Appl. Phys. Lett.*, vol. 107, no. 21, p. 212105, Nov. 2015.

[118] R. Yang, N. Su, P. Bonfanti, et al., "Advanced in situ pre-Ni silicide (Siconi) cleaning at 65nm to resolve defects in NiSix modules," *J. Vac. Sci. Technol. B*, vol. 28, no. 1, pp. 56–61, Jan. 2010.

[119] S. A. Campbell, *Fabrication engineering at the micro and nanoscale*, 3rd ed. New York: Oxford University Press, 2008.

[120] W. M. Duncan and G. H. Westphal, "GaAs Material Preparation and Characterization," *VLSI Electron. Microstruct. Sci.*, vol. 11, pp. 41–86, Jan. 1985.

[121] Z. Y. Zhou, C. X. Zheng, W. X. Tang, D. E. Jesson, and J. Tersoff, "Congruent evaporation temperature of GaAs(001) controlled by As flux," *Appl. Phys. Lett.*, vol. 97, no. 12, p. 121912, Sep. 2010.

[122] V. Borisenko and P. J. Hesketh, *Rapid Thermal Processing of Semiconductors*. Springer Science & Business Media, 2013.

[123] K. S. Jones, A. G. Lind, C. Hatem, S. Moffatt, and M. C. Ridgeway, "A Brief Review of Doping Issues in III-V Semiconductors," *ECS Trans.*, vol. 53, no. 3, pp. 97–105, May 2013.

[124] C. L. Hinkle, A. M. Sonnet, E. M. Vogel, et al., "GaAs interfacial self-cleaning by atomic layer deposition," *Appl. Phys. Lett.*, vol. 92, no. 7, p. 71901, Feb. 2008.

[125] T. Gougousi, "Atomic layer deposition of high-k dielectrics on III–V semiconductor surfaces," *Prog. Cryst. Growth Charact. Mater.*, vol. 62, no. 4, pp. 1–21, Dec. 2016.

[126] B. R. Yates, "Implantation and Activation of Ultra-Shallow Boron in Germanium," University of Florida, Gainesville, Fla., 2012.

[127] D. B. Williams and C. B. Carter, *Transmission Electron Microscopy: A Textbook for Materials Science*. Springer Science & Business Media, 2009.

[128] R. F. Egerton, *Physical Principles of Electron Microscopy: An Introduction to TEM, SEM, and AEM*. Springer Science & Business Media, 2006.

[129] T. S. Kuan and C.-A. Chang, "Electron microscope studies of a Ge–GaAs superlattice grown by molecular beam epitaxy," *J. Appl. Phys.*, vol. 54, no. 8, pp. 4408–4413, Aug. 1983.

[130] S. H. Vajargah, S. Y. Woo, S. Ghanad-Tavakoli, et al., "Atomic-resolution study of polarity reversal in GaSb grown on Si by scanning transmission electron microscopy," *J. Appl. Phys.*, vol. 112, no. 9, p. 93101, Nov. 2012.

[131] A. Beyer, B. Haas, K. I. Gries, et al., "Atomic structure of (110) anti-phase boundaries in GaP on Si(001)," *Appl. Phys. Lett.*, vol. 103, no. 3, p. 32107, Jul. 2013.

[132] C. A. Schneider, W. S. Rasband, and K. W. Eliceiri, "NIH Image to ImageJ: 25 years of image analysis," *Nat. Methods*, vol. 9, no. 7, pp. 671–675, Jul. 2012.

[133] M. Schaffer, B. Schaffer, and Q. Ramasse, "Sample preparation for atomic-resolution STEM at low voltages by FIB," *Ultramicroscopy*, vol. 114, pp. 62–71, Mar. 2012.

[134] Y. c. Park, B. c. Park, S. Romankov, et al., "Use of permanent marker to deposit a protection layer against FIB damage in TEM specimen preparation," *J. Microsc.*, vol. 255, no. 3, pp. 180–187, Sep. 2014.

[135] Y. Chriqui, L. Largeau, G. Patriarche, et al., "Direct growth of GaAs-based structures on exactly (001)-oriented Ge/Si virtual substrates: reduction of the structural defect density and observation of electroluminescence at room temperature under CW electrical injection," *J. Cryst. Growth*, vol. 265, no. 1–2, pp. 53–59, Apr. 2004.

[136] D. C. Hays, "Selective etching of compound semiconductors," 1999.

[137] N. Chand, J. Allam, J. M. Gibson, et al., "GaAs avalanche photodiodes and the effect of rapid thermal annealing on crystalline quality of GaAs grown on Si by molecular-beam epitaxy," *J. Vac. Sci. Technol. B*, vol. 5, no. 3, pp. 822–826, May 1987.

[138] J. E. Ayers, L. J. Schowalter, and S. K. Ghandhi, "Post-growth thermal annealing of GaAs on Si(001) grown by organometallic vapor phase epitaxy," *J. Cryst. Growth*, vol. 125, no. 1–2, pp. 329–335, Nov. 1992.

[139] A. Létoublon, W. Guo, C. Cornet, et al., "X-ray study of antiphase domains and their stability in MBE grown GaP on Si," *J. Cryst. Growth*, vol. 323, no. 1, pp. 409–412, May 2011.

[140] Woollam, John A., Johs, Blaine D., Herzinger, C. M., et al., "Overview of variable-angle spectroscopic ellipsometry (VASE): I. Basic theory and typical applications," *Opt. Metrol.*, vol. CR72, pp. 3–28, 1999.

[141] D. C. Look, *Electrical Characterization of GaAs Materials and Devices*. Wiley, 1992.

[142] H. W. Kim, "Effect of surface carbon and oxygen on the structural quality of silicon homoepitaxial films," *J. Mater. Sci.*, vol. 39, no. 1, pp. 361–363, 2004.

[143] C. S. C. Barrett, A. G. Lind, X. Bao, et al., "Quantitative correlation of interfacial contamination and antiphase domain boundary density in GaAs on Si(100)," *J. Mater. Sci.*, vol. 51, no. 1, pp. 449–456, Aug. 2015.

[144] T. F. Kuech and E. Veuhoff, "Mechanism of carbon incorporation in MOCVD GaAs," *J. Cryst. Growth*, vol. 68, no. 1, pp. 148–156, Sep. 1984.

[145] R. Butz and H. Lüth, "The surface morphology of Si (100) after carbon deposition," *Surf. Sci.*, vol. 411, no. 1–2, pp. 61–69, Aug. 1998.

[146] V. I. Vdovin, M. G. Mil'vidskii, and T. G. Yugova, "Antiphase boundaries in GaAs layers on Si and Ge," *J. Cryst. Growth*, vol. 132, no. 3–4, pp. 477–482, Sep. 1993.

[147] C. S. C. Barrett, T. P. Martin, X.-Y. Bao, et al., "Effect of bulk growth temperature on antiphase domain boundary annihilation rate in MOCVD-grown GaAs on Si(001)," *J. Cryst. Growth*, vol. 450, pp. 39–44, Sep. 2016.

[148] J. B. Posthill, J. C. L. Tarn, K. Das, T. P. Humphreys, and N. R. Parikh, "Observation of antiphase domain boundaries in GaAs on silicon by transmission electron microscopy," *Appl. Phys. Lett.*, vol. 53, no. 13, p. 1207, 1988.

[149] T. Kikkawa, H. Tanaka, and J. Komeno, "The growth of GaAs, AlGaAs, and selectively doped AlGaAs/GaAs heterostructures by metalorganic vapor phase epitaxy using tertiarybutylarsine," *J. Appl. Phys.*, vol. 67, no. 12, pp. 7576–7582, Jun. 1990.

[150] B. Vermang, H. Goverde, A. Lorenz, et al., "On the blistering of atomic layer deposited Al2O3 as Si surface passivation," in *2011 37th IEEE Photovoltaic Specialists Conference*, 2011, pp. 003562–003567.

[151] B. Vermang, H. Goverde, V. Simons, et al., "A study of blister formation in ALD Al2O3 grown on silicon," in *2012 38th IEEE Photovoltaic Specialists Conference*, 2012, pp. 001135–001138.

[152] O. Beldarrain, M. Duch, M. Zabala, et al., "Blistering of atomic layer deposition Al2O3 layers grown on silicon and its effect on metal–insulator–semiconductor structures," *J. Vac. Sci. Technol. Vac. Surf. Films*, vol. 31, no. 1, p. 01A128, Nov. 2012.

[153] C. Choi, N. Otsuka, G. Munns, et al., "Effect of insitu and exsitu annealing on dislocations in GaAs on Si substrates," *Appl. Phys. Lett.*, vol. 50, no. 15, pp. 992–994, Apr. 1987.

[154] H. L. Tsai and J. W. Lee, "Defect structures at the GaAs/Si interface after annealing," *Appl. Phys. Lett.*, vol. 51, no. 2, pp. 130–132, Jul. 1987.

[155] M. M. Al-Jassim, T. Nishioka, Y. Itoh, A. Yamamoto, and M. Yamaguchi, "Defect Reduction in MOCVD Grown Si/GaAs," *MRS Proc.*, vol. 116, Jan. 1988.

[156] R. W. Kaliski, C. R. Ito, D. G. McIntyre, et al., "Influence of annealing and substrate orientation on metalorganic chemical vapor deposition GaAs on silicon heteroepitaxy," *J. Appl. Phys.*, vol. 64, no. 3, pp. 1196–1200, Aug. 1988.

[157] N. Chand, R. People, F. A. Baiocchi, K. W. Wecht, and A. Y. Cho, "Significant improvement in crystalline quality of molecular beam epitaxially grown GaAs on Si (100) by rapid thermal annealing," *Appl. Phys. Lett.*, vol. 49, no. 13, pp. 815–817, Sep. 1986.

[158] J.-M. Baribeau, D. C. Houghton, P. MaignÉ, et al., "Characterization of GaAs and Ge Films on (100) Silicon," *MRS Proc.*, vol. 91, Jan. 1987.

[159] M. Yamaguchi, M. Tachikawa, Y. Itoh, M. Sugo, and S. Kondo, "Thermal annealing effects of defect reduction in GaAs on Si substrates," *J. Appl. Phys.*, vol. 68, no. 9, pp. 4518–4522, Nov. 1990.

[160] S. Goapper, L. Barbier, B. Salanon, A. Loiseau, and X. Torrelles, "Observation of domain structure and coarsening at Cu-Pd alloy vicinal surfaces," *Phys. Rev. B*, vol. 57, no. 19, p. 12497, 1998.

[161] J. F. Wager, "Energetics of self-diffusion in GaAs," *J. Appl. Phys.*, vol. 69, no. 5, pp. 3022–3031, Mar. 1991.

[162] L. Wang, L. Hsu, E. E. Haller, et al., "Ga self-diffusion in GaAs isotope heterostructures," *Phys. Rev. Lett.*, vol. 76, no. 13, p. 2342, 1996.

[163] U. M. Gösele, T. Y. Tan, M. Schultz, et al., "Diffusion in GaAs and Related Compounds: Recent Developments," *Defect Diffus. Forum*, vol. 143–147, pp. 1079–1094, 1997.

[164] H. D. Palfrey, M. Brown, and A. F. W. Willoughby, "Self-Diffusion in gallium arsenide," *J. Electron. Mater.*, vol. 12, no. 5, pp. 863–877, Sep. 1983.

[165] S. C. Ghosh, M. C. Biesinger, R. R. LaPierre, and P. Kruse, "The role of proximity caps during the annealing of UV-ozone oxidized GaAs," *J. Appl. Phys.*, vol. 101, no. 11, p. 114321, Jun. 2007.

[166] S. B. Zhang and J. E. Northrup, "Chemical potential dependence of defect formation energies in GaAs: Application to Ga self-diffusion," *Phys. Rev. Lett.*, vol. 67, no. 17, pp. 2339–2342, Oct. 1991.

[167] G. Radhakrishnan, O. McCullough, J. Cser, and J. Katz, "Secondary ion mass spectrometry study of ex situ annealing of epitaxial GaAs grown on Si substrates," *Appl. Phys. Lett.*, vol. 52, no. 9, pp. 731–732, Feb. 1988.

[168] A. Freundlich, A. Leycuras, J. C. Grenet, and C. Grattepain, "Defect-related Si diffusion in GaAs on Si," *Appl. Phys. Lett.*, vol. 53, no. 26, pp. 2635–2637, Dec. 1988.

[169] S. J. Pearton, D. L. Malm, L. A. Heimbrook, et al., "Heterointerface stability in GaAs-on-Si grown by metalorganic chemical vapor deposition," *Appl. Phys. Lett.*, vol. 51, no. 9, pp. 682–684, Aug. 1987.

[170]   S. O. Kasap, *Principles of electronic materials and devices*, 3rd ed. Boston: McGraw-Hill, 2006.

BIOGRAPHICAL SKETCH

Caleb Shuan Chia Barrett is the son of Michael and Shau-Ling Barrett. He grew up in Greenbelt, MD, and graduated from the Science and Technology Program at Eleanor Roosevelt High School. He then attended the University of Maryland where he majored in materials science and engineering. After graduating in 2013, he moved on to the University of Florida to pursue his Ph.D. in materials science and engineering under Dr. Kevin Jones. Along the way, he earned his master's degree in materials science and engineering in 2015. He has accepted an offer to work at Intel in Hillsboro, OR, after the completion of his Ph.D. to fund his future car collection and world explorations.